The Islamic University–Gaza

Research and Postgraduate Affairs

Faculty of Engineering

Master of Electrical Engineering

Communication Systems

الجامعـــــــة الإســـلاميـة - غزة

شئون البحث العلمي والدراسات العليا

كليـــــــــــة الهنـــــــــــدسة

ماجستيـــــر الهنـــدسة الكهربائية

أنظمـــــــة اتصـــالات

Design of Efficient Millimeter Wave Planar Antennas for 5G Communication Systems

تصميم هوائيات ذات كفاءة على تردد موجات المليمتر لأنظمة اتصالات الجيل الخامس

Mohammed H. Abu Saada

Supervised by

Dr. Talal F. Skaik

Assistant prof. of Electrical Engineering

Dr. Ramadan A. Alhalabi

Assistant prof. of Electrical Engineering

A thesis submitted in partial fulfillment
of the requirements for the degree of
Master of Electrical Engineering – Communication Systems Engineering

April/2017

إقـــــرار

أنا الموقع أدناه مقدم الرسالة التي تحمل العنوان:

Design of Efficient Millimeter Wave Planar Antennas for 5G Communication Systems

تصميم هوائيات ذات كفاءة على تردد موجات المليمتر لأنظمة اتصالات الجيل الخامس

أقر بأن ما اشتملت عليه هذه الرسالة إنما هو نتاج جهدي الخاص، باستثناء ما تمت الإشارة إليه حيثما ورد، وأن هذه الرسالة ككل أو أي جزء منها لم يقدم من قبل الآخرين لنيل درجة أو لقب علمي أو بحثي لدى أي مؤسسة تعليمية أو بحثية أخرى. وأن حقوق النشر محفوظة للجامعة الإسلامية غزة –فلسطين

Declaration

I hereby certify that this submission is the result of my own work, except where otherwise acknowledged, and that this thesis (or any part of it) has not been submitted for a higher degree or quantification to any other university or institution. All copyrights are reserves toIslamic University – Gaza strip paiestine

Student's name:	محمد حسن أبو سعدة	اسم الطالب:
Signature:	**محمد أبو سعدة**	التوقيع:
Date:	2017/5/21	التاريخ:

بسم الله الرحمن الرحيم

الجامعة الإسلامية غزة
The Islamic University of Gaza

مكتب نائب الرئيس للبحث العلمي والدراسات العليا هاتف داخلي 1150

الرقم: ج س غ/35/ Ref:

التاريخ: 2017/05/13م Date:

نتيجة الحكم على أطروحة ماجستير

بناءً على موافقة شئون البحث العلمي والدراسات العليا بالجامعة الإسلامية بغزة على تشكيل لجنة الحكم على أطروحة الباحث/ **محمد حسن محمود ابوسعدة** لنيل درجة الماجستير في **كلية *الهندسة*** قسم **الهندسة الكهربائية – أنظمة الاتصالات** وموضوعها:

تصميم هوائيات ذات كفاءة على تردد موجات المليمتر لأنظمة اتصالات الجيل الخامس

Design of Effcient Millimeter Wave planar antennas for 5G communication systems

وبعد المناقشة التي تمت اليوم السبت 16 شعبان 1438هـ، الموافق 2017/05/13م الساعة الحادية عشر صباحاً في قاعة مؤتمرات مبنى القدس، اجتمعت لجنة الحكم على الأطروحة والمكونة من:

د. طلال فايز سكيك	مشرفاً و رئيساً	.....
د. رمضان عبد الرحيم الحلبي	مشرفاً	.....
د. فادي ابراهيم النحال	مناقشاً داخلياً	.....
د. تامر كمال أبو فول	مناقشاً خارجياً	.....

وبعد المداولة أوصت اللجنة بمنح الباحث درجة الماجستير في كلية *الهندسة*/ قسم **الهندسة الكهربائية – أنظمة الاتصالات**.

واللجنة إذ تمنحه هذه الدرجة فإنها توصيه بتقوى الله ولزوم طاعته وأن يسخر علمه في خدمة دينه ووطنه.

والله ولي التوفيق،،،

نائب الرئيس لشئون البحث العلمي والدراسات العليا

أ.د. عبدالرؤوف علي المناعمة

Abstract

Fifth generation (5G) is the next major phase of mobile telecommunications standards beyond the current 4G, which will operate at millimeter-wave frequency band. In any wireless device, the performance of radio communications depends on the design of an efficient antenna. This thesis presents designs for microstrip antennas (single element and arrays at 28 GHz), where 28GHz is one of the standard frequencies of the 5G communications.

A parametric study to select the best single element design to use it in the array has been performed. The study included investigation on the impact of feeding technique, substrate dielectric constant, substrate thickness and substrate loss tangent on the antenna parameters. Different feeding techniques are studied, and gap-coupled feeder has been found the best in terms of bandwidth that is greater than 1 GHz.

Based on the best optimized single element patch, several microstrip antenna array designs at 28 GHz are proposed with number of elements up to 16 and those designs meet the requirements of 5G antennas. Commercial simulation software (CST) and (ADS) were utilized to design single element, linear and planar arrays.

Furthermore, dual polarized Linear and planar arrays were designed for handset mobiles and base stations respectively, with good isolation between vertical and horizontal ports (better than 20 dB).

ملخص البحث

الجيل الخامس من الاتصالات هو الجيل الذي يلي الجيل الرابع الحالي والمتوقع أن يبدأ العمل به في عام 2020 م. الترددات التي سيتم استخدامها في الجيل الخامس هي ترددات موجات المليمتر والتي تبدأ من 30 جيجا هيرتز فما فوق، حيث أن هذا البحث يقدم تصاميم لهوائيات بعنصر واحد ومصفوفات تعمل عند تردد 28 جيجا هيرتز.

تم عمل دراسة كاملة على المتغيرات المتعلقة بالمادة المصنوع منها الهوائي مثل (السماحية الكهربية للمادة العازلة، سمك المادة العازلة، وكذلك طرق تغذية هوائي الشرائح الدقيقة، ودراسة تأثيرها على أداء الهوائي مثل (كفاءة الهوائي، نطاق الترددات..).

وفق مواصفات هوائيات الجيل الخامس فإن النطاق الترددي يجب أن يكون أكبر من 1 جيجا هيرتز، وهذا تم تحقيقه باستخدام مغذي لهوائي الشرائح الدقيقة لا يلامسه مباشرة وإنما بوجود فجوة صغيرة بينهما.

كانت خلاصة هذه الدراسة اختيار أفضل تصميم وبناء مصفوفة الهوائيات الخطية واللوحية منه، حيث وصل عدد عناصر المصفوفة إلى 16 عنصر ليعطي كسب الى الهوائي يصل الى 17 ديسي بل، وتصميم مصفوفة هوائيات ثنائية القطبية تعمل للهاتف المحمول ولمحطة الارسال كل على حدة.

تم استخدام برامج التصميم الخاصة بالهوائيات مثل(CST)، (ADS).

DEDICATION

To

My Parents Hassan & Enayat

My Wife Islam

My children
Enayat, Anas, Tala, Leen

and
My Family

ACKNOWLEDGEMENT

First and the foremost, I would like to thank Almighty Allah for bestowing His blessings upon me and giving me the strength to carry out and complete this work.

I am extremely grateful to my supervisors Dr. Ramadan Alhalabi and Dr. Talal Skaik for their valuable advice, guidance, beneficial discussions and encouragement throughout my research. Apart from their valuable academic advice and guidelines, they have been extremely kind, friendly, and helpful. I am also very grateful to my thesis committee members, Dr. Tamer Abu Foul and Dr. Fady El-Nahal for their care, cooperation and constructive advices.

Special thanks to my colleagues and friends especially Eng. Belal A. Alsaati, Eng. Mohammed A. Matar, Eng. Mohammed A. Tubail, and Eng. Mohammed J. Hannona for their encouragements and various help that they provided throughout my graduate studies.

Special thanks to my friends Ahmed R. Qarrot, Abdallah H. Abu Saada, Zakaria A. Alshaghnouby, ,Mohammed Kh. Abu Salem, Mohammed Z. Aldahshan, Mohammed F. Kullab and Khalil Eslayyeh.

Also, I want to thank my Indian friend Sudipta Maity for his valuable advice and guidance.

I would like to give my special thanks to my parents, brothers, sister and my wife for their support, patience and love. Without their encouragement, motivation and understanding, it would have been impossible for me to complete this work. Finally, my sincere thanks are due to all people who supported me to complete this work.

Contents

List of Tables

List of Figures

Chapter 1
Introduction

Chapter 1

Introduction

1. 1 5G Communications

5G (5th generation mobile networks or 5th generation wireless systems) is a term used in some research papers and projects to denote the next major phase of mobile telecommunications standards beyond the current 4G. 5G is considered as beyond 2020 mobile communications technologies (Agarwal, 2017).

A new standard generation comes along every 10 years or so, since the first generation of mobile network standards appeared in 1982. These standards are developed to serve the current and future demands of the mobile users. But, the mobile traffic worldwide is increasing exponentially each year and the trend will likely continue for the expected future (Gampala &Reddy, 2016).

Worldwide mobile data traffic will most certainly continue to grow quickly in the next decade. Naturally there are growing concerns that the current 4G cellular network capacity will be unsustainable in the long term. In recent years, numerous research foundations and industry partners have been researching the concept of a 5th generation (5G) mobile network improvements in capacity, latency, and mobility (Hong W. , Ko, Lee, & Baek, 2015) . Due to spectrum shortage in the conventional microwave bands, millimeter wave (mm-Wave) bands have been attracting great attention as an additional spectrum band for 5G cellular networks (Kim, Bang, & Sung, 2014).

The main objectives of 5G will be targeted towards improving the capacity of the networks with better coverage at a lower cost. The most important and highly critical objective of all is the "capacity" as it directly relates to the growing user demand for faster and higher data rates. The general agreement among different research groups working on the futuristic 5G technologies is a peak data rate of 10 Gb/s for static users, 1 Gb/s for mobility users and no less than 100 Mb/s in urban areas. The technology being investigated to meet these high data rate targets is the massive MIMO (Gampala &Reddy, 2016). Massive MIMO: Extension of multi-user MIMO concept to hundreds of antennas at the base station is a promising solution to significantly increase user throughput and network capacity by allowing beamformed data transmission and interference management. The significantly increased path loss in very high-frequencies has to be compensated by higher antenna gains, which is made possible by increasing number of antennas at the base station (Ahmadi, 2016) . 5G research and development also aims at lower latency than 4G equipment to be sub-1ms and lower battery consumption (Revolvy, 2017).

Moving to the mm-Wave frequencies for 5G mobile stations, requires new techniques in the design of antennas for mobile-station (MS) and base-station (BS) systems. In order to achieve an efficient beam-steerable phased array antenna, which is one of the most important parts for 5G cellular systems, the smaller antennas arranged as an array can be employed (Ojaroudiparchin, Shen, &

Frolund, 2015). The number of devices could reach the tens or even hundreds of billions by the time 5G comes to fruition, due to many new applications beyond personal communications (Andrews, et al., 2014)

1. 2 Background

The generations of mobile communication systems are presented in Table (1.1). Mobile phone network has been historically divided into four generations, each generation has specific characteristics that distinguish it from other, each generation is different from the other in terms of frequency, data rate, maximum number of users and the geographical area covered by the network.

Table (1.1): summary of mobile communications generations (Hartley, 2017) (Uncategorized | mansipruthi, 2017) (Sahoo, Hota, & Barik, 2017)

Cellular phone generation	**1G**	**2G**	**3G**	**4G**	**5G**
1st year deployment	1981	1992	2001	2010	2020
Peak supported Data rate	2 Kbps	64 Kbps	2 Mbps	100 Mbps	10 Gbps
Frequency	900 MHz	900MHz and 1.8GHz	800/900 MHz 1.7 to 1.9 GHz 2100 MHz	800MHz 900MHz 1800MHz 2100MHz 2600MHz	28GHz 37 GHz 39 GHz 64 – 71 GHz
General functional description	Analogue cellular phones	Digital cellular phones (GSM/CDMA)	First mobile broadband utilizing IP protocols (WCDMA2000)	The mobile broadband on a unified standard (LTE)	Tactile internet – Enhance M2M communications network

1. 3 planar Antennas at mm-Wave Frequencies

In recent years, the demand for high speed cellular data and the need for more spectrum have motivated the use of millimeter wave (mm-wave) carrier frequencies for future cellular networks, where high gain adaptive antennas (Zhao, et al., 2013). The mm-Wave band has been attracting great attention, since an enormous amount of bandwidth is available (Kim, Bang, & Sung, 2014).

The millimeter-wave band is defined as the portion of the electromagnetic spectrum extending from 30 - 300 GHz with corresponding wavelengths range of 10 - 1 mm. Historically, mm-wave frequencies were used mostly for defense and radio astronomy applications mainly because of the high cost and limited availability of electronic devices at these frequencies. The recent advancement of silicon technology and the rapidly growing mm-wave applications markets (such as automotive radars, high-resolution imaging and high-definition video transfer requirements) necessitate the development of broadband, highly integrated, low power and low cost wireless systems including high-efficiency planar antennas (Alhalabi, 2010).

Integrated planar antennas have gained a lot of interest in the past years for mm-wave applications due to their low cost, ease of fabrication and potential for high efficiency operation. The small wavelength at mm-wave frequencies is an advantage for the design of small and efficient antennas. The size of the antenna is determined by the laws of physics; and for efficient radiation, the antenna size should be of the order of half wavelength or larger. Therefore, for f = 30 - 300 GHz (λ = 10 - 1 mm), it is feasible to build antennas that are physically small and at the same time electrically large enough to radiate efficiently. However, at mm-wave frequencies the losses are generally higher than at lower frequencies; and the antenna designer needs to carefully design the antenna and choose the appropriate substrate to minimize losses and achieve high radiation efficiency (Alhalabi, 2010).

Due to its small wave length, mm-wave antenna size can be made smaller than conventional cellular frequency wave. The small antenna size enables sharp beamforming or massive MIMO technology (Lee, Song, Choi, & Park, 2015).

In 5G requirements, the antenna should at least have a gain of 12 dB and bandwidth more than 1 GHz (Jamaluddin, Kamarudin, & Khalily, 2016).

1. 4 Why at 28 GHz?

Unused or underutilized Local Multipoint Distribution Service (LMDS) broadband spectrum exists at 28 GHz, and given the low atmospheric absorption, the spectrum at 28 GHz has very comparable free space path loss as today's 1-2 GHz cellular bands. In addition, but the rain attenuation and oxygen loss does not significantly increase at 28 GHz, and, in fact, may offer better propagation conditions as compared to today's cellular networks when one considers the availability of high gain adaptive antennas and cell sizes on the order of 200 meters (Zhao, et al., 2013). As shown in Figure (1.1) atmospheric absorption at 28 GHz is the negligible (0.06 dB/km) (Jr., Junhong Zhang, & Rappaport, 2013).

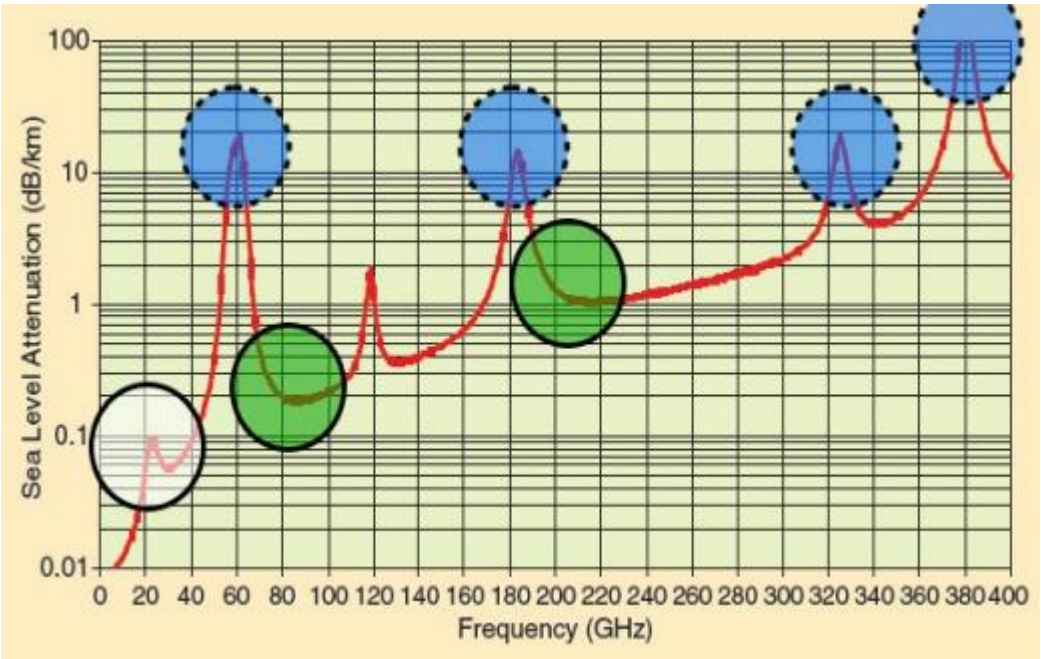

Figure (1.1): Air attenuation at different frequency bands (Jr., Junhong Zhang, & Rappaport, 2013)

1. 5 Literature review

Several mm-wave planar antenna configurations have been studied and designed for 5G communication systems:

In (Senic, zivkovic, simic, & Sarolic, 2014) a good parametric study on the loss tangent influence on antenna parameters. A similar parametric study is made in the thesis but using all substrate parameters (loss tangent $\tan\delta$, dielectric constant ε_r ,and substrate thickness.

A microstrip grid array antenna on an FR4 substrate in a standard PCB technology was presented in (Chen & Zhang, 2013). It shows a -10 dB S_{11} bandwidth of 7.16 GHz from 23.86 to 31.02 GHz and with a gain of 12.66 dB at 29.2 GHz. But using lossy material as FR4 leads to low radiation efficiency, as will be shown later in this study.

A 28 GHz mesh-grid antenna array is presented in (Hong, KwanghunBaek, Lee, & Kim, 2014) . The array offers a fan-beam like radiation pattern with the main radiating structure composed of an array of vias within a 10 layer FR4 PCB. The proposed array offers a -10 dB S11 bandwidth of > 3 GHz with 3.5 dB single element simulated gain with > 10.9 dB gain of a 16-element array. However, using multilayer technology in mobile antenna design leads in complexity in design and fabrication and this results to expensive device. Here in this thesis we propose antenna with single layer which is easy in fabrication and economic.

A 28 GHz wide scanning angle phased array with multi-polarization capabilities has been presented in (Hong W. , Ko, Lee, & Baek, 2015) The phased array uses a printed Yagi-Uda antenna fabricated on a 10-layer FR4 substrate with total thickness of 0.8 mm.

A 28 GHz slot antenna array with ~5% bandwidth with gain equal to 13dB was presented in (Alreshaid A. , Hammi, Sharawi, & Sarabandi, 2015). The occupied size of the presented 8 element array was only 29.9×28.7×0.13 mm3. A good bandwidth in this paper, but large size relatively, this study achieved 12.2dB gain in smaller size.

A switched beam planar array with center frequency at 28.5 GHz and with 1 GHz bandwidth was presented in (Alreshaid, Hammi, & Sharawi, 2015) and showed a gain of 8 – 12 dB. The beams radiated from the antenna array were steered to four different locations; ±20˚ and ± 45˚, the scanning angle must be larger than 45˚ in order mobile antenna work well.

Conformal tapered slot antenna array was presented in (Ashraf, Haraz, & Alshebeili, 2015) with a -10 dB S_{11} bandwidth of 14.8 GHz. Dielectric lenses were used to enhance the antenna gain to more than 20 dB over a wide frequency range (24 – 40 GHz). The system presents four orthogonal independent beams switched at the angle of ±14 degree along the co-ordinate axis. It is very short scanning angle.

Millimeter Wave Antenna Arrays for 5G Cellular Applications was designed in (Gampala &Reddy, 2016) to highlight the concept of massive MIMO that employs antenna arrays and beamforming techniques to address the high data rate demands. The antenna is designed at 28 GHz.

A new dense dielectric (DD) patch array antenna prototype operating at 28 GHz for future fifth generation (5G) is presented in (HARAZ, ELBOUSHI, ALSHEBEILI, & SEBAK, 2014). The proposed structure employs four circular-shaped DD patch radiator antenna elements fed by a 1-to-4Wilkinson power divider. The measured impedance bandwidth of the proposed array antenna ranges from 27 to beyond 32 GHz for a reflection coefficient (S_{11}) of less than 10 dB with a total realized gain more than 16 dB.The design based on multilayer technology which causes difficult fabrication and high cost.

A mm-Wave microstrip antenna array is designed in (Hu, Yu, Hsaio, & Lin, 2015) at 38 GHz by using a 64-element micorstrip patch antenna array with gain approximately equal 6.5 dB and bandwidth approximately equal 2 GHz. However, the gain is low (6.5dB) with respect to elements number which equals 64-elements.

A small beamforming antenna for the handset phone was designed in (Jang, Khattak, Jeon, Kim, & Kahng, 2015) with a feed network adapted to the optimized feeding scheme. It is revealed that the proposed four element 24-GHz resonance array antenna fits the placement in the top side of a handset phone. The antenna efficiency is over 70 % and the peak-gain is greater than 8 dB up to 10.5 dB at the aforementioned target millimeter-wave frequency.

However, the radiation efficiency is low (70%) and the feeding technique is inset-feed which has low bandwidth.

1. 6 Thesis motivation

In this research, a comprehensive study of different parameters that affect antenna performance, (such as antenna type, feeding technique, substrate dielectric constant, substrate thickness, substrate loss tangent, etc.…), was carried out. The outcome of this study serves as a design guide and is very useful for 5G mm-wave antenna designers. The usefulness of the study is illustrated through the design of a planar antenna optimized for 5G communication systems. The proposed antenna is designed in the 28 GHz range and has the following design characteristics:

The proposed antenna has a wide bandwidth of > 1 GHz over which the antenna has a good 50 Ω impedance matching with S_{11} < -10 dB with stable radiation patterns able to support the expected high data rates of the future 5G networks.

The proposed antenna has a high radiation efficiency to compensate for the extra path loss at mm-wave frequencies. The higher antenna efficiency will also relief the power amplifier requirements and will enhance the cell phone battery life.

It has a multi-polarization capability to reduce the polarization mismatch losses since the mobile phone orientation does not remain fixed during normal use.

The proposed antenna design was optimized in a multi element array configuration to achieve higher gain for better signal to noise ratio (SNR).

1. 7 Thesis overview

The thesis consists of five chapters:

Chapter one is an introduction about 5G communications, and its frequency band. Several antennas designs for 5G antenna are introduced in the literature review.

Chapter two provides an overview of the theory of Antenna. The work in chapter 2 presents the antenna parameters which describe the behavior of antenna, later in the same chapter, Microstrip patch antenna and its design procedures are presented.

In chapter 3, a parametric study is performed to choose the best design for 28GHz antenna. The parametric study contains the microstrip antenna parameters such as (feeding technique, substrate dielectric constant, substrate thickness, substrate loss tangent).

In chapter four antenna array designs are presented, the array is constructed from the best design in chapter 3. Single and dual polarized antenna array are also presented to satisfy 5G communication requirements.

The last chapter presents the conclusions drawn from the current work and also future work.

Chapter 2
Antenna Theory

Chapter 2

Antenna Theory

2.1 Introduction

Antenna can be defined as " the transition between a guided EM wave and a free-space EM wave and vice-versa (Kraus, Antennas, 1988) as we can see in Figure (2.1):

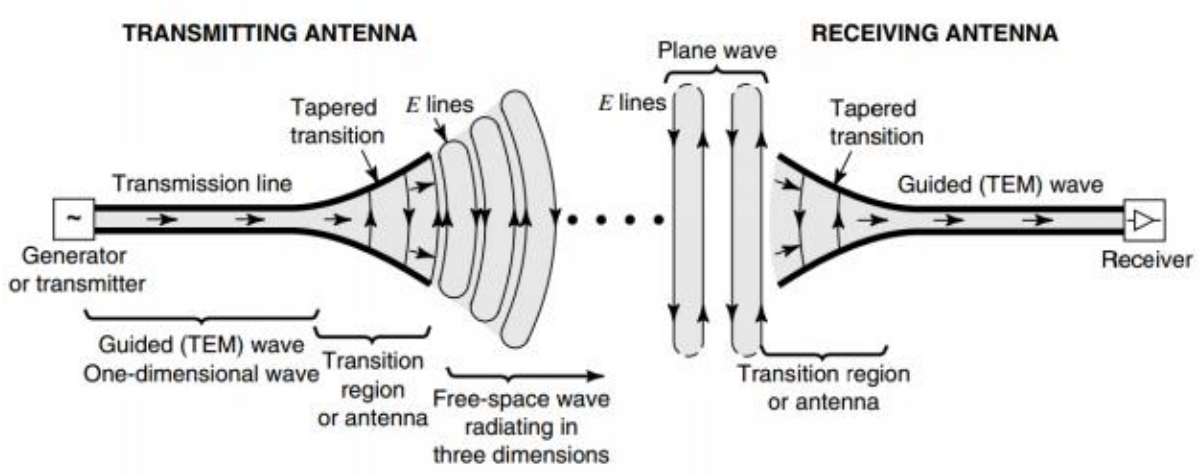

Figure (2.1): The antenna as a transition structure, for a transmitting antenna and for a receiving (Kraus & Marhefka, 2002).

Antenna can be made as a transmitter or as a receiver, it is reciprocal device, as shown in Figure (2.1) an antenna represents the area of transition between free-space wave and guided wave. Thus, an antenna is a transducer or transition device, between a guided wave and free-space wave, or vice versa (Kraus & Marhefka, 2002). The guiding device or transmission line can be either a coaxial line or a hollow pipe (waveguide) (Balanis C. , 2005).

The antenna system can be modeled as an electrical circuit, as in Figure (2.2) we can see A transmission-line Thevenin equivalent of the antenna system in the transmitting mode, where the source is represented by an ideal generator, the transmission line is represented by a line with characteristic impedance Z_c, and the antenna is represented by a load Z_A [$Z_A = (R_L + R_r) + jX_A$] connected to the transmission line. R_L is referred to the conduction and dielectric losses associated with the antenna structure so $R_L = R_c + R_d$ while R_r, is used to represent the radiation resistance, which represents radiation by the antenna. The reactance X_A is used to represent the imaginary part of the impedance associated with radiation by the antenna. The aim here is to transform all the energy from the generator to the to the radiation resistance R_r, but this is ideal case (Balanis C. , 2005).

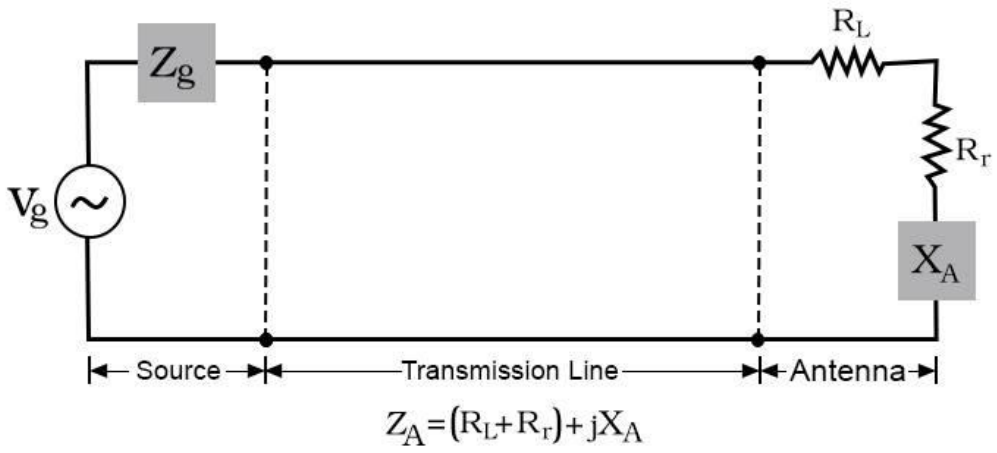

Figure (2.2): Transmission-line Thevenin equivalent of antenna in transmitting mode (Balanis C. , 2005)

2.2 **Maxwell's equations**

Electromagnetic theory is fundamental to understanding of microwave antennas, (SILVER, 1949) and its present form was founded by James Clerk Maxwell (1831-1879), whose efforts led to the discovery of electromagnetic waves , The laws of electromagnetism that Maxwell put together in the form of four equations are presented in Table (2.1): (Sadiku, 2007)

Table (2.1): Generalized Forms of Maxwell's Equations (Sadiku, 2007)

Differential Form	Integral Form	Remarks
$\nabla \cdot \mathbf{D} = \rho_v$	$\oint_s \mathbf{D}.d\mathbf{S} = \oint_v \rho_v dv$	Gauss's law
$\nabla \cdot \mathbf{B} = 0$	$\oint_s \mathbf{B}.d\mathbf{S} = 0$	Nonexistence of isolated magnetic charge
$\nabla \times \mathbf{E} = -\frac{\partial \mathbf{B}}{\partial t}$	$\oint_L \mathbf{E}.dI = -\frac{\partial}{\partial t}\int \mathbf{B}.d\mathbf{S}$	Faraday's law
$\nabla \times \mathbf{H} = \mathbf{J} + \frac{\partial \mathbf{D}}{\partial t}$	$\oint_L \mathbf{H}.dI = \int_s \left(\mathbf{J} + \frac{\partial \mathbf{D}}{\partial t}\right).dS$	Ampere's circuit law

The first and the second are Gauss' laws for the electric and magnetic fields, the third is Faraday's law of induction, the forth is Ampere's law as amended by Maxwell to include the displacement current $\partial \mathbf{D}/\partial t$.

$\partial \mathbf{D}/\partial t$ in Ampere's law is displacement current term which is essential in predicting the existence of propagating electromagnetic waves. The quantities $\mathbf{E}$ and $\mathbf{H}$ represent the electric and magnetic field intensities and are measured in units of [volt/m] and [ampere/m], respectively.

The quantities **D** and **B** are the electric and magnetic flux densities and are in units of [coulomb/m^2] and [weber/m^2], or [Tesla].

The quantities ρ and **J** are the volume charge density and electric current density (charge flux) of any external charges (that is, not including any induced polarization charges and currents.) They are measured in units of [coulomb/m^3] and [ampere/m^2]. The right-hand side of the second equation is zero because there are no magnetic monopole charges (Orfanidis, 2004).

2.3 Antenna Parameters

In order to understand the performance of an antenna, definitions of various parameters are necessary (Balanis C. , 2005), that are used to characterize the performance of an antenna when designing and measuring antennas. We can classify antenna parameters in to two kinds, first antenna parameters from the field point of view which include the radiation pattern, beamwidth, directivity, gain, polarization and the bandwidth, and the second antenna parameters from the circuit point of view which include input impedance, radiation resistance, reflection coefficient, return loss, VSWR and bandwidth (Huang & Boyle, Antennas from Theory to Practice, 2008).

2.3. 1 Radiation Pattern

The radiation pattern of an antenna is a plot of the radiated field/power as a function of the angle at a fixed distance, which should be large enough to be considered far field (Huang & Boyle, Antennas from Theory to Practice, 2008).

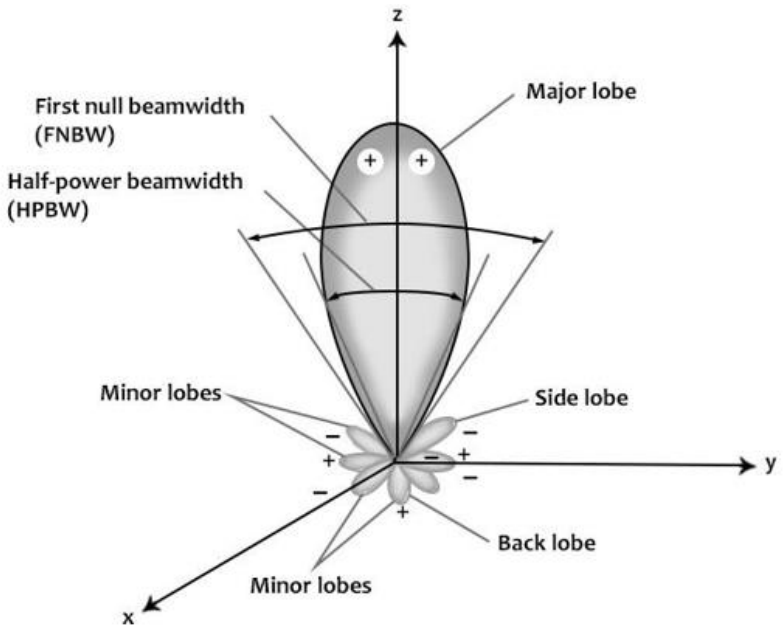

Figure (2.3): Radiation lobes and beamwidths of an antenna pattern [1]

Since the radiation pattern is the variation of the radiated electric field over a sphere centered on the antenna, *r* is constant and we have only θ and φ variations of the field. We can normalize the

field expression such that its maximum value is unity (Stutzman & Thiele, 2013):

$$f(\theta,\phi) = \frac{E_\theta}{E_\theta(\max)} \tag{2.1}$$

where $f(\theta,\phi)$ is the normalized field pattern and E_θ (max) is the maximum value of the magnitude of E_θ over a sphere of radius r.

Radiation Pattern Lobes can be classified into major or main, minor, side, and back lobes as shown in Figure (2.3), A major lobe (also called main beam) is defined as "the radiation lobe containing the direction of maximum radiation." A minor lobe is any lobe except a major lobe.

There are three common radiation patterns that are used to describe an antenna's radiation property:

Isotropic- An ideal lossless antenna having equal radiation in all directions, **Directional**- An antenna having the property of radiating or receiving electromagnetic waves more effectively in some directions than in others and **Omnidirectional**- An antenna having an essentially non-directional pattern in a given plane and a directional pattern in any orthogonal plane. Directional or omnidirectional radiation properties are needed depending on the practical application. Omnidirectional patterns are normally desirable in mobile and hand-held systems.

2.3. 2 Beamwidth

The definition of beamwidth of an antenna pattern is the angular separation between two identical points on opposite side of the pattern maximum. There are a number of beamwidths in an antenna pattern. The Half-Power Beamwidth (HPBW) is the most important one, which is defined by IEEE as (Balanis C. , 2005) : "In a plane containing the direction of the maximum of a beam, the angle between the two directions in which the radiation intensity is one-half value of the beam", the First Null Beamwidth (FNBW) is defined as the angular separation between the first nulls of the pattern. Both the HPBW and FNBW are shown in Figure(2.3).

2.3. 3 Directivity

Directivity is very important antenna parameter which defined as the ratio of the radiation intensity in a given direction from the antenna to the radiation intensity averaged over all directions. The average radiation intensity is equal to the total power radiated by the antenna divided by 4π. Simply, the directivity of a nonisotropic source is equal to the ratio of its radiation intensity in a given direction over that of an isotropic source. In mathematical form, it can be written as

$$\mathbf{D} = \mathbf{D}(\theta,\phi) = \frac{\mathbf{U}(\theta,\phi)}{\mathbf{U}_0} = \frac{4\pi\mathbf{U}(\theta,\phi)}{P_{rad}} \qquad \textbf{(2.2)}$$

If the direction is not specified, it implies the direction of maximum radiation intensity (maximum directivity) expressed as (Balanis C. , 2005)

$$\mathbf{D}_{\max} = \mathbf{D}_0 = \frac{\mathbf{U}_{\max}}{\mathbf{U}_0} = \frac{4\pi\mathbf{U}_{\max}}{P_{rad}} \qquad \textbf{(2.3)}$$

where

$\mathbf{D}$ = directivity (dimensionless)
$\mathbf{D}_0$ = maximum directivity (dimensionless)

$\mathbf{U}$ = radiation intensity (W/unit solid angle)
$\mathbf{U}_{\max}$ = maximum radiation intensity (W/unit solid angle)
$\mathbf{U}_0$ = radiation intensity of isotropic source (W/unit solid angle)
P_{rad} = total radiated power (W)

2.3. 4 Antenna Efficiency

There are a number of antenna efficiencies, the total antenna efficiency e_0 is used to take into account losses at the input terminals and within the structure of the antenna (Balanis C. , 2005), such losses may be due, referring to Figure (2.4), to
1. reflections because of the mismatch between the transmission line and the antenna
2. I ^{2}R losses (conduction and dielectric)

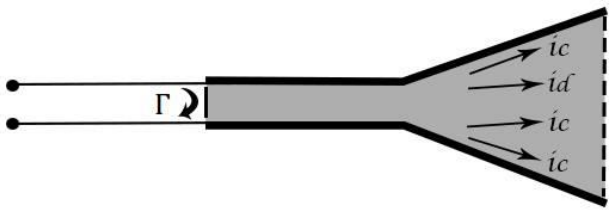

Figure (2.4): antenna losses (Reflection, conduction and dielectric)

In general, the overall efficiency can be written as (Balanis C. , 2005) :

$$e_0 = e_r e_c e_d \qquad \textbf{(2.4)}$$

where

e_0 = total efficiency (dimensionless)

e_r = reflection(mismatch) efficiency = $(1-\left|\Gamma^2\right|)$ (dimensionless)

e_c = conduction efficiency (dimensionless)

e_d = dielectric efficiency (dimensionless)

Γ = voltage reflection coefficient at the input terminals of the antenna

$\Gamma = (Z_{in} - Z_0)/(Z_{in} + Z_0)$ where Z_{in} = antenna input impedance,

Z_0 = characteristic impedance of the transmission line]

2.3. 5 Antenna radiation efficiency

In general, an efficiency factor is the ratio of wanted power to total power supplied (Stutzman & Thiele, 2013), so antenna efficiency can be defined as the ratio between the radiated power (P_r) to the input power (P_{in}) (Volakis, 2007), Figure (2.5) shows the reference points for input and output power.

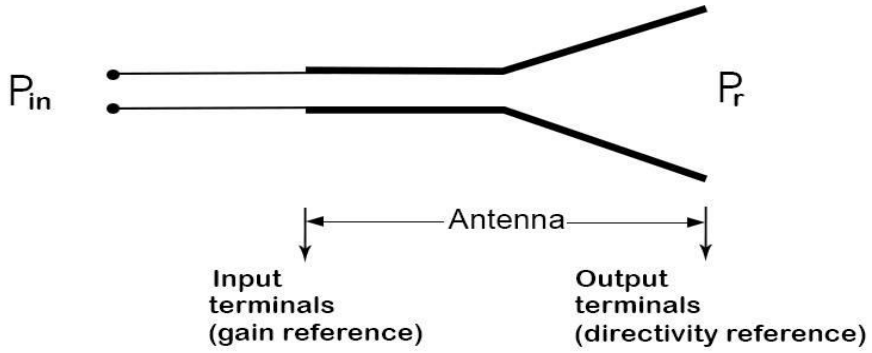

Figure (2.5): Antenna reference terminals (Balanis C. , 2005)

$$e_{cd} = e_c e_d = \text{antenna radiation efficiency} \qquad \textbf{(2.5)}$$

Total Antenna efficiency = (radiation efficiency) x (mismatch loss) (Bevelacqua, Antenna-theory.com, n.d.)

$$e = \frac{P_r}{P_{in}} = \frac{P_r}{P_r + P_0} \qquad \textbf{(2.6)}$$

where

P_r = power radiated

P_0 = power dissipated in ohmic losses on the antenna

$P_{in} = P_r + P_0$ = input power = power accepted by the antenna

2.3. 6 Antenna Gain

Gain is a useful measure that describe the antenna performance, the gain of the antenna is closely related to the directivity, it is a measure that takes into account the efficiency of the antenna as well as its directional capabilities (Balanis C. , 2005). The only difference between gain and directivity is the value of the power used. Directivity can be viewed as the gain of an antenna would have if all input power appeared as radiated power, that is, $P_{in} = P_r$. Gain includes the fact that real antennas do not behave in this fashion and some of the input power is lost on the antenna as (Stutzman & Thiele, 2013) :

$$G = e_r D \tag{2.7}$$

2.3. 7 Bandwidth

The bandwidth can be considered to be the range of frequencies, where on each side of a center frequency the antenna characteristics (such as input impedance, pattern, beamwidth, polarization, side lobe level, gain, beam direction, radiation efficiency) are within an acceptable value of those at the center frequency (at -10 dB) (Balanis C. , 2005). For narrowband antennas, the bandwidth is expressed as a percentage of the frequency difference (upper minus lower) over the center frequency of the bandwidth this called as fractional bandwidth of the antenna (FBW) (Balanis C. , 2005).

For example, a 5% bandwidth for 28 GHz antenna means that the bandwidth of our antenna is

28 GHz *0.05 = 1.4 GHz,

The fractional bandwidth FBW is given by (Antenna-Theory.com - Fractional Bandwidth, 2017):

$$FBW = \frac{f_H - f_L}{f_c} \tag{2.8}$$

where:

FBW – Fractional bandwidth

f_H – Upper frequency in Hz

f_L – Lower frequency in Hz

f_c – Centre frequency in Hz

2.3. 8 Input Impedance

Input impedance is defined as "the impedance presented by an antenna at its terminals or the ratio of the voltage to current at a pair of terminals or the ratio of the appropriate components of the electric to magnetic fields at a point." (Balanis C. , 2005) The input impedance of an antenna (antenna impedance) will be influenced by other antennas or objects that are nearby, antenna impedance is composed of real and imaginary parts as (Stutzman & Thiele, 2013) :

$$Z_A = R_A + jX_A \tag{2.9}$$

Antenna can be modeled as shown in Figure (2.6):

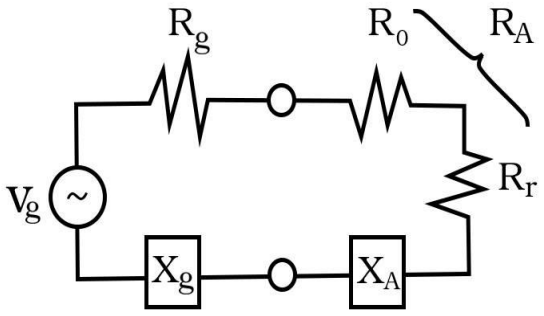

Figure (2.6): Equivalent model for a transmitting antenna (Stutzman & Thiele, 2013).

The input resistance, R_A , represents dissipation which occurs in two ways. Power that leaves the antenna and never returns (i.e., radiation) is one part of the dissipation. There are also ohmic losses just as in a lumped resistor. Electrically small antennas can have significant ohmic losses but other antennas usually have ohmic losses that are small compared to their radiation dissipation. The input reactance, X_A, represents power stored in the near fields of the antenna. The input resistance can be written as (Stutzman & Thiele, 2013)

$$R_A = R_r + R_0 \tag{2.10}$$

Where:

R_r: radiation resistance

R_0 : is the resistance associated with ohmic losses

2.3. 9 Polarization

Polarization of an antenna is the polarization of the wave transmitted from antenna which can be defined as " that property of an electromagnetic wave describing the time-varying direction and relative magnitude of the electric-field vector (Balanis C. , 2005). The polarization of a plane wave is the figure of the instantaneous electric field traces out with time at a fixed observation point as shown in Figure (2.7) (Stutzman & Thiele, 2013). In the far field at any point of an antenna the radiated wave can be represented by a plane wave whose electric-field strength is the same as that of the wave and whose direction of propagation is in the radial direction from the antenna (Balanis C. , 2005).

There are three types of antenna polarization as linear, circular, and elliptical:

linearly polarized: if the vector that describes the electric field at a point in space as a function of time is always directed along a line.

Elliptically polarized: if the electric field traces is an ellipse.

circularly polarized: if the electric field vector remains constant in length but rotates around in a circular path (Stutzman & Thiele, 2013).

Linear and circular polarizations are special cases of elliptical, and they can be obtained when the ellipse becomes a straight line or a circle, respectively.

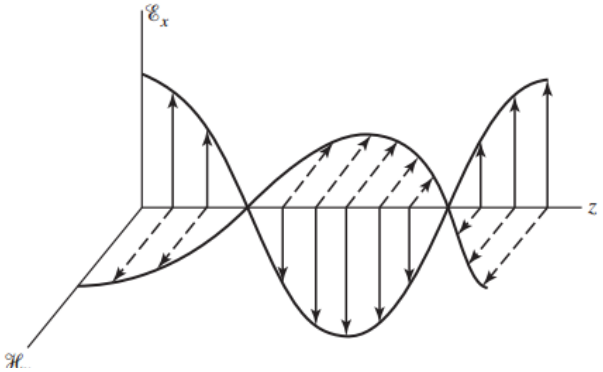

Figure (2.7): The spatial behavior of the electric (solid) and magnetic (dashed) fields of a linearly (vertical) polarized wave for a fixed instant of time (Stutzman & Thiele, 2013)

2.4 Microstrip Antennas

In recent years Microstrip antennas have been one of the most important topics in antenna theory and design, and are increasingly used in a wide range of modern microwave systems (Pozar D. M., 1992) . Microstrip "patch" antenna can be defined as that antenna which made from patches of conducting material on a dielectric substrate above a ground plane (Balanis C. , 2005). microstrip antennas are used because of their low cost, Low weight, low size, With simple feed (Nair, Bharati A., & S.S., 2015).

- **Microstrip Antenna Advantages and limitations:**

Microstrip antenna has many benefits when comparing with other microwave antennas types. These advantages are (Gang, Bhartia, Bahl, & Ittipiboon, 2001) (Bancroft, 2009)[13]

  - ❖ Low weight, low size, and thin profile configuration.
  - ❖ Ease to design and fabricate.
  - ❖ Low fabrication cost.
  - ❖ Many designs readily produce linear or circular polarization Dual frequency and dual polarization can be achieved easily.
  - ❖ Can easily conform to a curved surface of a vehicle or product.
  - ❖ It is easy to be integrated with microwave integrated circuits.
  - ❖ Feed lines and matching networks can be fabricated simultaneously with antenna structure.
  - ❖ An array of microstrip antennas can be used to form a pattern that is difficult to synthesize using a single element.
  - ❖ Smart antennas can be designed when microstrip antennas are combined with phase shifters or PIN-diode switches.

- **and the disadvantages are** (Gang, Bhartia, Bahl, & Ittipiboon, 2001) (Bancroft, 2009) (Radartutorial.eu, n.d.) :
  - ❖ Narrow bandwidth (1%), while mobiles need (8%).
  - ❖ Lower gain (~6 dB)
  - ❖ Poor antenna efficiency.
  - ❖ Sensitivity to environmental factors such as temperature and humidity.
  - ❖ An array suffers presence of feed network decreasing efficiency.

2.4.1 Basic Characteristics

The idea of the microstrip antenna dates back to the 1950's (Pozar D. , 1992). The antenna structure is shown in Figure (2.8) (a)Microstrip antenna consist of a very thin ($t \ll \lambda_0$, where λ_0 is the free-space wavelength) metallic strip (patch) placed a small fraction of a wavelength ($h \ll \lambda_0$, usually $0.003\lambda_0 \le h \le 0.05\lambda_0$) above a ground plane. (Balanis C. , 2005).

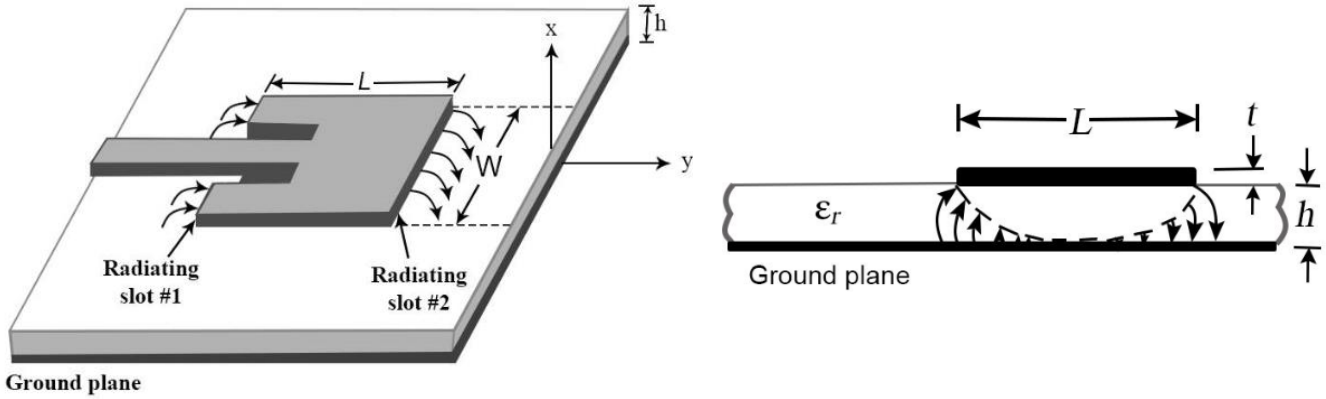

(a)Microstrip antenna (Balanis C. , 2005)

(b)Side view (Balanis C. , 2005)

Figure (2.8): Microstrip antenna and coordinate system.

The maximum pattern of the patch is normal to the patch (broadside radiator). For a rectangular patch, (L) represents the length of the patch which usually $\lambda_0 / 3 < L < \lambda_0 / 2$, which controls the antenna frequency and (W) represents the patch width which is smaller than λ_0 but it can not be too small otherwise the antenna becomes a microstrip line but not a radiator (Huang & Boyle, Antennas from Theory to Practice, 2008). The width controls the input resistance of the patch antenna .The ground plane is separated by a dielectric sheet (the substrate), as shown in Figure (2.8) (b) (Balanis C. , 2005). A patch antenna has again between 5-6 dB and exhibits 3dB beamwidth between 70^o and 90^o (Gang, Bhartia, Bahl, & Ittipiboon, 2001). The patch is fed by a microstrip line which structure is similar to microstrip antenna. The radiation from microstrip line is sometimes undesired. The microstrip line radiation can be reduced if thin substrate is used with higher relative dielectric constant. On the other hand, thick substrates with low permittivity are used for microstrip antennas because the radiation is the target of the antenna (Gang, Bhartia, Bahl, & Ittipiboon, 2001).

2.4.2 Feeding techniques:

Microstrip patch antennas have radiating elements on the upper side of its dielectric substrate, feeding of this patch is by a microstrip line or a coaxial probe through the ground plane which was used early (Gang, Bhartia, Bahl, & Ittipiboon, 2001). Both the microstrip feed line and the probe possess inherent asymmetries which generate higher order modes which produce cross-polarized radiation (Balanis C. , 2005). After that a number of new feeding configurations have been improved, such as proximity-coupled microstrip feed and aperture coupled microstrip feed (Gang, Bhartia, Bahl, & Ittipiboon, 2001), the antenna feeding techniques are as follow:

1- **Coaxial-line feeds**: where the inner conductor of the coax is attached to the radiation patch while the outer conductor is connected to the ground plane (Balanis C. , 2005). But in this study coaxial probe feeder is excluded because coaxial connectors cannot be used to feed printed antennas as their operation is limited to frequencies below 26.5 GHz (Ayoub & Christodoulou, 2014),This technique gives good results up to 20 GHz, but not for mm-Waves. (Liu, Gaucher, Pfeiffer, & Grzyb, 2009).

2- Microstrip (coplanar) feeds

It is a natural choice to excite the microstrip antenna by a microstrip line because the patch can be considered an extension of the microstrip line, and both easily can be fabricated on the same plane simultaneously (Gang, Bhartia, Bahl, & Ittipiboon, 2001). The microstrip feed line width is usually much smaller compared to the patch. The microstrip-line feed is simple to match by controlling the inset position and rather simple to model. However, as the substrate thickness increases, surface waves and spurious feed radiation increase, which for practical designs limit the bandwidth (typically 2–5%) (Balanis C. , 2005). Microstrip (coplanar) feeds include more than one configuration such as Inset Feed, Quarter-Wavelength Transmission Line and Coupled (Indirect) Feeds:

A) **Inset Feed**:

The input impedance of the patch at the edge is high 150–300 ohms (Balanis C. , 2005). If the feeder is connected at the antenna edge as shown in Figure (2.9) impedance mismatch will occur, so the feeder must be modified. Since the current is low at the ends of a half-wave patch and increases in magnitude toward the center the input impedance (Z=V/I) could be reduced if the patch was fed closer to the center. (Bevelacqua, Antenna-theory.com, 2017)

One method of doing this is by using an inset feed (a distance *R* from the end) as shown in Figure (2.10). The inset length can be calculated from (Huang & Boyle, Antennas from Theory to Practice, 2008)

$$R_{in}(x = x_0) = R_{in}(x = 0)\cos^2\left(\frac{\pi}{L}x_0\right) \qquad \textbf{(2.11)}$$

where:

x_0 : inset length

$R_{in}(x = 0)$: the antenna resistance at the edge in ohm

L: the length of the Microstrip antenna

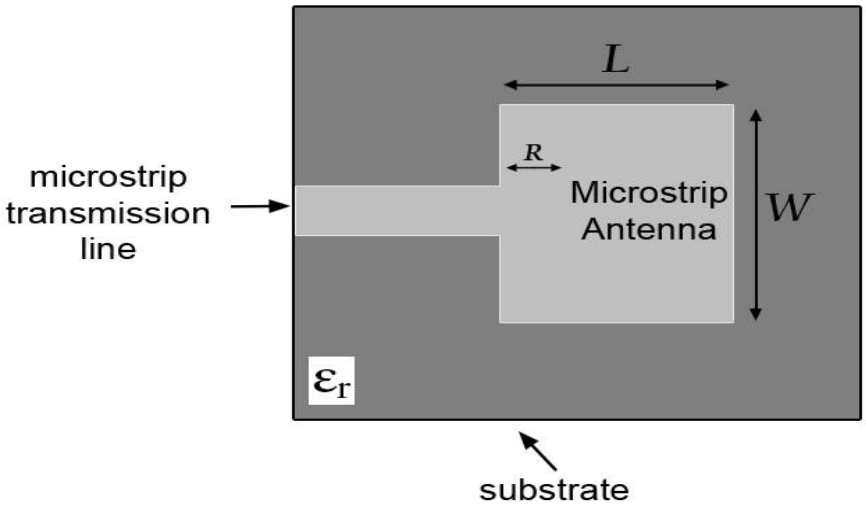

Figure (2.9): unmatched microstrip antenna
(Bevelacqua, Antenna-theory.com, 2017)

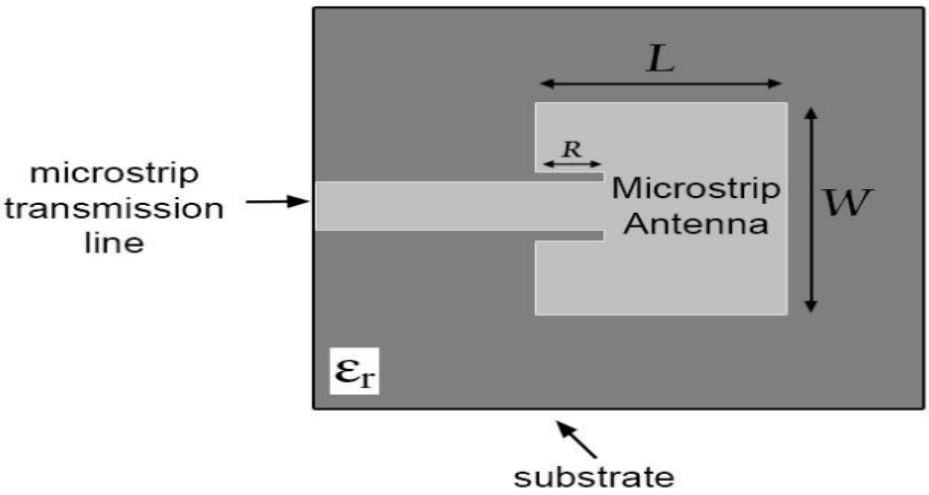

Figure (2.10): Patch Antenna with an Inset Feed.
(Bevelacqua, Antenna-theory.com, 2017)

B) Fed with a Quarter-Wavelength Transmission Line:

A quarter-wavelength transmission line with characteristic impedance Z_1 can be used to match microstrip antenna to a transmission line of characteristic impedance Z_0 (Bevelacqua, Antenna-theory.com, 2017) as shown in Figure (2.11):

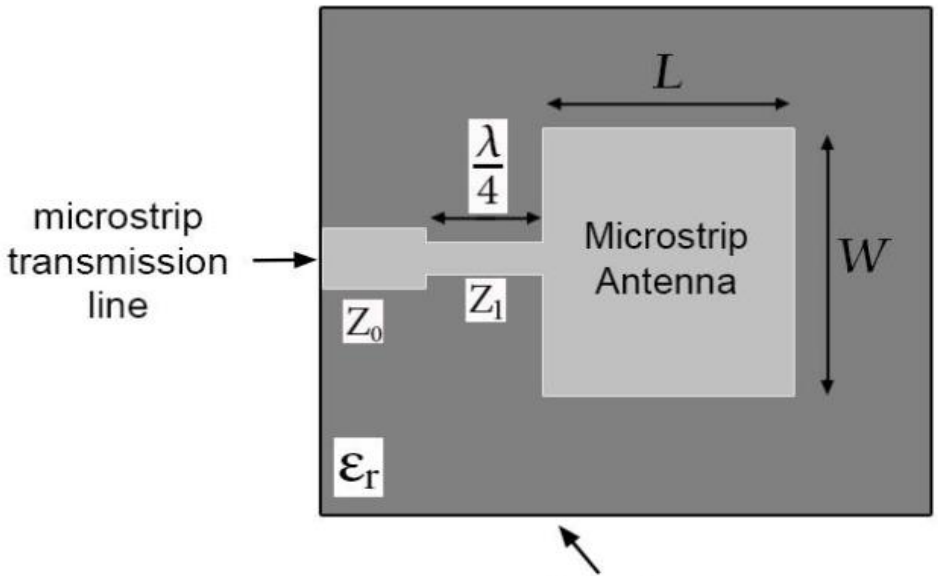

Figure (2.11): Patch antenna with a quarter-wavelength matching section (Bevelacqua, Antenna-theory.com, 2017) .

The target is to match antenna input impedance (Z_A) to the transmission line (Z_0), after transformation the impedance seen from the beginning of the quarter-wavelength line becomes by (Pozar D. M., Microwave Engineering, 2012) :

$$Z_{in} = Z_0 = \frac{Z_1^2}{Z_A} \qquad \textbf{(2.12)}$$

$$Z_1 = \sqrt{(Z_0 * Z_A)} \qquad \textbf{(2.13)}$$

C) Gap Coupled Feeds:

Sometimes microstrip antenna are not directly fed at its edge. Alternatively, gap coupled fed can be used where etched gap separates the microstrip feeder from the microstrip antenna as shown in Figure (2.12), so power moves from feeder to antenna indirectly by coupling (Bevelacqua, Antenna-theory.com, 2017).

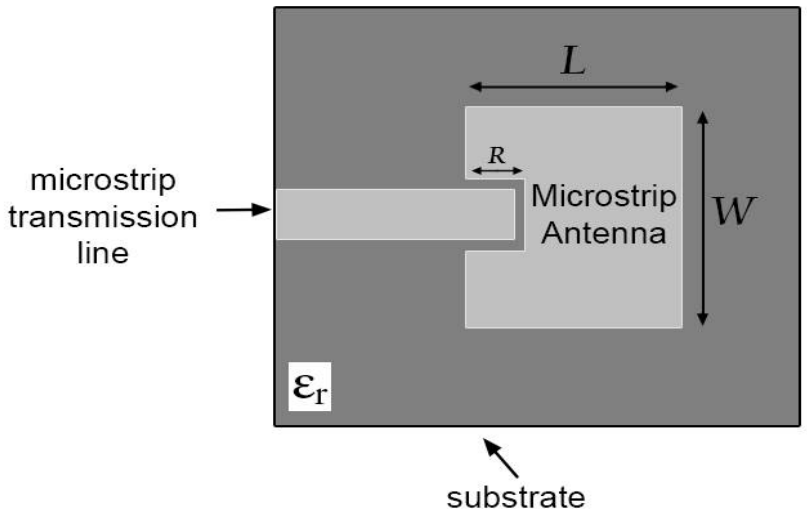

Figure (2.12): Gap Coupled (indirect) inset feed.

Gap coupled feed strip is good choice as the patch can be considered as an extension of the feed strip, and both can be fabricated together on one plane, without much wastage of the substrate material. The gap-coupled capacitive feed strip requires a narrow gap width for efficient coupling of power (S.Sarkar, 2013).

The advantage of the gap coupled feed is that it provides good impedance bandwidth (S.Sarkar, 2013). Figure (2.13) shows the equivalent circuit of electromagnetically gap- coupled capacitive feed strip.

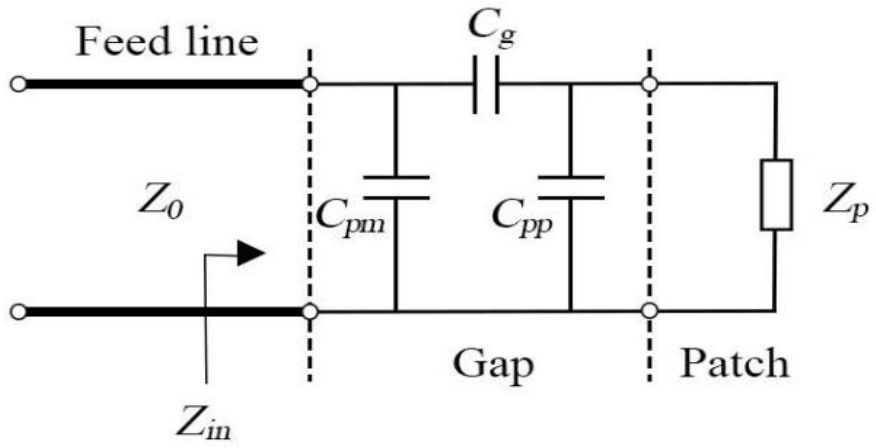

Figure (2.13): Equivalent circuit of a rectangular patch fed by a single gap (Ononchimeg, Bang, & Ahn, 2010) .

3) Aperture-coupling feeds

Non-contacting feeds have been developed for microstrip antennas in recent years. The aperture coupling feeder is one of the non-contacting feeds, its structure as shown in Figure (2.14) consists of two substrates separated by a ground plane. The microstrip feed line lies on the bottom side of

the lower substrate, slotted ground plane is between the two substrates, the energy from the feed line is coupled to the patch through that slot (Balanis C. , 2005) (Pozar D. , 1992). The upper substrate can be made with a lower permittivity to produce broadly wide fringing fields, yielding better radiation. The lower substrate is made with a high value of permittivity for tightly coupled fields that do not produce spurious radiation (Bevelacqua, Antenna-theory.com, 2017). The disadvantage of this method is increased difficulty in fabrication. The patch is shielded from the feeder radiation by the ground plane and minimizes interference of spurious radiation for pattern formation and polarization purity.

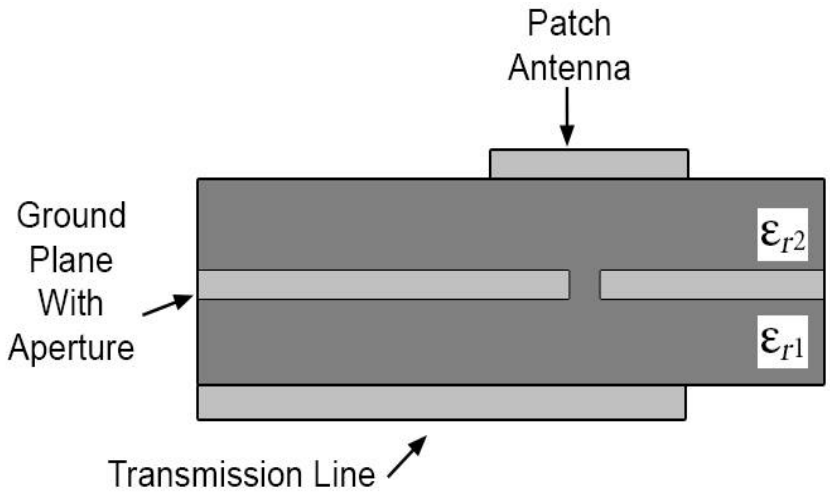

Figure (2.14): Aperture coupled feed (Bevelacqua, Antenna-theory.com, 2017)

4) Proximity coupling feed:

A structure of this antenna is shown in Figure (2.15). It has two substrate layers with an open end microstrip line between the two substrates (the top of the lower substrate) and the patch on the top layer, the two layers can be selected to reduce spurious radiation from the open end of the microstrip and to increase the bandwidth. This type of feeding has the largest bandwidth ~13%, and the improvement of the bandwidth value can be controlled by changing the open stub parameters (Garg, Microstrip antenna design handbook, 2001). The fabrication of a Proximity feed is somewhat more difficult (Balanis C. , 2005).

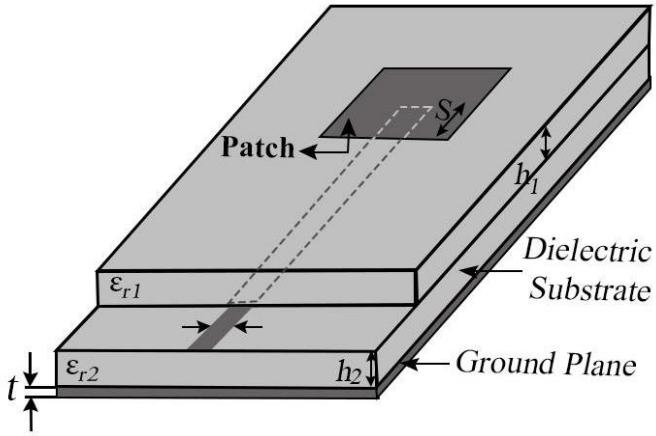

Figure (2.15): Patch antenna fed by proximity coupling *(Grilo & Correra, 2015)* .

2.4.3 Designing Rectangular Microstrip Antenna

Designing a rectangular microstrip antenna, needs to choose the substrate material with thickness *h*, dielectric permittivity "constant" *εr* and the target center "resonant" frequency *fr* in Hz, then determine the antenna dimensions: antenna width *W* and length *L*.

This can be calculated by the following steps (Huang & Boyle, Antennas from Theory to Practice, 2008):

Step 1: For efficient radiator, calculate the width W from the equation (2.14)

$$W = \frac{c}{2 f_r \sqrt{\frac{2}{\varepsilon_r + 1}}} \qquad \textbf{(2.14)}$$

where c is the free space light velocity

step 2: Determine the effective dielectric constant ε_{eff} from equation (2.15) :

$$\varepsilon_{eff} = \frac{\varepsilon_r + 1}{2} + \frac{\varepsilon_r - 1}{2\sqrt{1+12\frac{h}{W}}} \qquad \textbf{(2.15)}$$

step 3: Determine the incremental length ΔL generated by the fringing fields from equation (2.16):

$$\Delta L = 0.412h\frac{(\varepsilon_{eff}+0.3)(\frac{W}{h}+0.264)}{(\varepsilon_{eff}-0.258)(\frac{W}{h}+0.8)} \quad \textbf{(2.16)}$$

step 4: Determine the effective length L_{eff} of the patch by equation (2.17) then determine the actual length L of the patch by equation (2.18):

$$L_{eff} = \frac{c}{2f_r\sqrt{\varepsilon_{eff}}} \quad \textbf{(2.17)}$$

$$L = L_{eff} - 2\Delta L \quad \textbf{(2.18)}$$

After that the antenna can be simulated using any simulation tool such as ADS Agilent or CST, and its parameters can be optimized to obtain optimum characteristics.

Chapter 3
Single element design

Chapter 3

Single Element Design

The design of an efficient printed antenna requires a good understanding of how different design parameters affect the antenna performance. These parameters, for printed antennas, include the selection of substrate with appropriate dielectric constant (ε_r), dielectric loss tangent ($\tan\delta$), substrate thickness (h), antenna shape and feeding technique. This chapter presents the simulation results of a parametric study of these parameters at mm-Wave frequencies (27 - 29 GHz). This study can serve as a design guide for researchers and antenna designers who are willing to design efficient mm-Wave microstrip patch antennas for 5G communications.

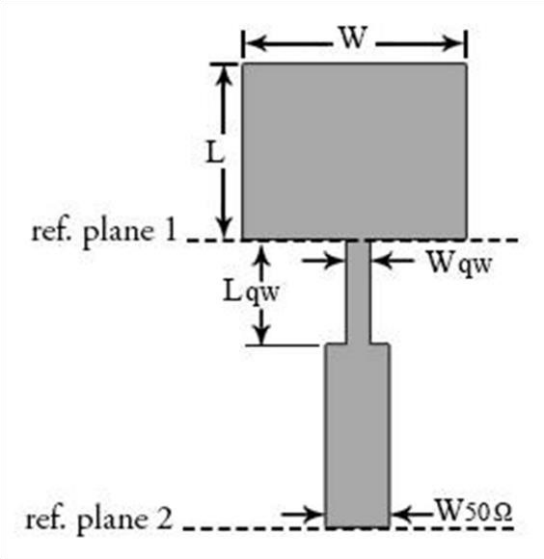

Figure (3.1): edge-fed microstrip patch antenna (top view).

3.1 Antenna Substrate:

The antenna substrate has a direct impact on the antenna size and performance. The main substrate parameters that need to be considered when designing planar antennas are:

- Substrate thickness (h).
- Dielectric constant (ε_r).
- Substrate Loss Tangent ($\tan\delta$).
- Copper cladding thickness (t).

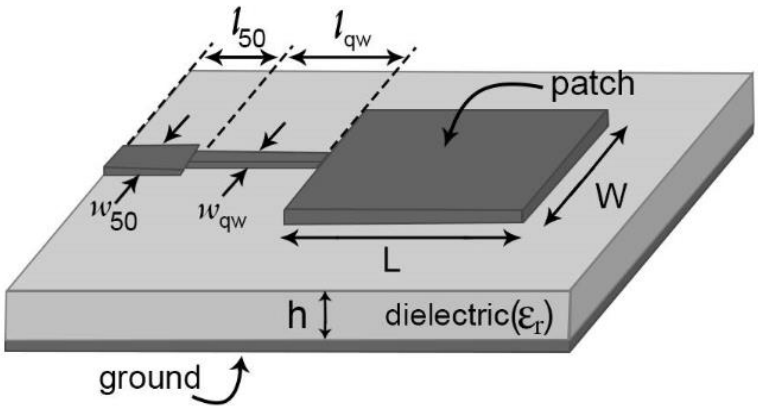

Figure (3.2): 3D geometry for edge-fed microstrip patch antenna

3.1.1 Substrate Thickness:

A low loss Teflon-based RT/duroid 5880 substrate (RT/duroid® 5880 Laminates, 2017) was chosen to perform the study of the substrate thickness impact on antenna performance. This substrate has a dielectric constant ε_r = 2.2 and loss tangent $\tan\delta$ = 0.0009. An edge-fed microstrip patch antenna was used in the study as shown in Figure (3.1) and Figure (3.2). Figure (3.3) presents the simulated real and imaginary parts of the antenna input impedance for five different substrate thicknesses. The simulated input impedance is referenced at ref. plane 1 (see Figure (3.1). The antenna dimensions were slightly adjusted for each substrate thickness so that the antenna resonates at ~28 GHz. It can be seen from Figure (3.3) (a) that as the substrate thickness increases from 0.127 mm to 0.787 mm, the real part of the input impedance increases from ~ 207 Ω to ~ 322 Ω at 28 GHz. This increase in the real part of the antenna impedance can be attributed to an increase in the antenna radiation efficiency or an increase in the antenna losses. The real part of the antenna input impedance can be written as (Stutzman & Thiele, 2013) :

$$R_A = R_r + R_{loss} \qquad \textbf{(3.1)}$$

Where R_A is the total real part of the antenna input impedance, R_{loss} is the part of the antenna input resistance that accounts for different loss mechanisms in the antenna (conductor losses, dielectric losses, surface waves, etc…) while R_r is the radiation resistance which represents the part of the input power to the antenna that is transferred into radiated electromagnetic waves.

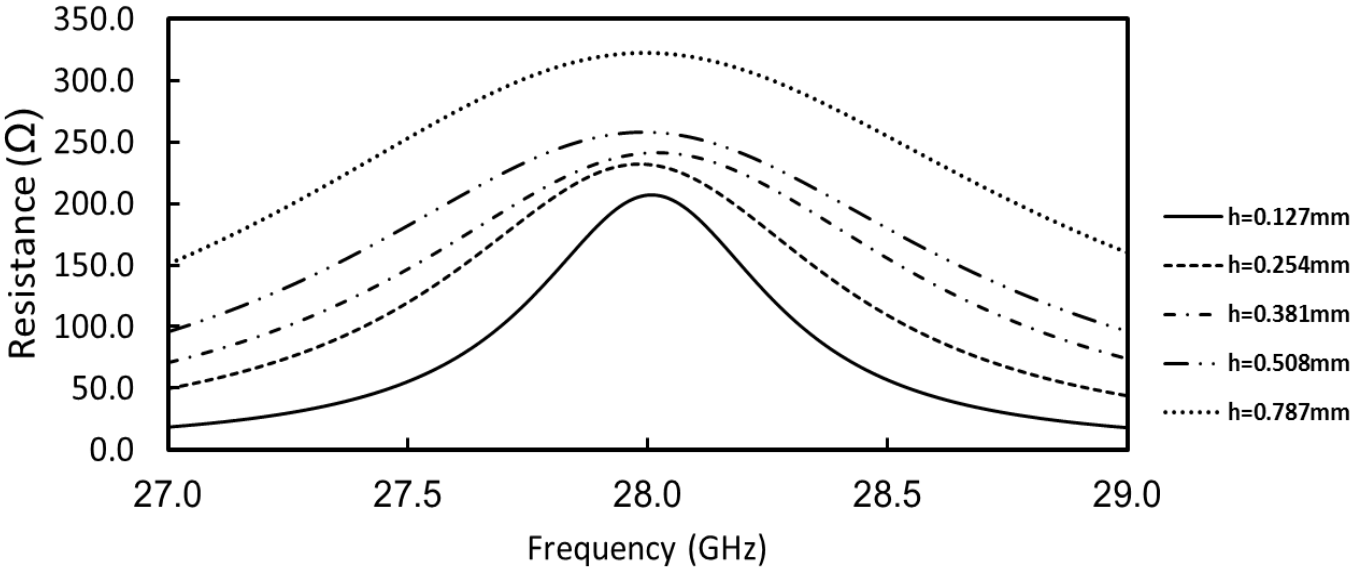

(a)

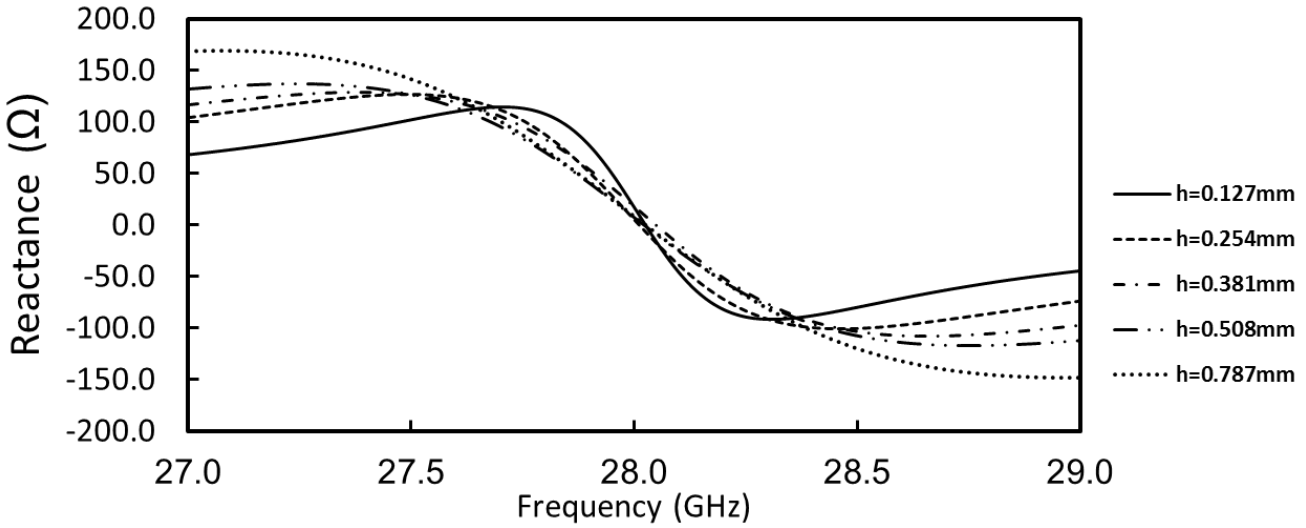

(b)

Figure (3.3): simulated (a) real and (b) imaginary parts of the antenna input impedance for five different substrate thicknesses

The simulated radiation efficiency is presented in Figure (3.4). It can be seen from the figure that the radiation efficiency increases from 81.1% for substrate thickness of 0.127 mm to 92.8% for substrate thickness of 0.381 mm. This increase in radiation efficiency explains the increase in antenna resistance from 207Ω at 0.127mm substrate thickness to 241Ω at 0.381mm substrate thickness. The efficiency then starts to decrease again and reaches an efficiency of 88.2% at substrate thickness of 0.787 mm. The low efficiency at 0.127 mm substrate thickness can be explained by the fact that at such a low thickness, the microstrip patch is very close to the ground plane. The electric field lines are therefore strongly attached to the ground plane.

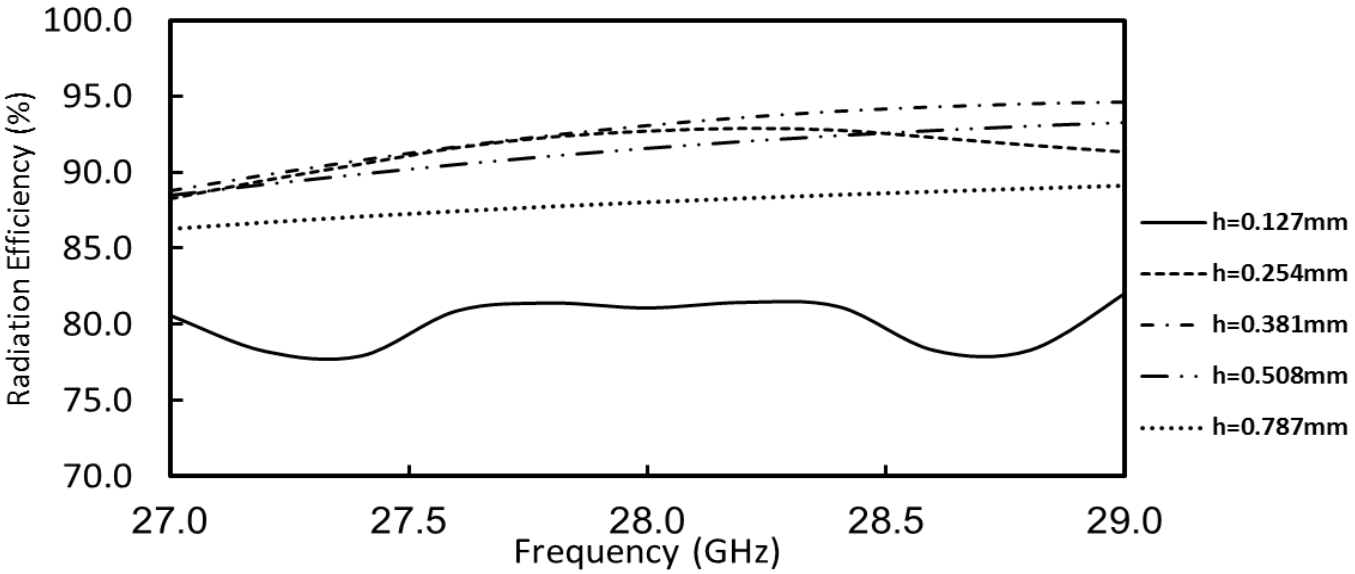

Figure (3.4): Simulated radiation efficiency vs. frequency at different substrate thickness.

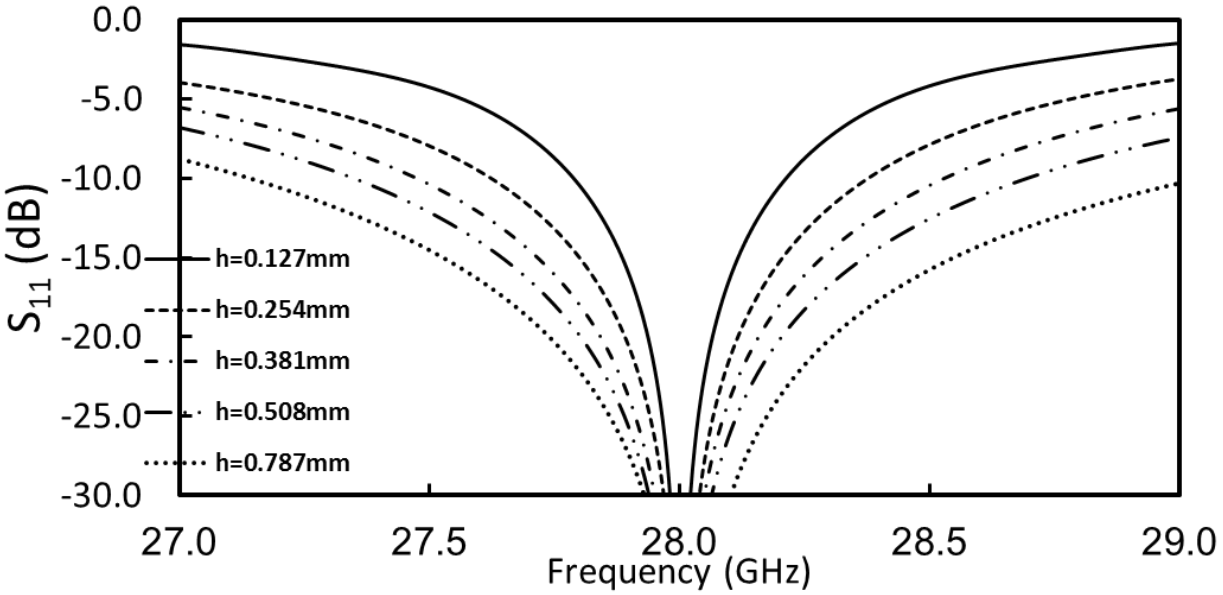

Figure (3.5): Simulated antenna S_{11} vs. frequency at different substrate thickness

(at ref. plane 2).

This means more energy is being stored, and less power is being radiated. As the thickness increases, the capacitance to ground is reduced and more power is being radiated which results in an improved efficiency. As the thickness increases further, more power is coupled to substrate modes and the efficiency decreases again. The coupling to unwanted substrate modes means higher losses and increased value of R_{loss}. This explains the reason behind the continuous increase in the antenna resistance beyond 0.381 mm substrate thickness.

The simulated S_{11} (referenced at ref. plane2) is presented in Figure (3.5). It is clear from the figure that the antenna bandwidth increases as the substrate thickness increases. The bandwidth increase is due to the reduction in the antenna Quality factor (Q) either due to the increased radiation resistance or increased losses in the antenna.

In summary, the antenna substrate thickness is limited on the lower and upper boundaries by different mechanisms. On the lower end, the substrate thickness is limited by the fact that smaller substrate thickness means higher capacitance to ground. This results in reduced fringing fields and lower radiation. It also results in higher Quality factor (Q) and reduced bandwidth. On the upper end, the substrate thickness is limited by two mechanisms. The first one is the excitation of unwanted substrate modes. The higher the antenna substrate thickness, the more power is lost and coupled to the substrate modes which in turn lowers the antenna radiation efficiency. The second mechanism that limits the maximum allowable substrate thickness for microstrip line-fed antennas is the fact that the width of a 50 Ω microstrip line increases as the substrate thickness increases and it can be wider than the width of the microstrip antenna itself.

The simulation results suggest a suitable substrate thickness of ~ 0.381mm ($0.036\lambda_0$ at 28 GHz) for optimum antenna performance which falls within the substrate thicknesses recommended in page 812 in (Balanis C. , 2005) and presented here:

$$0.003\lambda_0 \le h \le 0.05\lambda_0 \qquad \textbf{(3.2)}$$

The simulated antenna impedance matching bandwidth (S_{11} < -10 dB) and radiation efficiency at 28 GHz vs. substrate thickness are summarized below in Table (3.1):

Table (3.1): Simulated antenna parameters at different substrate thicknesses

Substrate thickness (mm)	Impedance matching absolute bandwidth (MHz)	Fractional bandwidth (%)	Antenna radiation Efficiency (%) @ 28 GHz
0.127	423	1.51	81.05
0.254	745	2.7	92.68
0.381	961	2.4	92.83
0.508	1170	4.2	91.21
0.787	1893	6.8	88.22

3.1.2 Dielectric Constant (ε_r):

The Substrate dielectric constant **(** ε_r) affects the antenna performance in a similar way to the substrate thickness. A lower value of **(** ε_r) for the antenna substrate means lower capacitance to ground. This will increase the fringing field at the patch periphery, and thus the radiated power (Garg, Microstrip antenna design handbook, 2001)**.** On the other side, a higher value of **(** ε_r) results in higher capacitance from the patch antenna to the ground plane and therefore more energy storage and less power radiation. There are numerous substrates that can be used for the design of microstrip antennas, and their dielectric constants are usually in the range of $2.2 \leq \varepsilon_r \leq 12$. The ones that are most desirable for good antenna performance are thick substrates whose dielectric constant is in the lower end of the range because they provide better efficiency, larger bandwidth, loosely bound fields for radiation into space, but at the expense of larger element size (Pozar D. , 1992).

Figure (3.6) presents the simulated S_{11} of an edge-fed microstrip patch antenna on two different substrates with two different dielectric constants (ε_r = 2.2 and 4.4). The dielectric losses in the

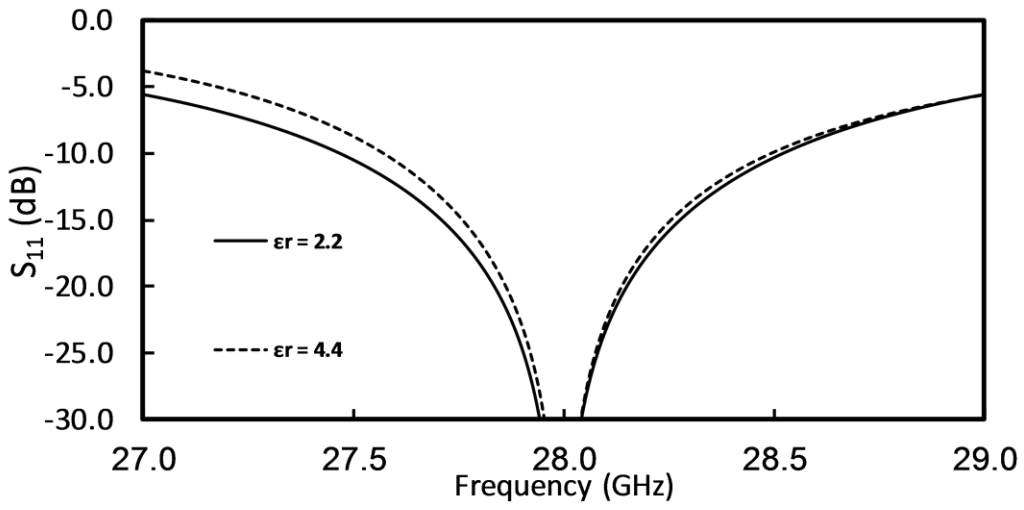

Figure (3.6): simulated S_{11} for two different substrate dielectric constants. Substrate thickness = 0.381 mm.

substrates were assumed to be negligible and the loss tangents of the two substrates were assumed to be 0. A slight improvement in the antenna S_{11} bandwidth can be seen in the ε_r = 2.2 when compared to the ε_r = 4.4 case. This bandwidth improvement is clearly due to the improved antenna radiation (lowered Q). Figure (3.7) presents the simulated radiation efficiency vs. frequency at two different substrate dielectric constants. As expected, the radiation efficiency for the ε_r = 2.2 case is higher than the ε_r = 4.4 case since the fields are less tight to the ground plane in the ε_r = 2.2

case, which means the capacitance to ground is lower. Table (3.2) summarizes the simulation results.

Table (3.2): Simulated antenna parameters at two different Dielectric Constant (ε_r) values, substrate thickness = 0.381 mm, $\tan\delta = 0$

Dielectric constant (ε_r)	Impedance matching absolute bandwidth (MHz)	Fractional bandwidth (%)	Antenna radiation Efficiency (%) @ 28 GHz
2.2	1061	3.8	94.1
4.4	933	3.3	89.6

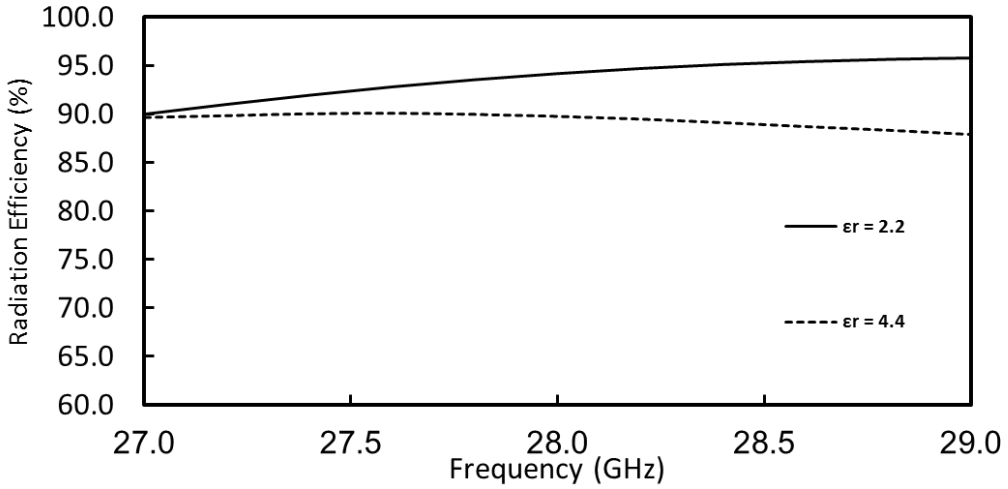

Figure (3.7): simulated radiation efficiency vs. frequency. (substrate thickness =0.381mm)

3.1.3 Substrate Loss Tangent:

Different loss mechanisms affect the antenna performance in different ways. These losses include: conductor losses, dielectric losses and surface wave losses. The dielectric loss tangent represents the losses associated with substrate dielectric material. The loss tangent ($\tan\delta$) of the antenna substrate can be expressed by $\tan\delta = 1/Q_d$,where Q_d is the quality factor associated with dielectric losses (losses in the antenna substrate dielectric material) which is defined as the ratio of stored energy to the power lost in the antenna substrate dielectric constant as shown in equation (3.3) in (Garg, Microstrip antenna design handbook, 2001) pg. 281.

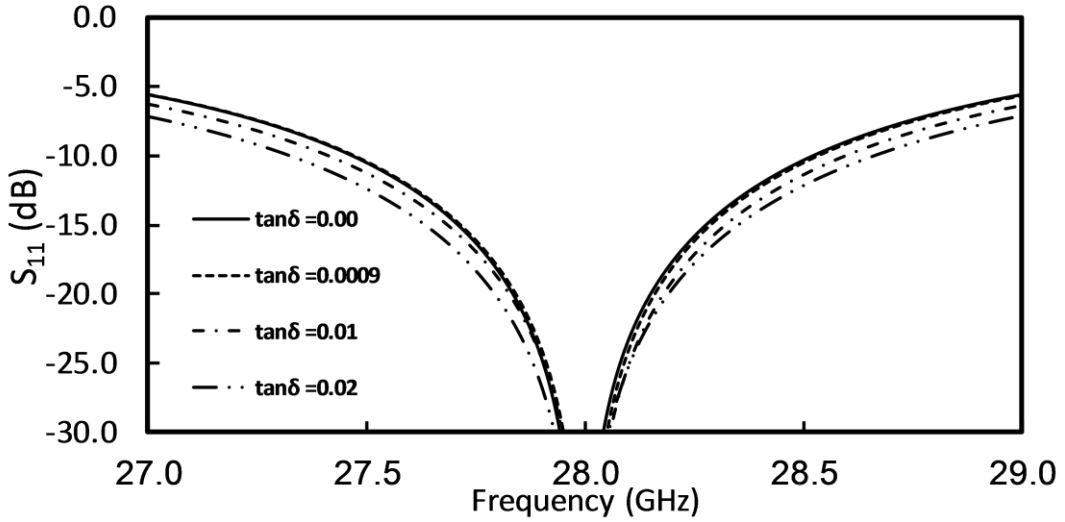

Figure (3.8): simulated antenna S_{11} vs. freq for different substrate loss tangent. h = 0.381mm, ε_r = 2.2

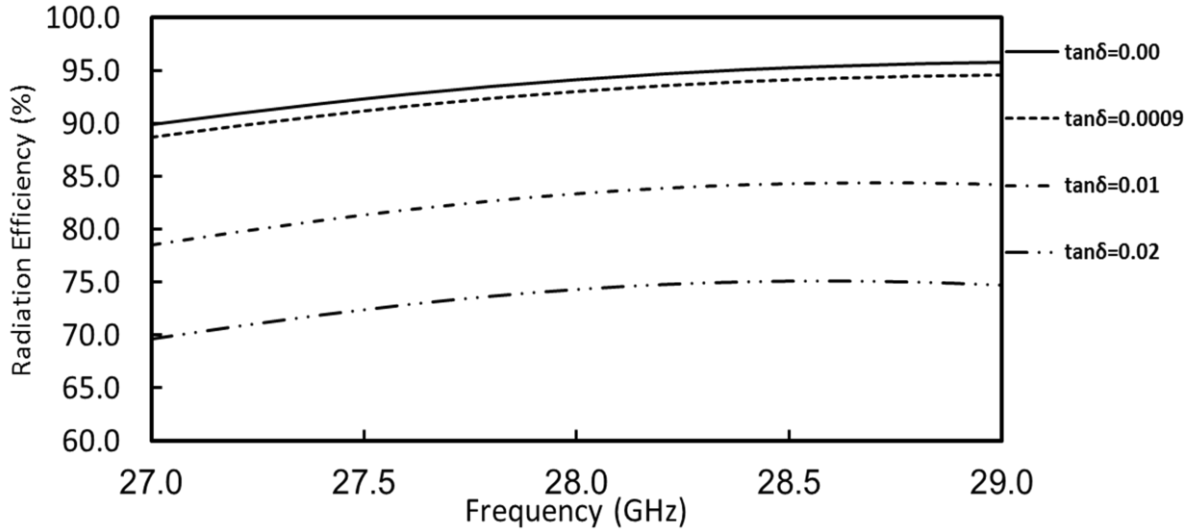

Figure (3.9): simulated radiation efficiency vs. frequency for different substrate loss tangent.

h = 0.381mm, ε_r = 2.2

$$Q = \frac{\omega_r W_T}{P_d} \quad \textbf{(3.3)}$$

Where

P_d : represents the power dissipated in the antenna substrate dielectric material.

ω_r : is the resonant frequency

W_T : is the total energy stored per cycle at the resonant frequency

It can be seen in Figure (3.8) and Figure (3.9) as the antenna loss tangent increases, the antenna quality factor is reduced which results in lower radiation efficiency but it also results in improved antenna matched S_{11} bandwidth.

3.1.4 Copper cladding depth selection:

metallic loss (in neper per meter) increases with frequency. Metallic loss of one microstrip line can be calculated using the equation (3.4) (Advanced millimeter-Wave Technologies, 2009) :

$$\alpha_c = \frac{\pi \mu_0 f}{Z_0 W} \delta_s \quad \textbf{(3.4)}$$

Where:

α_c (dB/unit length): conductor loss in the strip conductor

f : operated frequency

W : the line width

δ_s : the skin depth

where δ_s is the skin depth, Z_0 is the characteristic impedance and W the line width. from this equation we can notice that metallic losses increases by increasing δ_s , so if we want to select one of the standard δ_s values (8µm , 17 µm , 35 µm ,70 µm) from RT/duroid 5880 datasheet , we can choose the lowest value (8µm) in order to achieve lowest ohmic losses .

3.2 Feeding techniques:

In this study, we aim to investigate different feeding techniques specification mentioned in chapter 2 in order to obtain the best one, where the feeding technique selection depends on the application of the antenna. The best technique here is according to antenna efficiency, broad bandwidth, easy to use in antenna array and easy fabrication.

Substrate thickness and loss tangent values for all designs are 0.381mm and 0.0009 respectively.

The input impedance of the antenna should match with the source impedance which for all RF sources and microwave sources is 50 Ω (Chakravarthy, 2016)

A) **Inset Feed**:

When the patch is fed by a source, the edge nearer to the source has infinite impedance because of zero current at the open circuit edge and at the middle of the patch, the impedance is zero because of maximum current at the patch center. Hence, a 50 Ω input impedance feed point is selected by moving closer to the patch center by length equal to R as presented in Figure (2.10).

According to equation (2.11), $R_{in}(x=0)$ at ref. plane 1 =241 Ω, $R_{in}(x=x_0)$ = 50 Ω, after calculating this equation x_0 is founded to equal 0.1 mm, hence the antenna is matched with 50 Ω feeding line.

B) **Fed with a Quarter-Wavelength Transmission Line:**
The structure of this feeding technique is presented in Figure (2.11) and the formula for matching the antenna with 50 Ω in equation (2.13), so we can calculate the impedance easily using this formula

$$Z_1 = \sqrt{241*50} = 110\,\Omega$$

Using lineCalc tool in ADS agilent 2014, the transformer width can be calculated to be 0.27 mm, with length equal to 2 mm, hence the antenna is matched with 50 Ω feeding line.

C) Gap Coupled Feeds:

This feeding technique is similar to inset feed technique, but the feeder does not touch the antenna, the feeding here is indirect by a very small gap, the equivalent circuit for this type is illustrated in Figure (2.13), as a capacitive load in order to increase the antenna bandwidth to be larger than 1 GHz. There is no formula to calculate the gap width around the 50Ω feeder line as shown in Figure (3.10). A parametric study was made to obtain the best results as in Table (3.1).

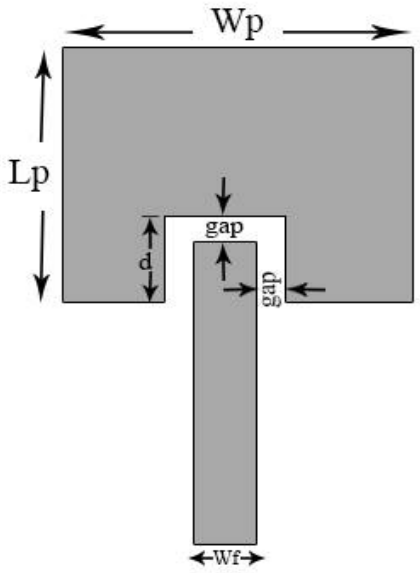

Figure (3.10): single element geometry with gap coupled feeding

Table (3.3): parametric study for gap width and inset length on antenna parameters

gap = 0.1 mm	Impedance matching absolute bandwidth (MHz)	Fractional bandwidth (%)	Antenna radiation Efficiency (%) @ 28 GHz
d =0.9	1040	3.7	90
d =1.0	1110	3.96	91
d =1.2	1234	4.4	91.8
d =1.35	1245	4.44	91.8
d =1.45	1226	4.38	91.9
d =1.5	1216	4.34	91.8

After that another value of gap = 0.03 was selected with changing the value of d, the results was as follow :

gap = 0.03 mm	Impedance matching absolute bandwidth (MHz)	Fractional bandwidth (%)	Antenna radiation Efficiency (%) @ 28 GHz
d=0 (flat patch)	1285	4.58	91.3
d =0.07	1376	4.91	91.8
d =0.08	1396	4.98	91.8
d =0.09	1410	5.03	91.7
d =0.1	1416	5.06	91.6
d =0.2	1471	5.25	91.2
d =0.3	1485	5.3	90.1
d =0.4	1427	5.1	89.3

Here the d value is fixed at 1.13 mm and different values of gap were used

d=1.13mm	Impedance matching absolute bandwidth (MHz)	Fractional bandwidth (%)	Antenna radiation Efficiency (%) @ 28 GHz
gap = 0.05	1267	4.5	88.8
gap = 0.09	1274	4.55	91.9
gap = 0.1	1215	4.34	91.6
gap = 0.12	1089	3.89	90.6
gap = 0.14	860	3.07	88.3
gap = 0.19	440	1.57	83

From the previous results, one design is selected to be the optimum design according to bandwidth and radiation efficiency value with constrain of gap value to be equal or greater than 0.1 mm in order to be easy for fabrication. It can be observed that at gap=0.1 mm and d=1.35mm the bandwidth is equal to 1245 and the radiation efficiency is equal to 91.8 % which the optimum values in this design.

D) **Aperture-coupling feeds**

It is Non-contacting feeder, an electromagnetic coupling between feeder and microstrip patch occurs cross the ground aperture as shown in the antenna structure in Figure (2.14). The dimensions in Figure (3.11) were useful in selecting the optimum values of width and length of the slot in the ground and the thickness of the lower substrate.

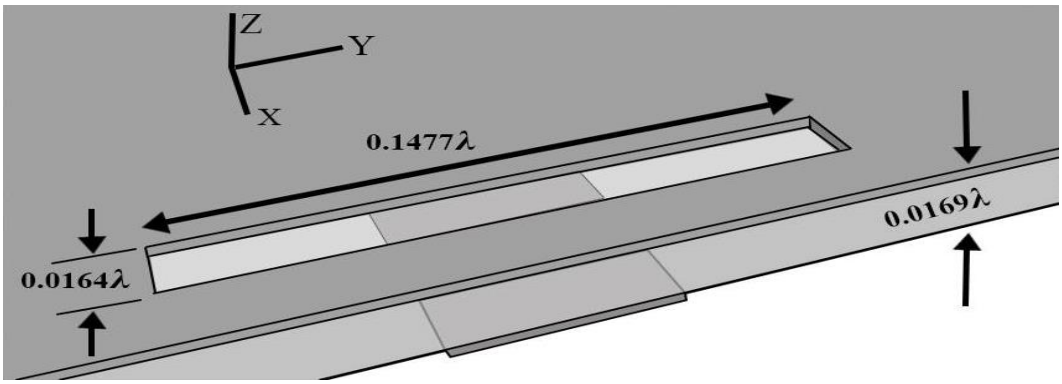

Figure (3.11): feed substrate and slot dimensions (Civerolo, 2010)

The upper substrate thickness is 0.381 mm with dielectric constant ε_r =2.2, where the lower substrate has the same thickness and ε_r =4.5 with a high value of permittivity for tightly coupled fields that do not produce spurious radiation, the slot dimensions were 2*0.4 mm^2.

E) Proximity coupling feed:

This type of feeding is also Non-contacting feeder, the feeder is between two substrates as shown in Figure (2.15), with the same layers used in the previous design, the open stub parameters controls the impedance matching to be 50Ω.

The results of simulation for different feeding techniques illustrated in Figure (3.12) and Figure (3.13).

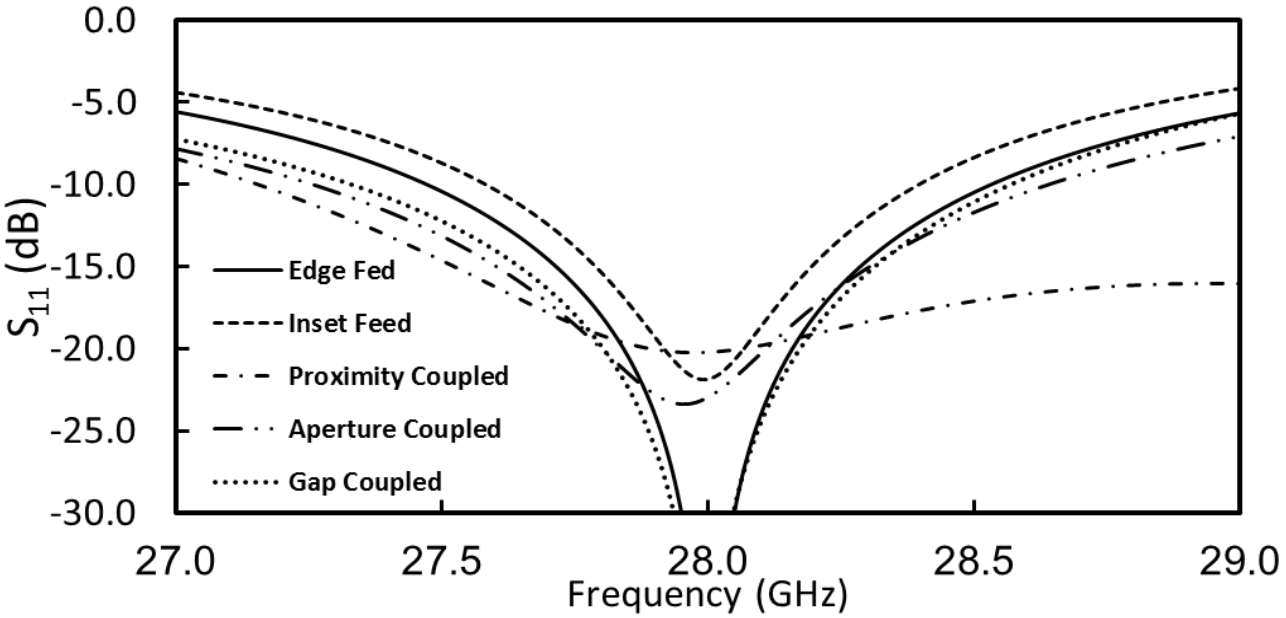

Figure (3.12): simulated antenna S_{11} vs. freq for different feeding techniques tangent. h = 0.381mm, ε_r = 2.2

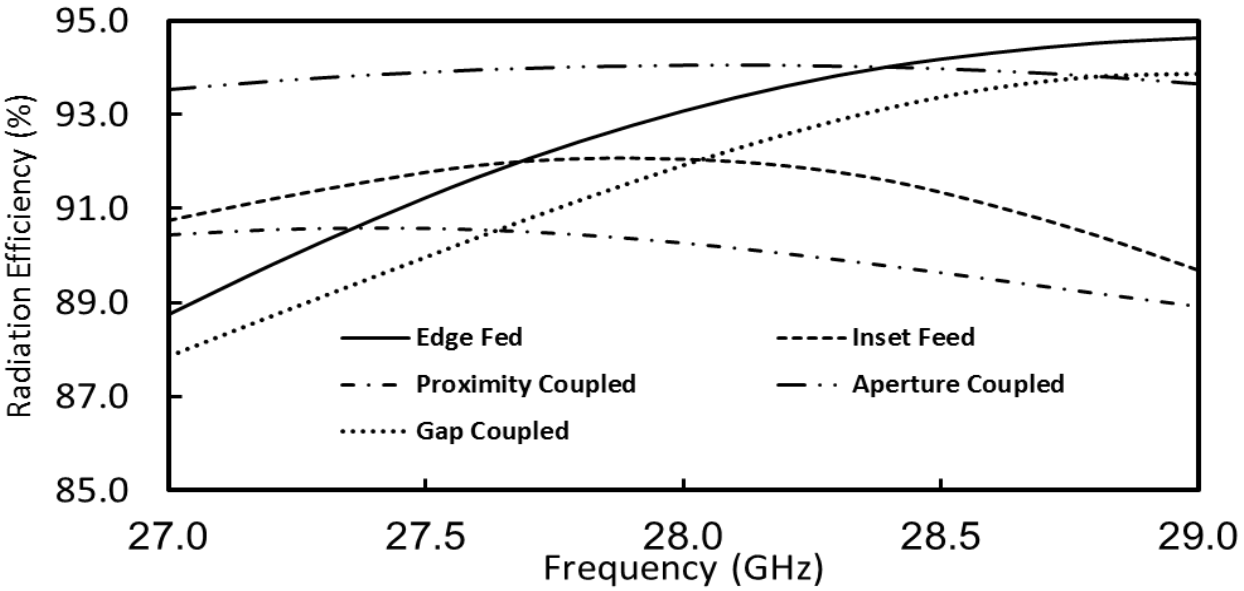

Figure (3.13): simulated radiation efficiency freq for different feeding techniques tangent. h = 0.381mm, ε_r = 2.2

And the results can be summarized in Table (3.4):

Table (3.4): Simulated antenna parameters at different feeding techniques

Feeding technique	Impedance matching absolute bandwidth (MHz)	Fractional bandwidth (%)	Antenna radiation Efficiency (%) @ 28 GHz
Edge feed	1061	3.79	93
Inset feed	816	2.91	91.6
Gap coupled feed	1225	4.38	91.8
Aperture-coupling feeds	1385	4.95	91.7
Proximity coupling feed	3474	12.4	83.5

From the previous results, the selected design is a gap coupled feed, it has wide band width=1.225 GHz, high efficiency =91.8%, easy to fabricate and easy to use in antenna arrays.

3.3 Single element patch antenna design

Based on the simulations results of the above parametric study, a 0.381 mm thickness low loss Teflon based RT/duroid 5880 (RT/duroid® 5880 Laminates, 2017) substrate was chosen for the antenna design. The initial antenna width was obtained from equation (2.14), the width value was equal to 4.232 mm.

The effective dielectric constant of the microstrip antenna was then calculated from equation (2.15). The extension of the length ΔL was calculated using equation (2.16)**Error! Reference source not found.** The actual length of the patch is determined by solving equation (2.18) for L to be equal to 3.375 mm.

A full electromagnetic simulation of the antenna was then performed using computer simulation technology (CST) 3D simulator.

The antenna input impedance is simulated at ref. plane 1 and is shown in Figure (3.14). The antenna dimensions were slightly modified to get a resonance at 28 GHz. The simulated input impedance = ~ 241 at 28 GHz. A quarter wave 111 Ω microstrip line was used to match the antenna impedance to 50 ohms. The simulated S_{11} of the antenna at ref plane 2 is presented in Figure (3.15). A good simulated radiation efficiency as illustrated in Figure (3.16). 2D and 3D radiation patterns are presented in Figure (3.17), Figure (3.18) and Figure (3.19). This was the initial design, after the feeding technique was modified to be gap-coupled feeder, as mentioned previously. The simulation results are also summarized in Table (3.5):

Table (3.5): Simulated antenna parameters for gap-coupled feeding technique

Substrate thickness (mm)	Impedance matching bandwidth (S_{11} < -10 dB) MHz	Fractional bandwidth (%)	Antenna radiation Efficiency (%) @ 28 GHz
0.381	1225	4.38	91.8

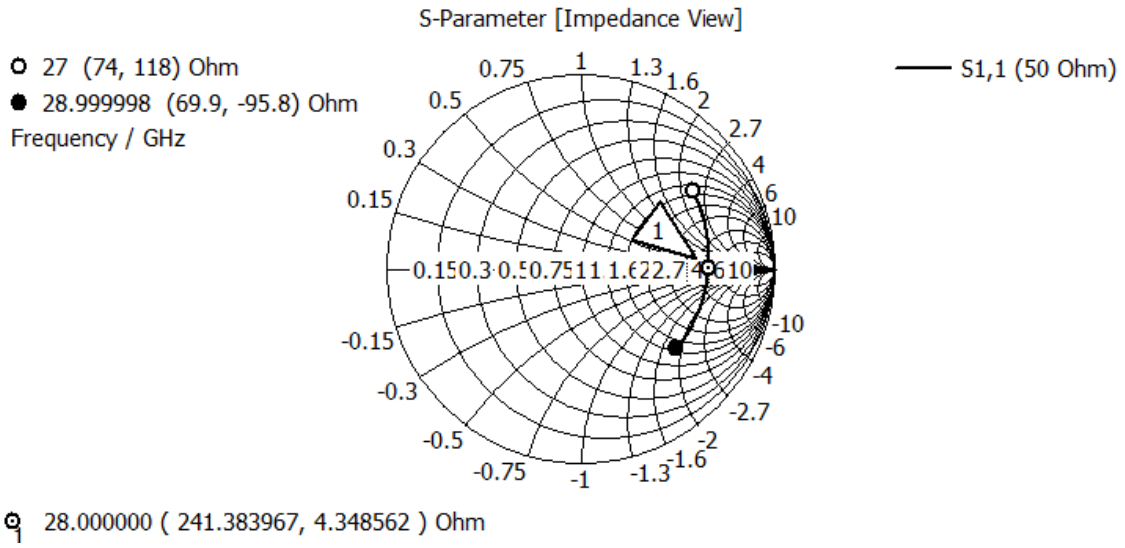

Figure (3.14): simulated input impedance at ref. plane 1

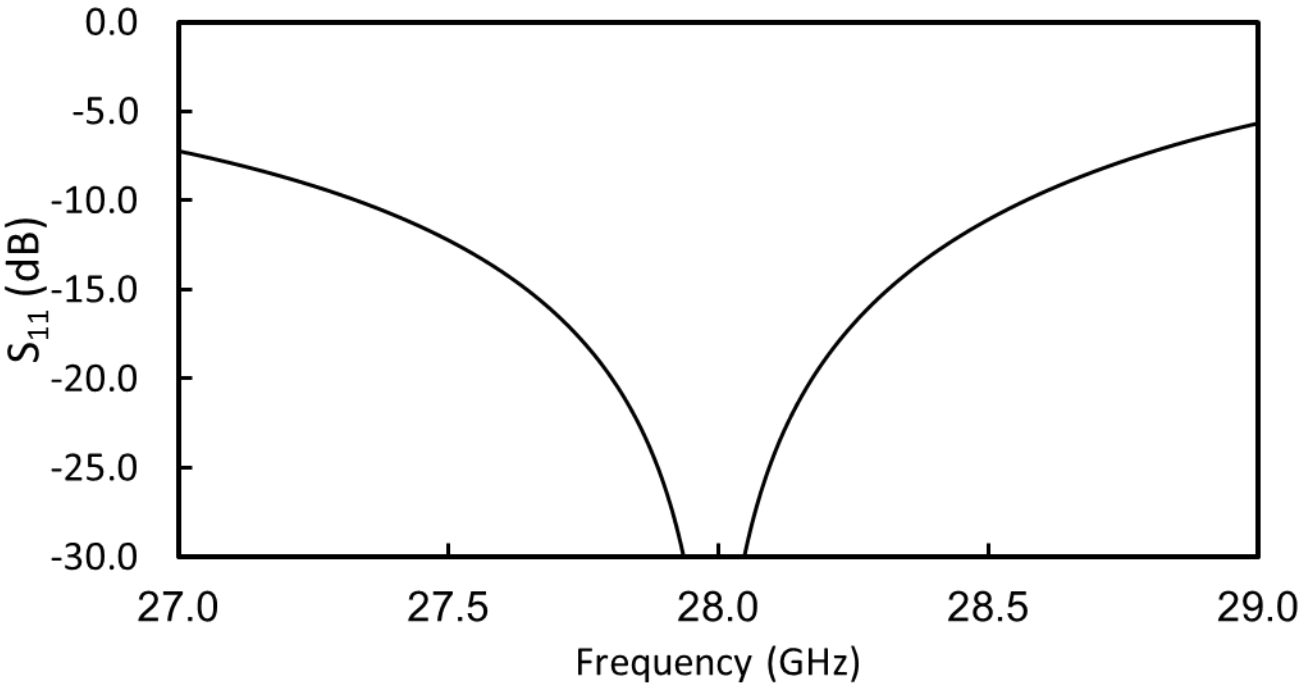

Figure (3.15): Simulated antenna S_{11} vs. frequency for single elements at ref. plane 2

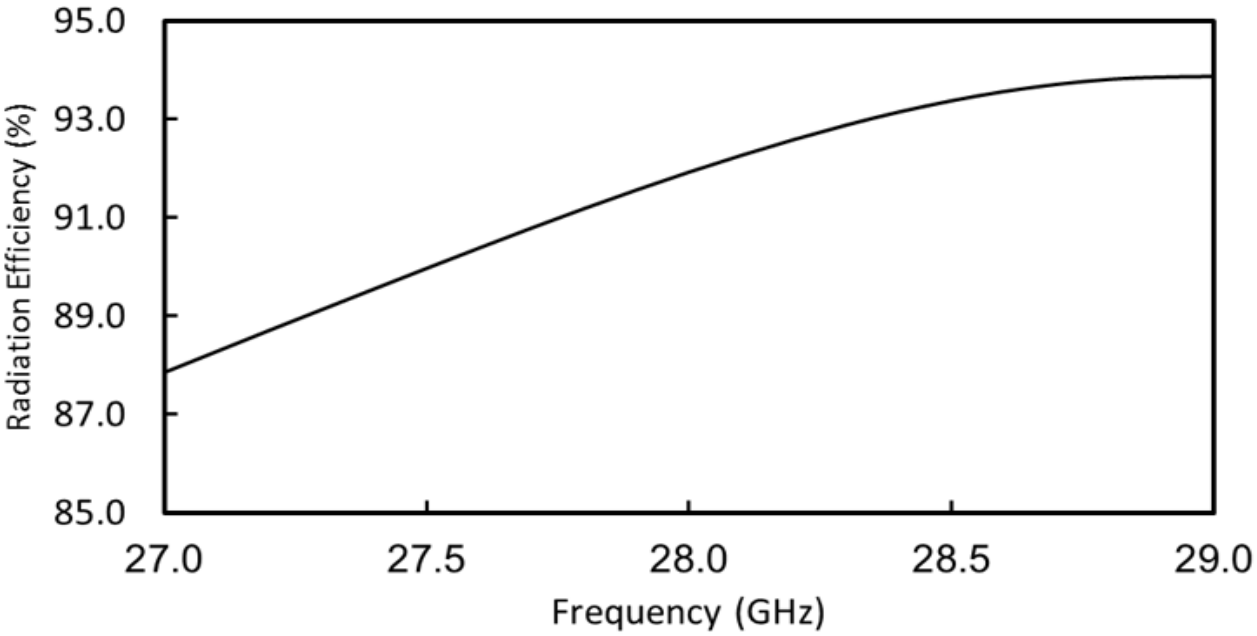

Figure (3.16): Simulated radiation efficiency vs. frequency for single elements

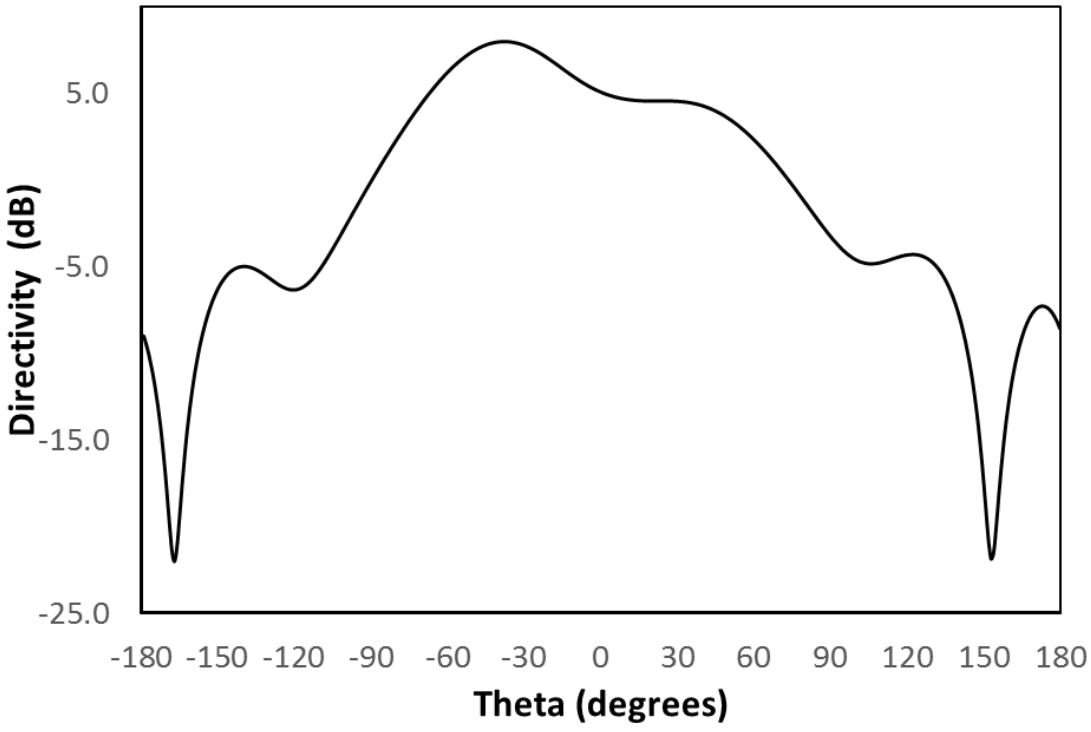

Figure (3.17): Simulated radiation pattern at 28 GHz, E-plane

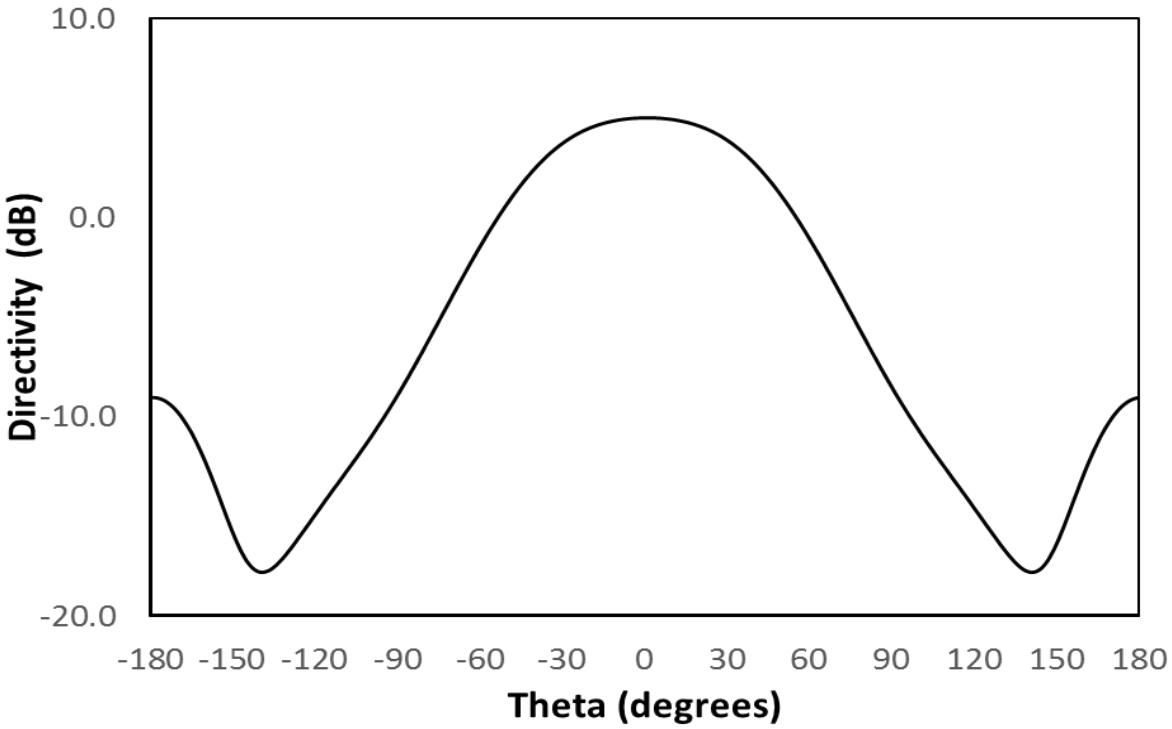

Figure (3.18): Simulated radiation pattern at 28 GHz, H-plane

The tilt in the radiation pattern in figure (3.19)may be because the asymmetry in antenna feeding.

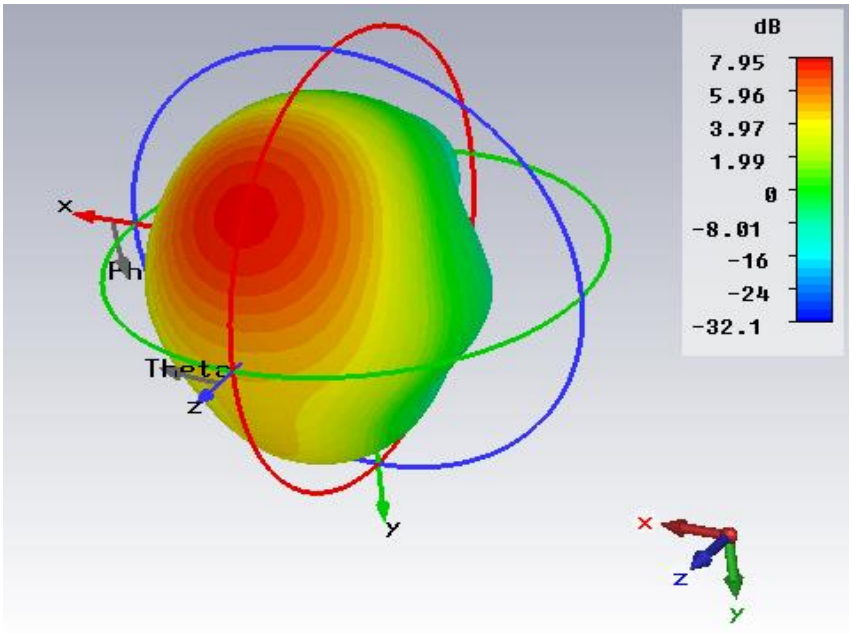

Figure (3.19): 3D radiation pattern (realized gain)

Chapter 4
Antenna Array Design

Chapter 4

Antenna Array Design

4. 1 Introduction

For 5G applications, the antenna needs to have high gain of > 12 dB and directive beam that can be steered in a certain direction (Jamaluddin, Kamarudin, & Khalily, Rectangular Dielectric Resonator Antenna Array for 28 GHz Applications, 2016). It might be hard to achieve such high gain using single small antenna. However, several small antennas can be grouped together in an antenna array to achieve such high gain directive pattern that can be electronically scanned in a certain direction. Shaping the array radiation pattern can be achieved by appropriate element to element spacing and appropriate excitation adjustment of the magnitude and phase of the currents feeding individual elements of the array. The array elements can be spatially distributed to form a linear, planar or volume array. Linear arrays have narrow radiation beam in the plane containing the array axis while have a wide beam in the orthogonal plane. This characteristic of linear array pattern is useful in the case of 5G handset applications as it only requires 1-D scanning to cover large area.

This chapter starts with a brief analysis of antenna array factor. A study of mutual coupling between adjacent elements and feeding techniques are then presented. Finally, the simulation results of several linear and planar antenna arrays are presented.

The main parameters that affect the overall performance of an antenna array are (Balanis C. A., 2008) :

1. Distance between adjacent elements.
2. Geometry (e.g., linear, circular, or planar arrangement of the radiating elements).
3. Amplitude current excitation of each individual element.
4. Phase excitation of each individual element.
5. Radiation pattern of each individual element.

4. 2 The Array Factor for Linear Arrays

The basic configuration for elements in an array is the linear array which is illustrated in Figure (4.1): , where the variable resistance symbol indicates attenuators and the other symbol indicates phase shifters. The pattern characteristics of an array can be explained for operation as a transmitter or receiver, since antennas usually satisfy the conditions of reciprocity. The output of each element can be adjusted in amplitude and phase by the attenuators and phase shifters. Amplitude and phase control provide custom shaping of the radiation pattern and for scanning of the pattern in space. (Stutzman & Thiele, 2013)

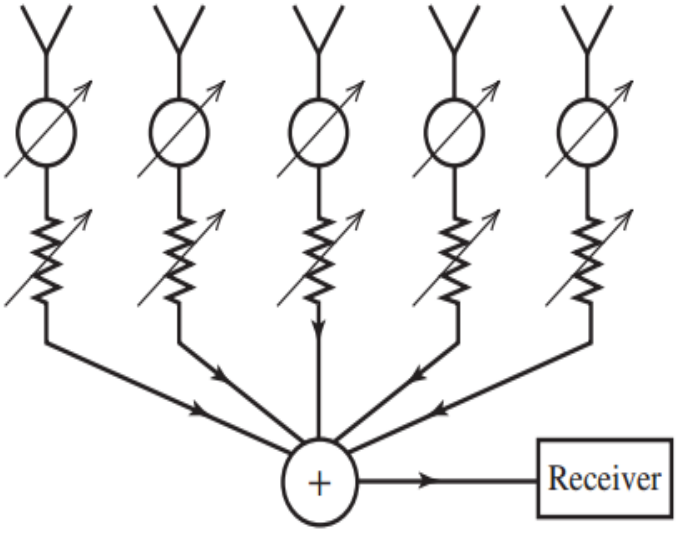

Figure (4.1): A typical linear array (Stutzman & Thiele, 2013).

By replacing each element by an isotropic radiator, the array factor corresponding to the linear array of Figure (4.1) can be found, while maintaining the element locations and excitations, the array is receiving a plane wave arriving at an angle θ from the line of the elements as shown in Figure (4.2), and all the planes with equal phase. Each element is excited with phase ξ_n, due to the spatial phase delay effect of the incoming plane wave. The amplitudes of excitation are constant, taken to be unity, because a plane wave has uniform amplitude, as shown in Figure (4.2). The resulting excitations of $1e^{j\xi_0}$, $1e^{j\xi_1}$ for each element, then The array factor for this receiving array as in Figure (4.2), is then the sum of the isotropic radiator receiving antenna responses $\{1e^{j\xi_0}, 1e^{j\xi_1}, \ldots\}$ weighted by the amplitude and phase shift appeared by complex currents $\{ I_0 , I_1, \ldots\}$ introduced in the transmission path connected to each element. The array factor of the array is thus (Stutzman & Thiele, 2013) :

$$AF = I_0 e^{j\xi_0} + I_1 e^{j\xi_1} + I_2 e^{j\xi_2} + ... \qquad \textbf{(4.1)}$$

where ξ_0, ξ_1 , … are the phases of an incoming plane wave at the element locations.

The formula (4.1) is general for any geometry. Now we consider linear arrays with elements equally spaced along the z-axis as illustrated in Figure (4.3). The phase of the arriving plane wave is set to zero at the origin for suitability, thus ξ_0 = 0. The received waves arriving at Element 1 lag the received waves arriving at the origin by a distance of *dcosθ*. The corresponding phase of waves at Element 1 relative to the origin is $\xi_1 = \beta d \cos\theta$, the spatial phase delay. Using this result in equation (4.1) gives (Stutzman & Thiele, 2013)

$$AF = I_0 + I_1 e^{j\beta d\cos\theta} + I_2 e^{j\beta_2 d\cos\theta} + ... = \sum I_n e^{j\beta_n d\cos\theta} \qquad \textbf{(4.2)}$$

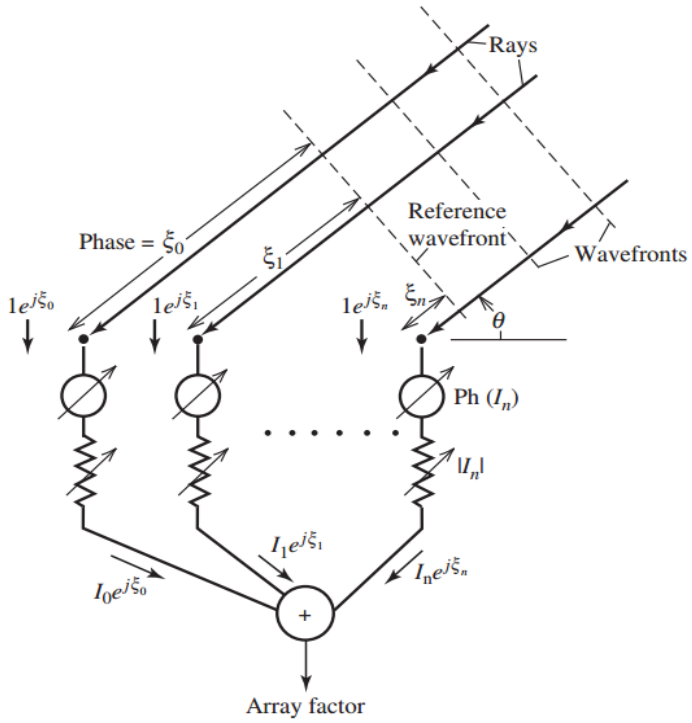

Figure (4.2): Equivalent configuration of the array in Figure (4.1) for determining the array factor (Stutzman & Thiele, 2013).

Now the array considered to be transmitting. If the current has a linear phase headway (i.e., relative phase between adjacent elements is the same), the phase can be separated explicitly as

$$I_n = A_n e^{jn\alpha} \tag{4.3}$$

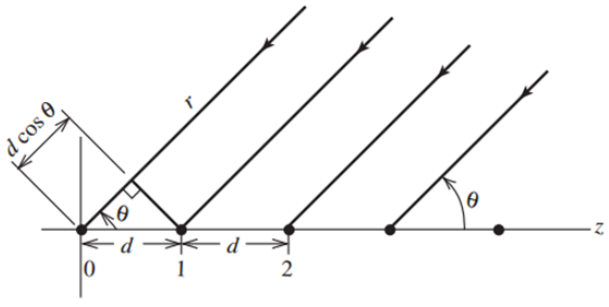

Figure (4.3): Equally spaced linear array of isotropic point sources (Stutzman & Thiele, 2013).

where the $n+1th$ element leads the nth element in phase by α . Then (4.3) become (Stutzman & Thiele, 2013)

$$AF = \sum_{n=0}^{N-1} A_n e^{jn(\beta d \cos\theta + \alpha)} \quad \textbf{(4.4)}$$

Define

$$\psi = \beta d \cos\theta + \alpha \quad \textbf{(4.5)}$$

Then

$$AF = \sum_{n=0}^{N-1} A_n e^{jn\psi} \quad \textbf{(4.6)}$$

Generally, the far-field pattern of an array is given by the multiplication pattern of the single element and the array factor, as in Figure (4.4) (Balanis C. A., 2008) :

$$Total\ Pattern\ =\ Element\ Factor\ \times\ Array\ Factor \quad \textbf{(4.7)}$$

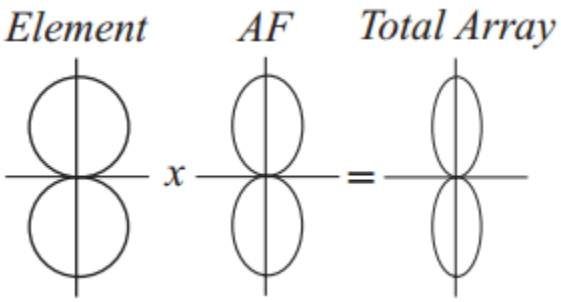

Figure (4.4): Array radiation pattern (Huang & Boyle, Antennas from Theory to Practice, 2008)

4. 3 Antenna Array feeding Configuration

The proper configuration selection depends on many factors, such as bandwidth, the required antenna gain, insertion loss, beam angle, grating/sidelobe level, power-handling capability, and polarization.

4.3.1 Parallel Feed

The essential configuration of a one-dimensional parallel feed consists of a branching network of two-way power dividers as shown in Figure (4.5). A corporate feed is the most widely used parallel feed configuration, the major advantages of parallel feed are, the power is equally split at each junction, the beam position is independent of the frequency provided that the distances from the input port to each radiating element are identical, finally the feed is broadband (Garg, Bhartia, Bahl, & Ittipiboon, Microstrip antenna design handbook, 2001), so the bandwidth of a parallel-fed microstrip array is limited by two factors: the bandwidth of the patch element and the impedance

matching circuit of the power dividing transmission lines, such as the quarter-wave transformer. A series-fed array can achieve a bandwidth on the order of 1% or less, while a parallel-fed array can achieve a bandwidth of 15% or more, depending on the design (Balanis C. A., 2008) . the beam direction can be controlled by incorporating suitable phasors or line extensions. The disadvantages of parallel feed is that it requires long transmission lines between the input port and radiating elements, this causes large value of insertion loss, thereby reducing the overall efficiency of the array (Garg, Bhartia, Bahl, & Ittipiboon, Microstrip antenna design handbook, 2001).

In the design, all the radiating elements are usually identically matched to the feed lines by suitable method such as quarter-wave transformer. In order to obtain a symmetrical corporate feed network, the number of the radiating elements is 2^n where n is an integer (Garg, Bhartia, Bahl, & Ittipiboon, Microstrip antenna design handbook, 2001).

The parallel-fed array is the relative ease with which both amplitude and phase for each element can be designed independently, while in a series-fed array one element's change will generally impact all other elements (Balanis C. A., 2008).

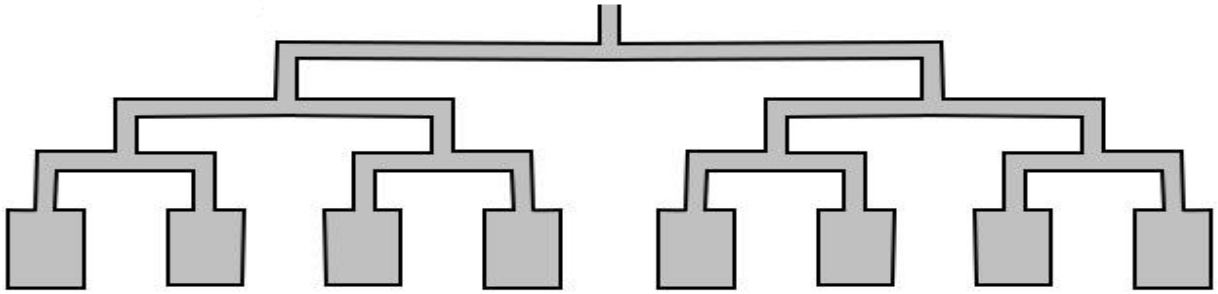

Figure (4.5): Configurations of parallel feed microstrip array (Balanis C. A., 2008).

4.3.2 Series Feed

Multiple elements are arranged linearly and fed serially by a single transmission line consisting a series feed configuration as shown in Figure (4.6), series feed has the lowest insertion loss but generally has the least polarization control and the narrowest bandwidth. It has the narrowest bandwidth because the line goes through the patches, and thus the phase between adjacent elements is not only a function of line length but also of the patches' input impedances.

Since the patches are amplitude weighted with different input impedances, the phases will be different for different elements and will change more drastically as frequency changes due to the narrowband characteristic of the patches (Balanis C. A., 2008)

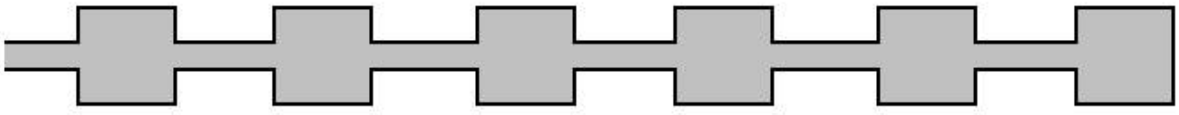

Figure (4.6): Configurations of series feed microstrip array

4.3.3 Capacitively coupled fingers

There is another shape of linear array, patches are fed by means of capacitive coupling along the resonant edges as illustrated in Figure (4.7). The gap between each element and the main transmission line is adjusted to give good coupling. The main disadvantage of this feed type is narrow bandwidth and potential of grating lobes problem due to λ_g element spacing (Huang & Boyle, Antennas from Theory to Practice, 2008) .

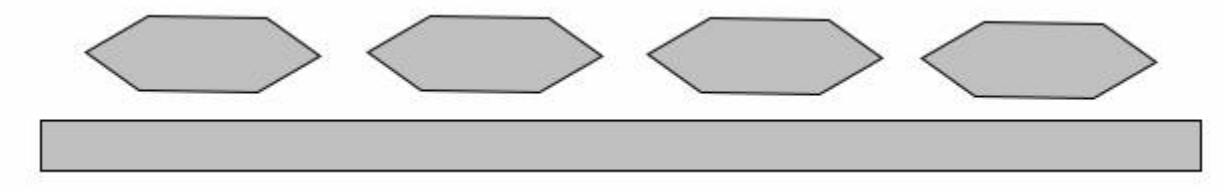

Figure (4.7): Configuration of microstrip Lozenge array

4. 4 Mutual coupling

4.4.1 introduction

When designing linear antenna array for 5G we aim to have the largest scanning angle without having grating lobes. This can be achieved by keeping inter-element spacing less than half-wavelength according to (4.8) (Stutzman & Thiele, 2013).

$$d < \frac{\lambda}{1+|\cos\theta_0|} \qquad \textbf{(4.8)}$$

Where:

λ : wavelength in free space

d: inter-element space, from center to center

θ_0 : is the main beam pointing angle with respect to the line of the array corresponding to the largest scan angle off broadside.

The goal here is to obtain 180^o scanning angle, this can be achieved when θ_0=0, and $\cos 0 = 1$ which results in $d < 0.5\lambda$. This small distance between adjacent elements can cause an increase in the undesired mutual coupling. This affects the current distribution and hence the input impedance as well as the radiation pattern of individual elements. The most significant effects are on the antenna input impedance, which is a very important parameter for a single antenna as well as for an antenna array (Huang & Boyle, Antennas from Theory to Practice, 2008). A smaller spacing is more desirable for a compact array because it helps to suppress the grating lobes when scanning. On the other hand, a smaller spacing result in higher coupling (Tang, et al., 2016).

4.4.2 Mutual coupling concept

Mutual coupling inside antenna array is usually caused by two reasons: the first is signal leakage via conducting currents on the metallic background or surface wave along substrates; the 2nd is radio leakage received from space between antenna elements (Pan, Tang, & Qi, 2017). Two patches are coupled through all present media, i.e., substrate and air, when they are placed close to each other. The coupling through substrate layer happens through surface waves, and the coupling through the air medium is the direct patch-to-patch near field coupling (Ghosh1, Ghosal, Mitra, & Chaudhuri, 2016). To explain the effect of mutual coupling on array performance, an equivalent lumped-element circuit model for electrically coupled RF/microwave resonators is given (HONG & LANCASTER, 2001) in Figure (4.8), where L and C are the self-inductance and self-capacitance, so that $(LC)^{-1/2}$ equals the angular resonant frequency of uncoupled resonators, and C_m represents the mutual capacitance. Now, if we look into reference planes T1–T1' and T2–T2', we can see a two-port network that may be described by the following set of equations (HONG & LANCASTER, 2001):

$$I_1 = j\omega C V_1 - j\omega C_m V_2 \qquad \textbf{(4.9)}$$

$$I_2 = j\omega C V_2 - j\omega C_m V_1 \qquad \textbf{(4.10)}$$

The conclusion from equations (4.9) and (4.10), if the mutual coupling occurred between two adjacent elements, then each element represents a current source for the other one, this will affect the antenna array mainly in the following ways (Hui) :

1. change the array radiation pattern

2. change the matching characteristic of the antenna elements (change the input impedances)

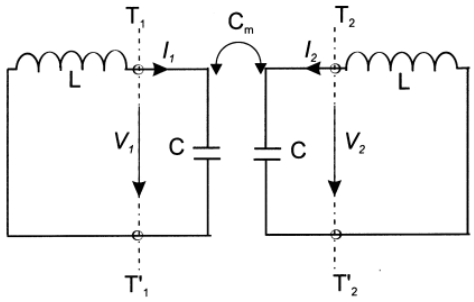

Figure (4.8): Synchronously tuned coupled resonator circuit with electric coupling. (Pozar D. M., Microwave Engineering, 2012).

4.4.3 Reduction of Mutual Coupling

Owing to the recent move toward millimeter wave bands and the massive improvement in manufacturing technologies, the demand of size reduction in modern communication industry has become a hot topic. However, the undesirable mutual coupling (MC) effects arise. It is detrimental to antenna operations through changing the array radiation pattern, and the matching impedance of the radiating elements. Moreover, in phased antenna arrays, strong electromagnetic (EM) interactions between radiating elements yields scan blindness and efficiency degradation (Al-Hasan, Denidni, & Sebak, 2014).

Different methods have been used to enhance the isolation between antenna array elements, electromagnetic band gap (EBG) in the substrate as in (Yu & Zhang, 2003) , using waveguide metamaterials as in (Yang, Liu, Zhu, & Cui, 2012) and resonators, such I-shaped resonator as in (K. & Parui, 2013).

In this study, the effect of defected ground structure (DGS) in reducing the mutual coupling between adjacent elements is investigated. A modified ground plane structure that can enhance the performance of the closely packed radiating elements is proposed and studied. DGS can be defined as an etched lattice shape in the ground plane of planar circuits such as microstrip lines or microstrip antennas as shown in Figure (4.9) (a). It has been used mostly for size reduction of microwave amplifiers, suppression of the higher order harmonics in antennas, cross polarization reduction in microstrip antennas and mutual coupling reduction in antenna arrays (Arya, Patnaik, & Kartikeyan, 2011).

DGS is able to provide a wide band-stop characteristic in some frequency bands with only one or small number of unit cells. Due to their excellent pass and rejection frequency band characteristics and easy to design and fabricate, DGS circuits are widely used in various active and passive microwave and millimeter-wave devices such as filters, dividers, couplers, amplifiers, resonators and antennas. This defect disturbs the shield current distribution in the ground plane and changes characteristics of a transmission line such as line capacitance and inductance (Salehi, Motevasselian, Tavakoli, & Heidari, 2006).

The DGS is considered as an equivalent circuit consisting of capacitance and inductance as given in Figure (4.9) (b). The equivalent inductive part increases due to the defect and produces equivalently the high effective dielectric constant, that is, slow wave property, the slotted gap plays a very important role to find the resonance behavior of the DGS by varying in the inductance (L) and capacitance(C). (Arya, Patnaik, & Kartikeyan, 2011).

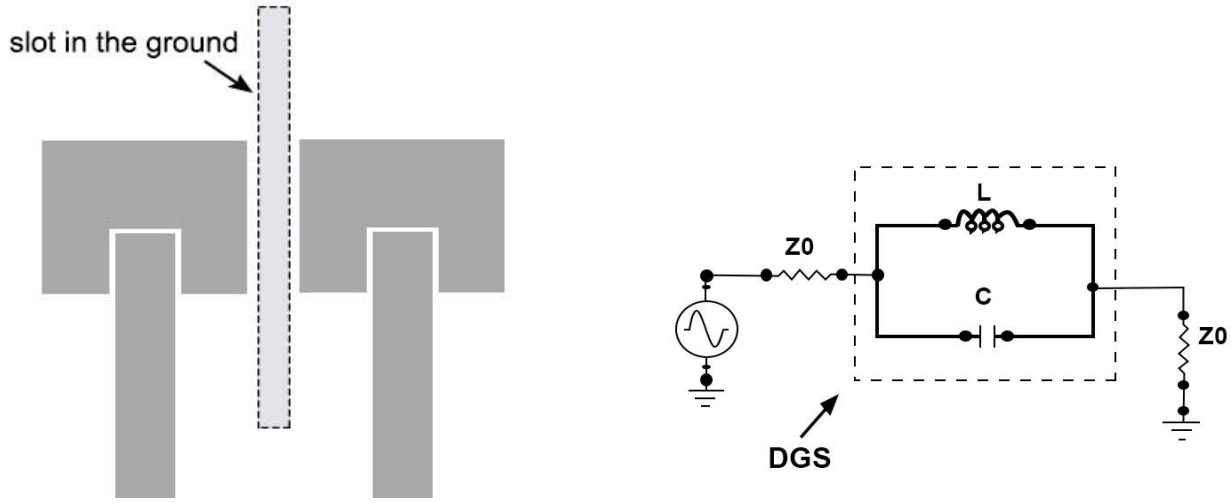

(a) (b)

Figure (4.9): (a) two adjacent antennas with DGS between them (b) L-C equivalent of DGS

4. 5 Design and results

The space influence between two adjacent elements was studied firstly without using any mutual reduction method. Different values of inter-element space from center to center were used, where the antenna length equal 3.19 mm and its width equal 4.232 mm, the gap around the feeder equal 0.1 mm and the width of the feeder is 1.187 mm (50Ω transmission line width at 28 GHz).

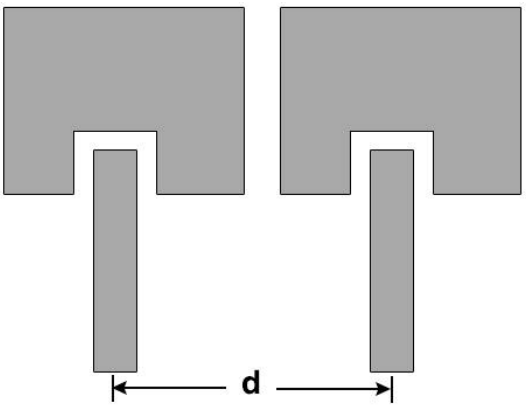

Figure (4.10): two adjacent antennas for mutual coupling study

Table (4.1): inter-element space impact on mutual coupling

Physical spacing (d) in (mm)	Space between adjacent elements	S_{21}
4.819	0.45λ	-9.5
5.355	0.5λ	-12.5
6.42	0.6λ	-17
7.497	0.7λ	-21
8.032	0.75λ	-23
5.568	0.8λ	-24.7
9.639	0.9λ	-28.3
10.71	λ	-31.2

It can be noted from Table (4.1) that as space increases the mutual coupling decreases, and it is acceptable at values lower than -20 dB, this value satisfies when space equal 0.7 λ, but this space doesn't satisfy the condition in equation (4.8) to obtain the largest scanning angle without appearance of grating lobes, which requires a space $\leq 0.5\ \lambda$. As mentioned in section 4.4.3, using Defected Ground Structure is a good choice to reduce mutual coupling between adjacent elements. In Figure (4.10) the mutual coupling between two antennas separated 5.355 mm (0.5λ) from each other and with rectangular slot in the ground between them was simulated. The dimensions of this rectangular slot were optimized in order to obtain the best isolation value. The simulation results show that a mutual coupling (S_{21}) of less than -20 dB along the -10 dB S_{11} matching bandwidth of the antenna was achieved for a slot dimensions of (8.3*0.8) mm^2, where the slot dimensions are obtained after optimized a parametric study. The simulation results before and after placing DGS are shown in Figure (4.11), Figure (4.12), Figure (4.13) and can be summarized in Table (4.2):

Table (4.2): comparison between simulated results with and without DGS

Performance Parameter	Without DGS	With DGS
S_{21} at 28GHz	-12.12	-24.5
Bandwidth (MHz)	1285	1426
Radiation efficiency (%)	88	91.1

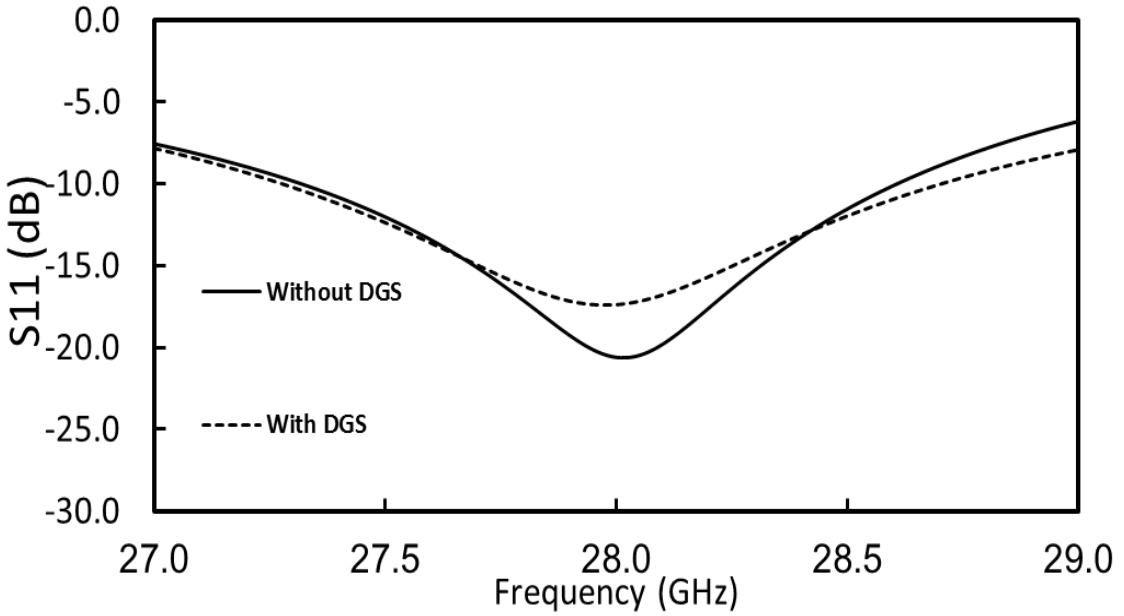

Figure (4.11): Simulated antenna S_{11} vs. frequency between two adjacent elements with and without DGS, slot dimensions of (8.3*0.8) mm^2

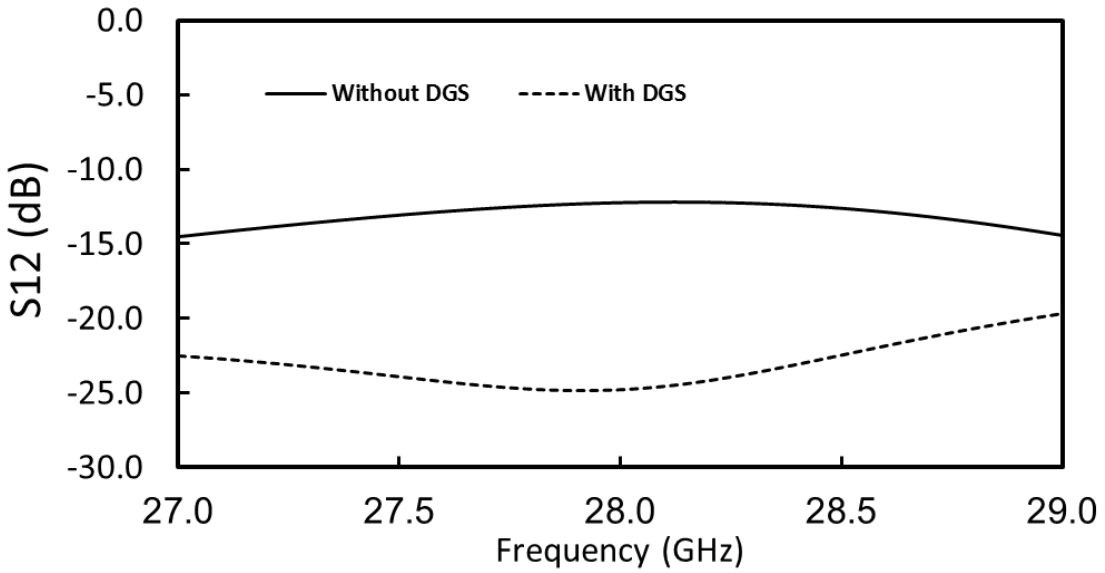

Figure (4.12): Simulated antenna S_{21} vs. frequency between two adjacent elements with and without DGS, slot dimensions of (8.3*0.8) mm^2

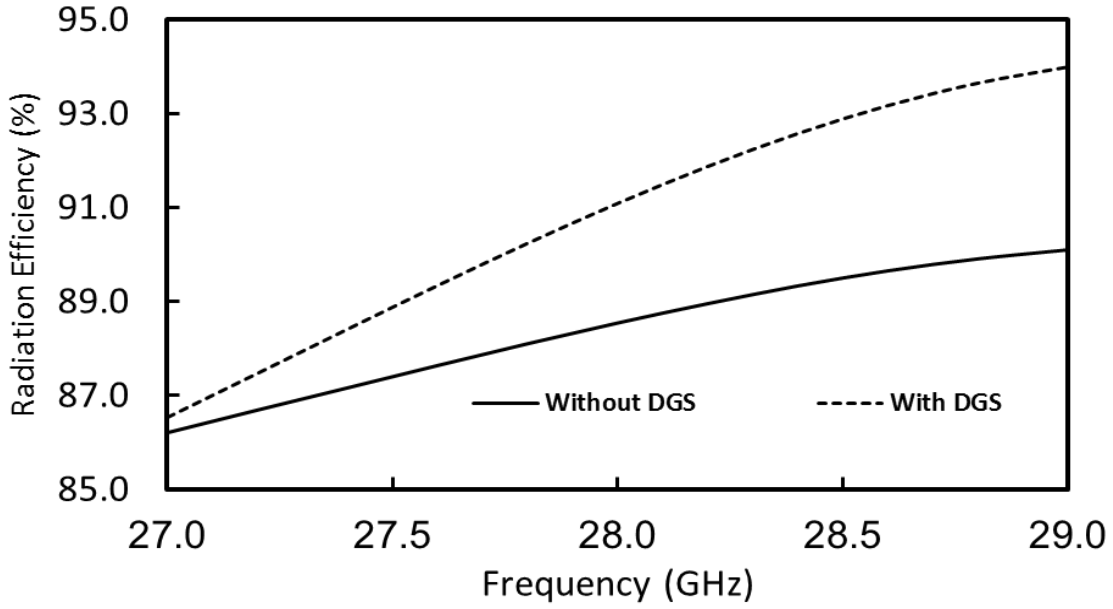

Figure (4.13): simulated radiation efficiency for two adjacent elements with and without DGS, slot dimensions of (8.3*0.8) mm^2

4.5.1 Two Elements Linear Antenna Array:

In this section, 2x1 linear antenna array is presented, after studying how to treat the mutual coupling between array elements using DGS, the array configuration is presented in Figure (4.14). Figure (4.15) presents the simulated S_{11}. The array has an S_{11} <-10 dB bandwidth greater than 2GHz. The simulated gain of the array is presented in Figure (4.16). The 2-element array has a max gain of 9.01 dB at 28 GHz. Figure (4.17) presents 3D radiation patterns of the array. The array has a half power beamwidth (HPBW) of 45.2 degree and 96.4 degree in the E and H planes respectively.

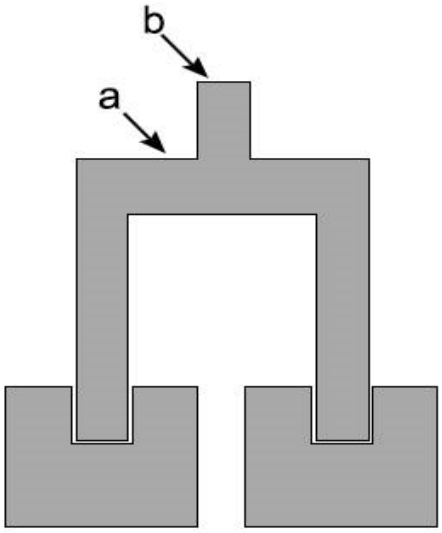

Figure (4.14): 2x1 linear antenna array

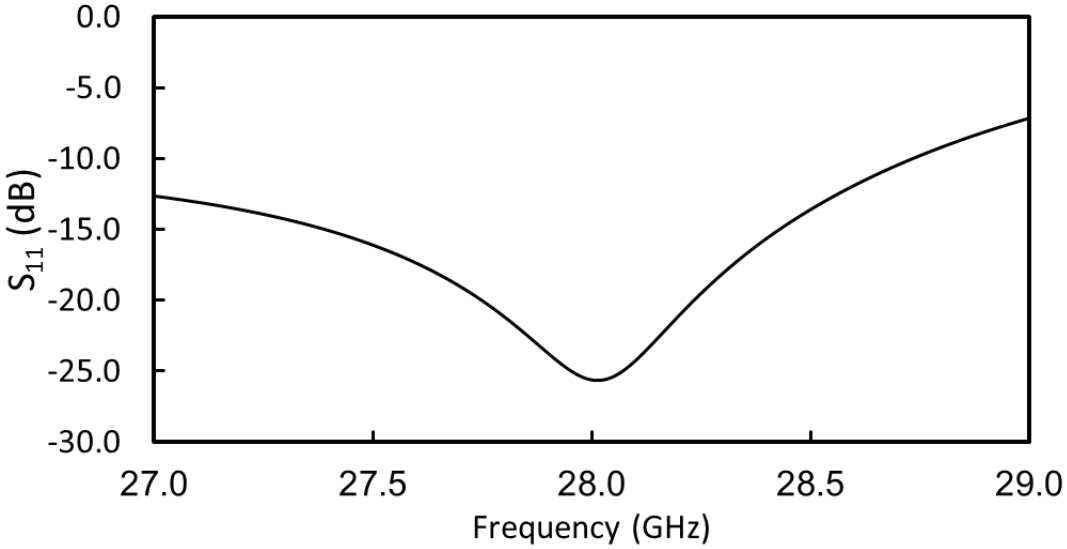

Figure (4.15): Simulated antenna S_{11} vs. frequency for 2x1 linear antenna array

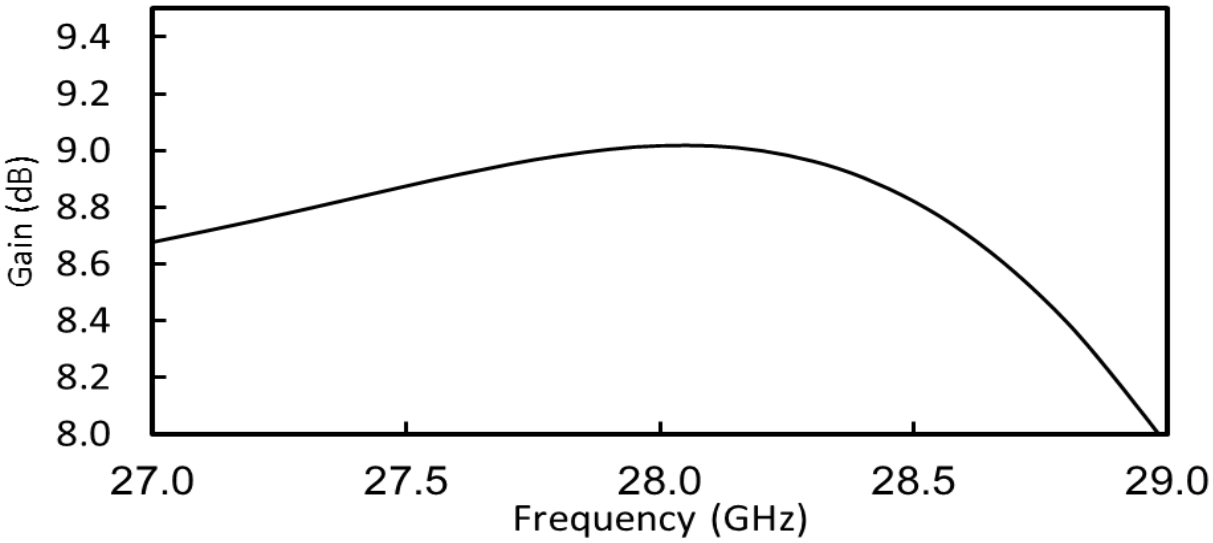

Figure (4.16): Simulated gain vs. frequency for 2x1 linear antenna array

The power is equally split at each junction, so the impedance matching for this array is by using a junction power divider, each antenna feeder has 50Ω, at point (a) the total impedance is 25Ω, it needed to match with 50Ω as at point (b) using quarter wave transformer.

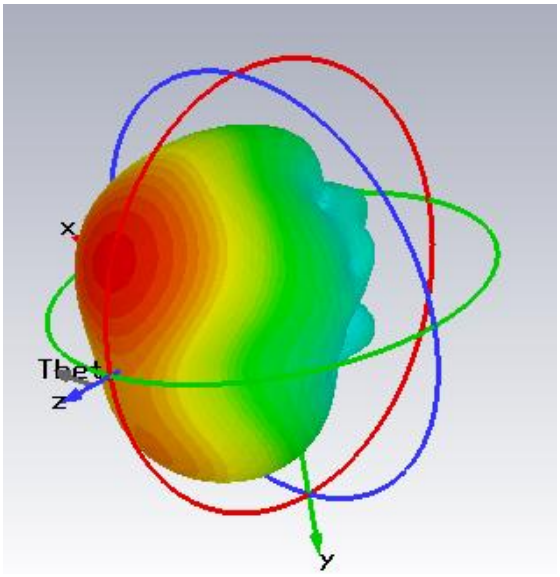

Figure (4.17): 3D radiation pattern for 2x1 linear antenna array pattern (realized gain)

4.5.2 Four Element Linear Antenna Array:

Based on the results of the previous 2x1 array, a new design for 4x1 linear array is presented in Figure (4.18). The simulated S_{11} of the array is presented in Figure (4.19). The array has an S_{11} <- 10 dB bandwidth of 1.38 GHz. Figure (4.20) presents the simulated gain of the array. The 4-

element array has a max gain of 12.02 dB at 28.5 GHz. Figure (4.21) presents the radiation patterns of the array. The array has a half power beamwidth (HPBW) of 23.8 degree and 44.7 degree in the E and H planes respectively. The impedance matching was made by quarter-wavelength transformer, where line a is 50Ω, line b is 70.71Ω and line c is 100 Ω and the feeder line is 50Ω.

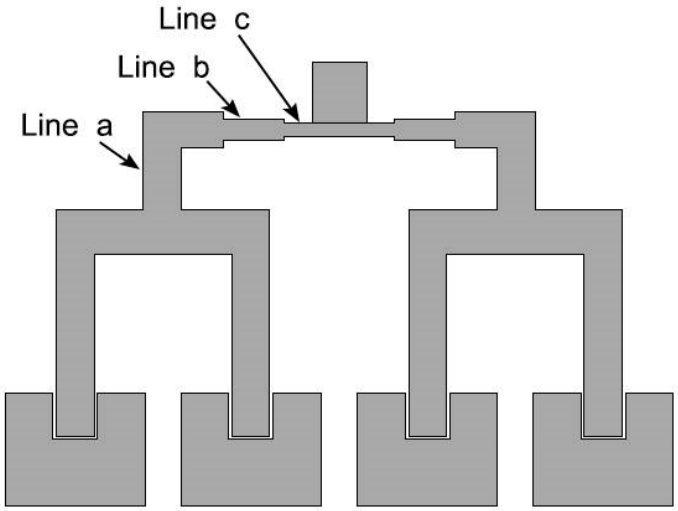

Figure (4.18): 4x1 linear antenna array

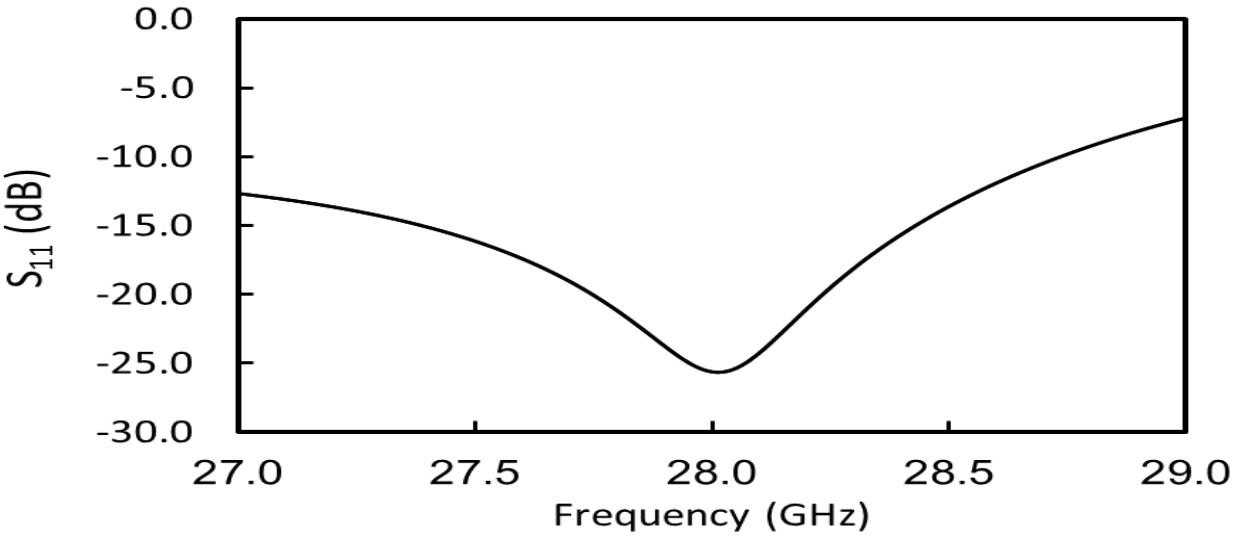

Figure (4.19): Simulated antenna S_{11} vs. frequency for 4x1 linear antenna array

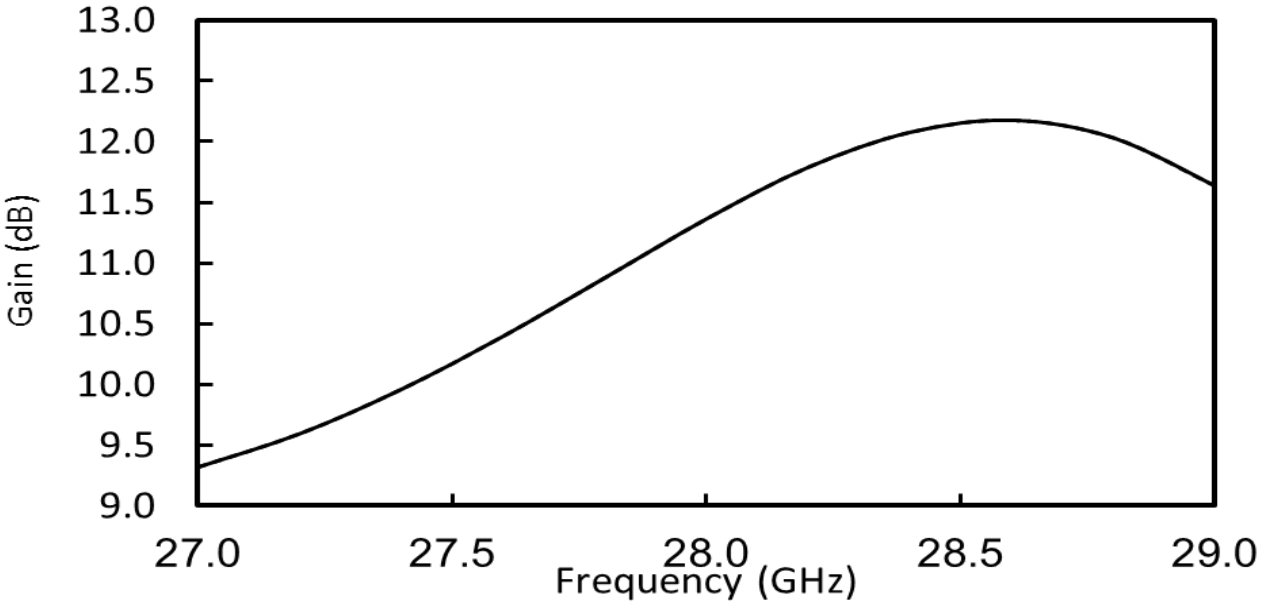

Figure (4.20): Simulated gain vs. frequency for 4x1 linear antenna array

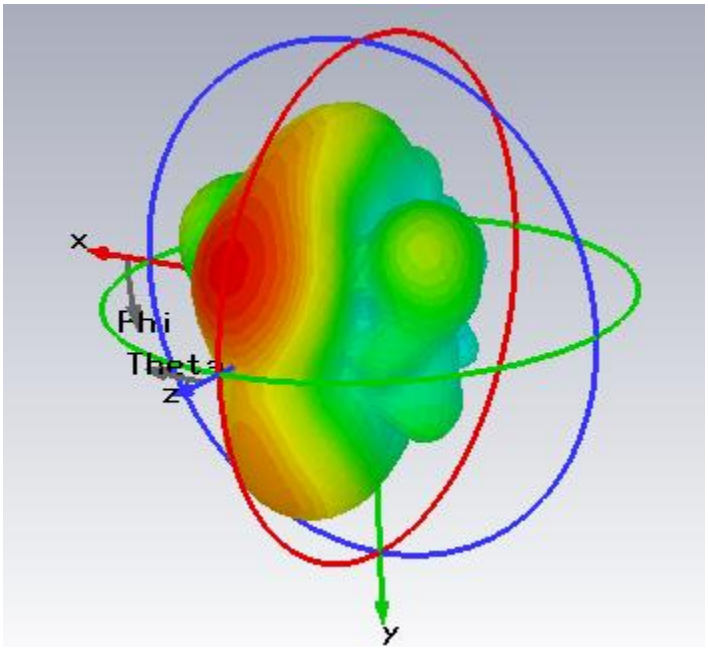

Figure (4.21): 3D radiation pattern for 4x1 linear antenna array pattern (realized gain)

4.5.3 Eight Elements Linear Antenna Array:

A 8x1 linear array is presented in Figure (4.22). The simulated S_{11} of the array is presented in Figure (4.23). The array has an S_{11} <-10 dB bandwidth more than 2 GHz. Figure (4.24) presents the simulated gain of the array. The 8-element array has a max gain of 14.6 dB at 28.4 GHz. Figure (4.25) presents the radiation patterns of the array. The array has a half power beamwidth (HPBW) of 13.1 degree and 35.4 degree in the E and H planes respectively.

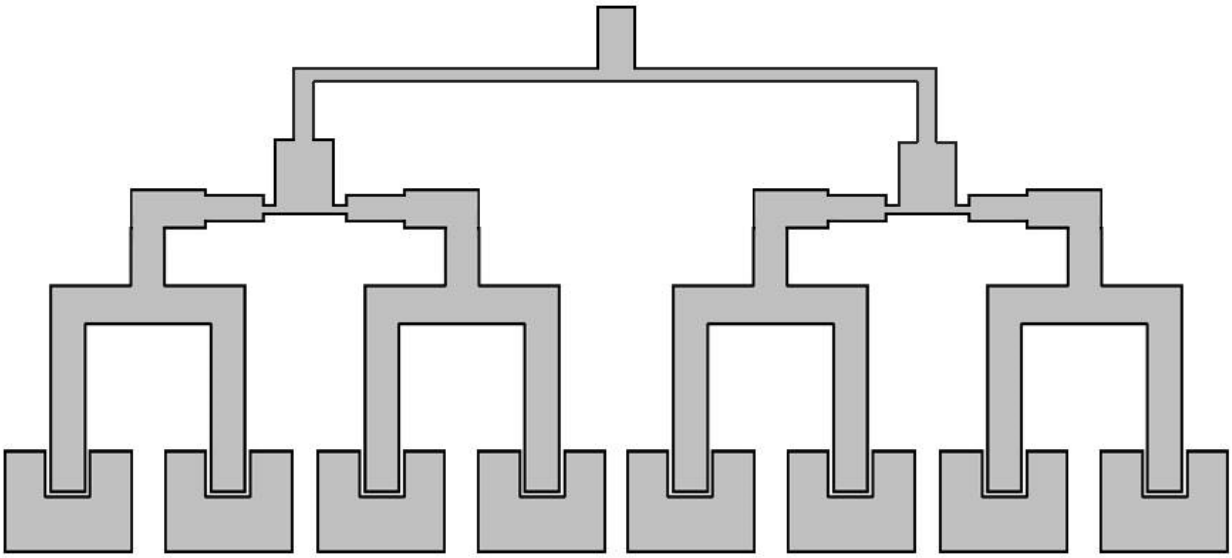

Figure (4.22): 8x1 linear antenna array

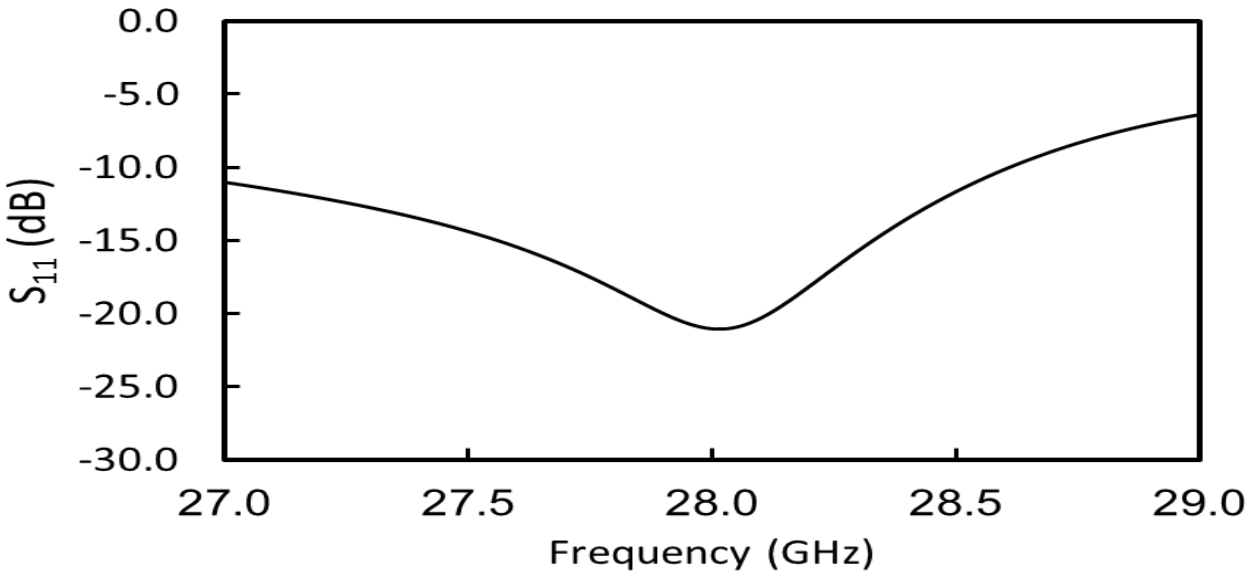

Figure (4.23): Simulated antenna S_{11} vs. frequency for 8x1 linear antenna array

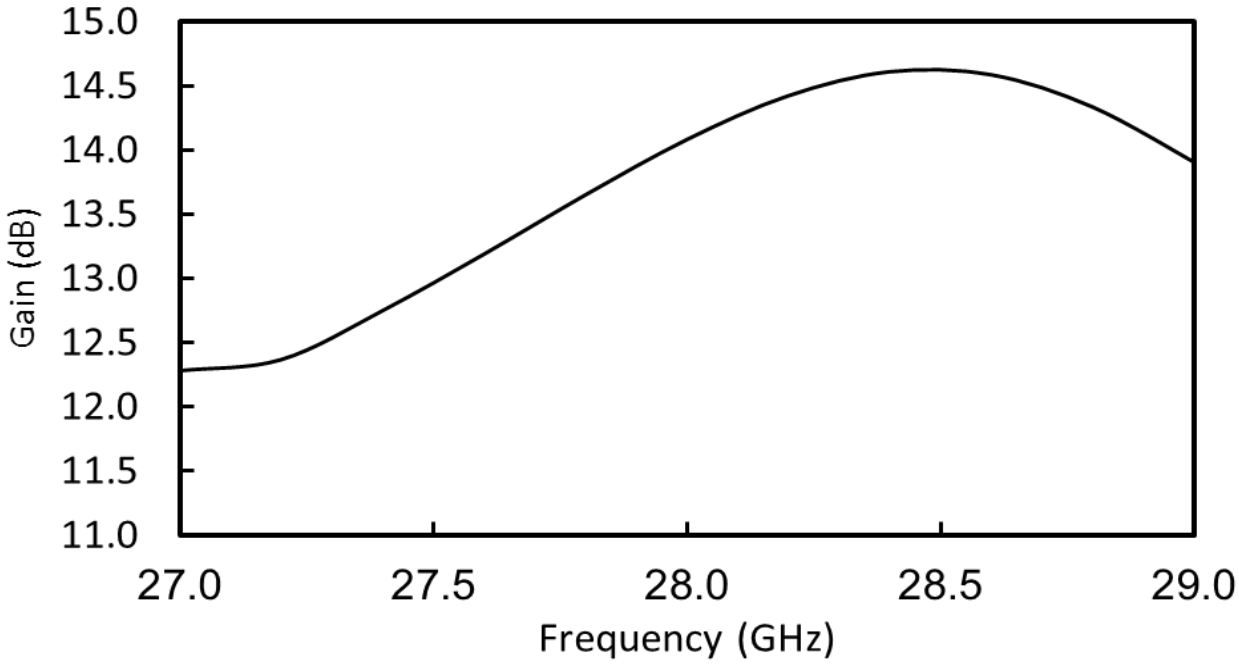

Figure (4.24): Simulated gain vs. frequency for 8x1 linear antenna array

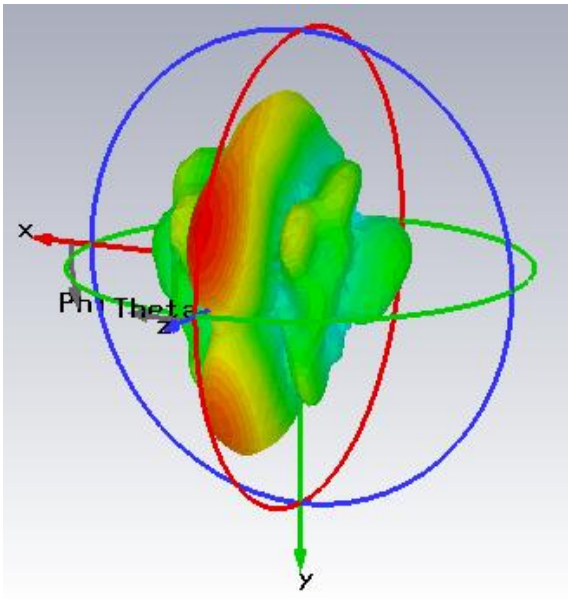

Figure (4.25): 3D radiation pattern for 8x1 linear pattern (realized gain)

4.5.4 Sixteen Element Linear Antenna Array:

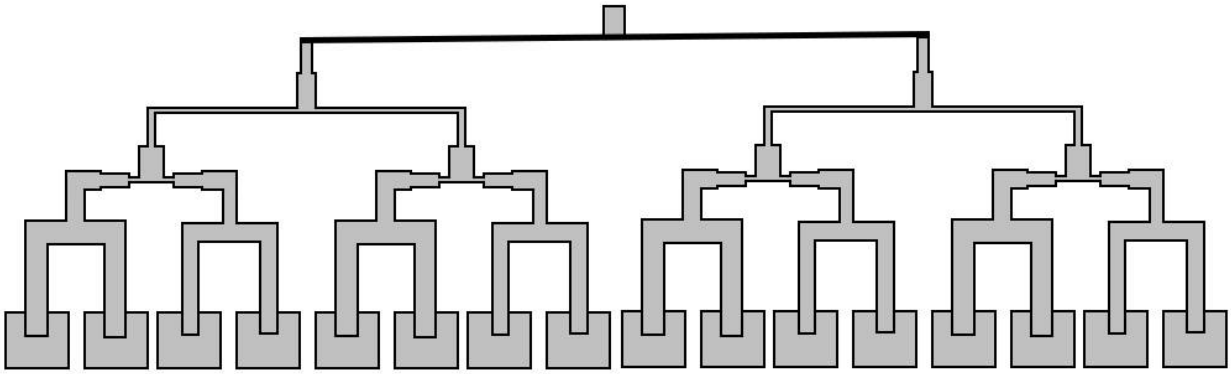

Figure (4.26): 16x1 linear antenna array

A 16x1 linear array is presented in Figure (4.26). The simulated S_{11} of the array is presented in Figure (4.27) . The array has an S_{11} <-10 dB bandwidth greater than 2 GHZ. Figure (4.28) presents the simulated gain of the array. The 16-element array has a max gain of 17.3 dB at 28.4 GHz. Figure (4.29) presents 3D radiation patterns of the array. The array has a half power beamwidth (HPBW) of 6.4 degree and 26.9 degree in the E and H planes respectively. The simulated gain vs. frequency of the 2, 4, 8 and 16 element linear arrays are compared in Figure (4.30).

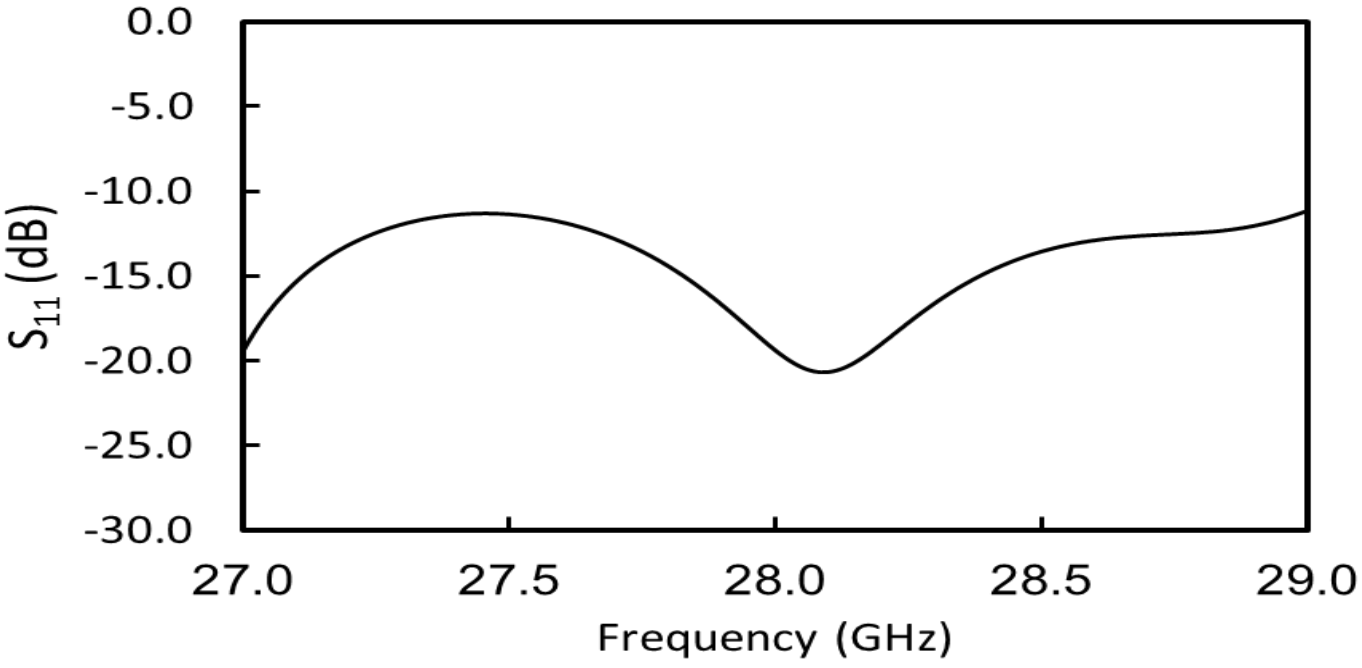

Figure (4.27): Simulated antenna S_{11} vs. frequency for 16x1 linear antenna array

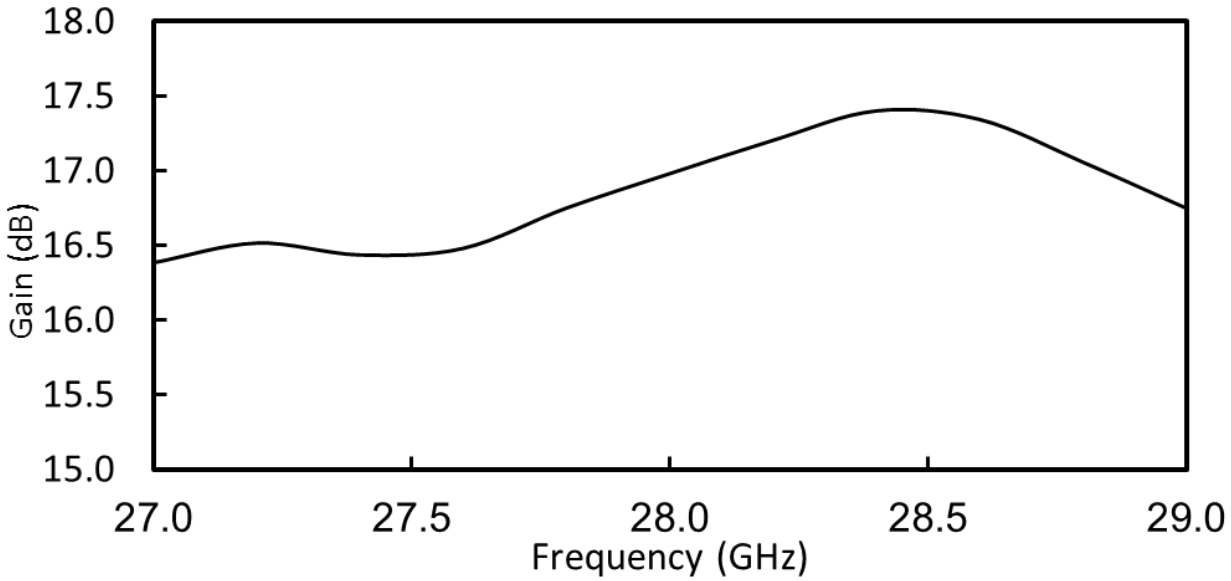

Figure (4.28): Simulated gain vs. frequency for 16x1 linear antenna array

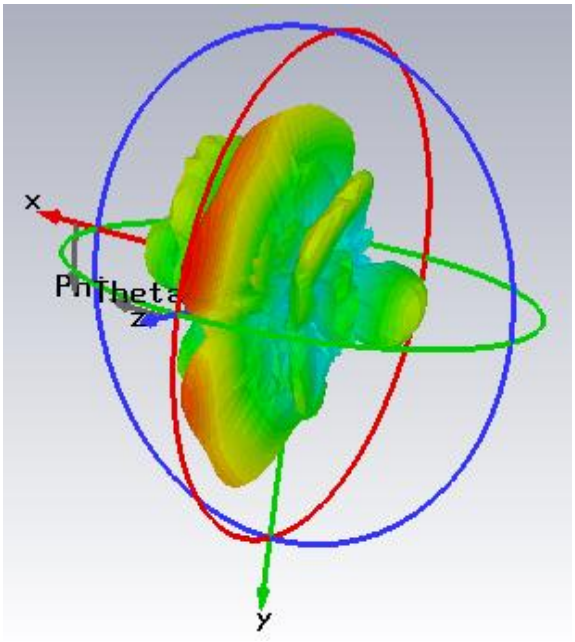

Figure (4.29): 3D radiation pattern for 16x1 linear antenna array pattern (realized gain)

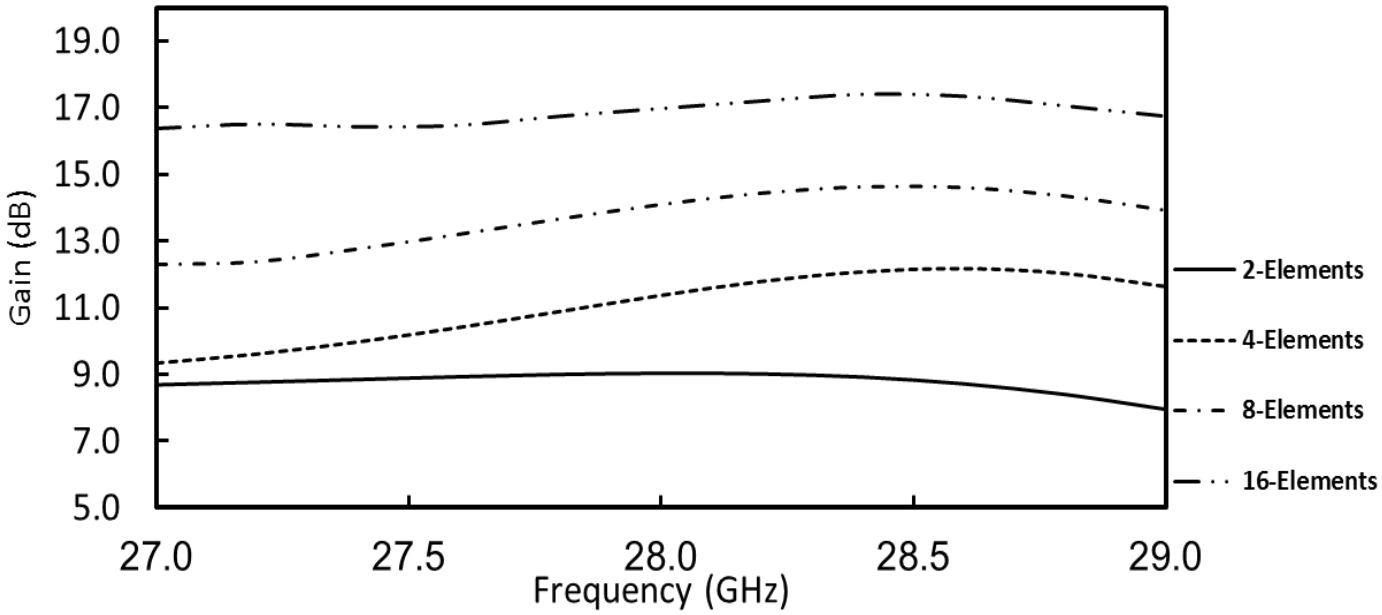

Figure (4.30): simulated gain vs. frequency of the 2, 4, 8 and 16 element linear arrays

4.5.5 Corner-fed single element antenna

Dual polarized antennas can be very efficient in a dense multipath environment since it is usually difficult for the received signal to have a pure linear polarization a corner-fed antenna is very useful method in dual-polarized antenna because it provides good isolation between two edge connected ports (Zhong, Yang, & Cui, Corner-Fed Microstrip Antenna Element and Arrays for Dual-Polarization Operation, 2002). A corner-fed patch antenna geometry is presented in Figure (4.31).

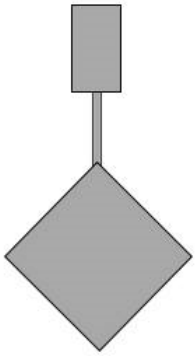

Figure (4.31): Corner-fed patch antenna geometry

The antenna impedance at the corner is higher than edge center impedance. The simulated corner impedance is equal ~441Ω. A 148.5 Ohm quarter-wavelength transformer transmission line is used

to match the antenna with 50Ω. The simulated S_{11} is presented in Figure (4.32) and 3D radiation pattern is shown in Figure (4.33).

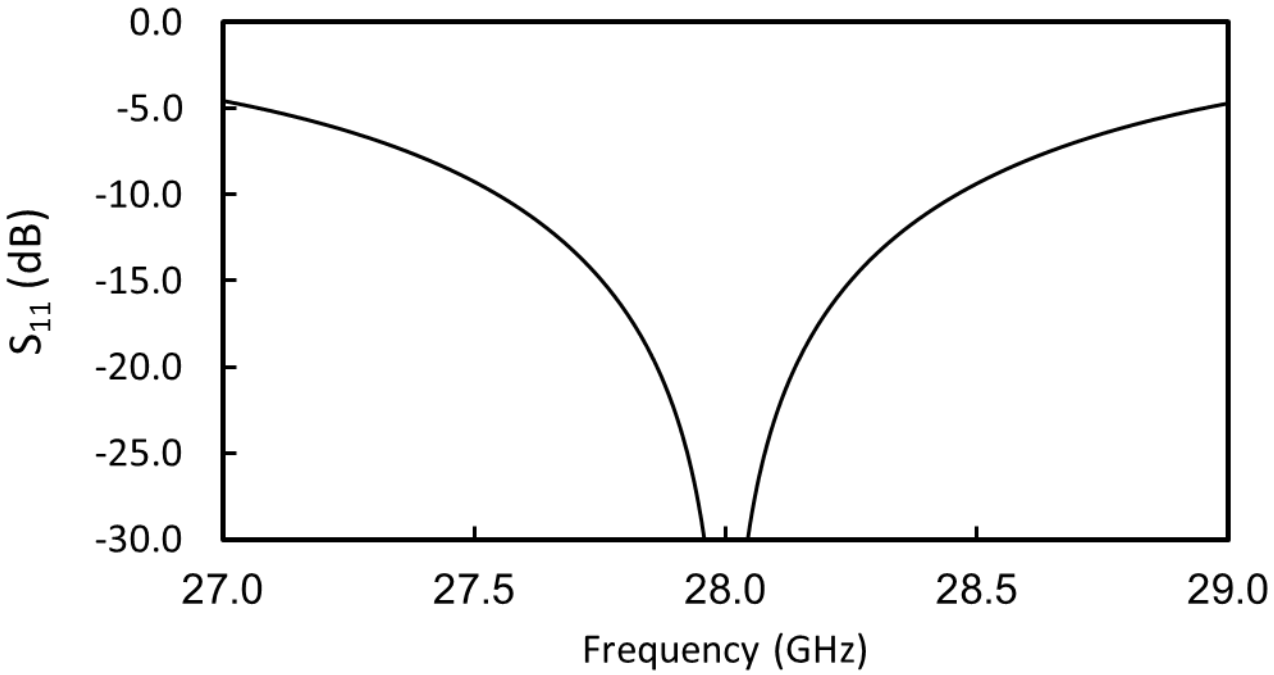

Figure (4.32): Simulated antenna S_{11} vs. frequency for single element corner fed antenna

The antenna has a matched S_{11} <-10dB bandwidth of 909 MHz. The antenna has a simlated gain of peak value of 6.87 dB at 28 GHz.

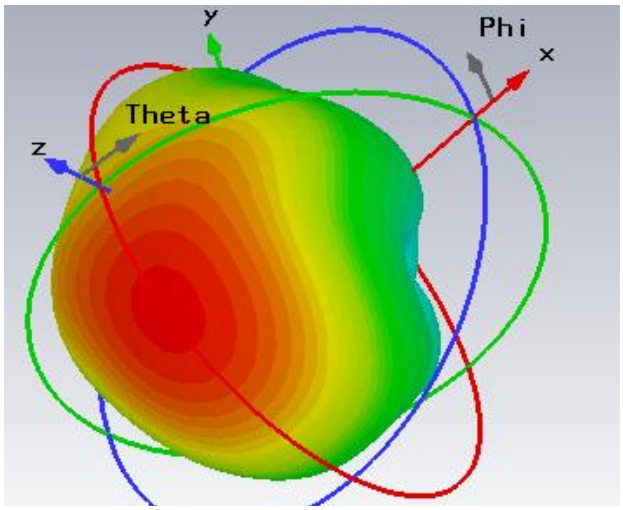

Figure (4.33): 3D radiation pattern for corner fed antenna pattern (realized gain)

4.5.6 4x1 Linear array of corner fed microstrip patch antenna:

A four-element linear array is presented in Figure (4.34). The simulated S11 of the array is presented in Figure (4.35). The array has an S_{11} <-10 dB bandwidth of 1290 MHz. Figure (4.36) presents the simulated gain of the array. The 4-element array has a max gain of 12.1 dB at 28.2 GHz. Figure (4.37) presents the radiation patterns of the array. The array has a half power beamwidth (HPBW) of 23.9 degree and 44.9 degree in the E and H planes respectively.

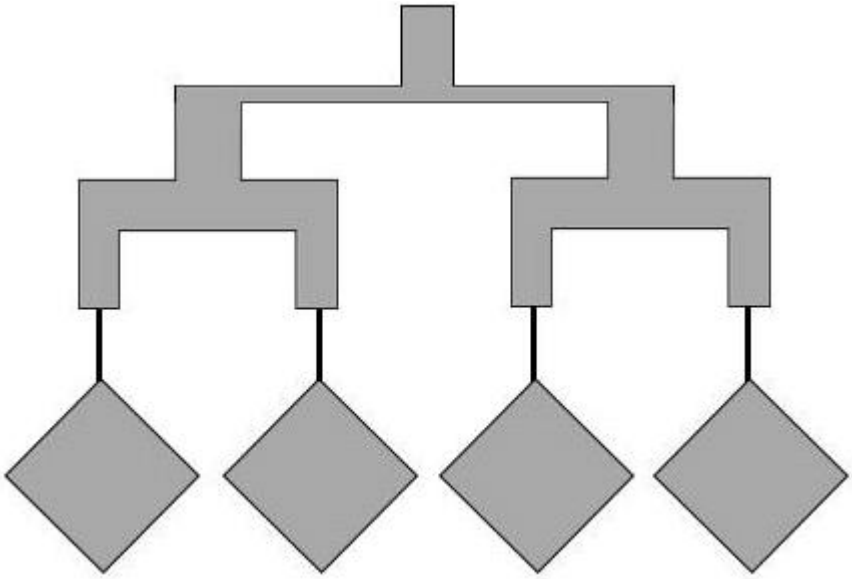

Figure (4.34): four-element corner fed linear array

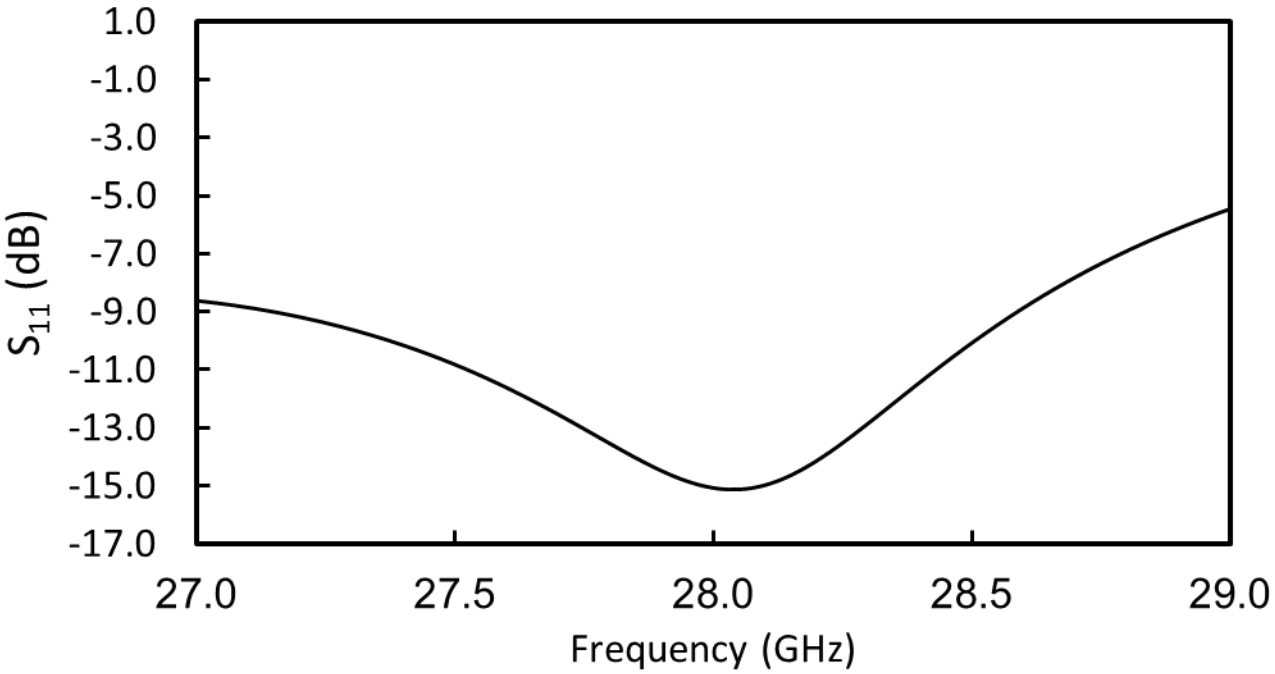

Figure (4.35): Simulated antenna S_{11} vs. frequency for corner fed four element linear array antenna

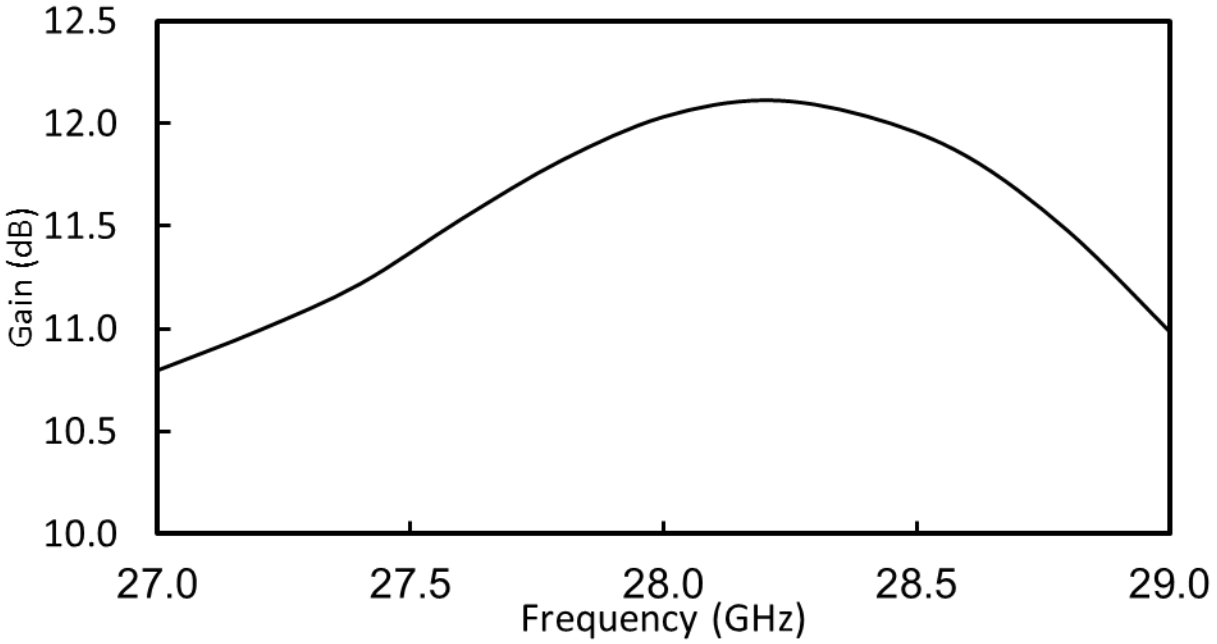

Figure (4.36): Simulated gain vs. frequency for corner fed four element linear array antenna

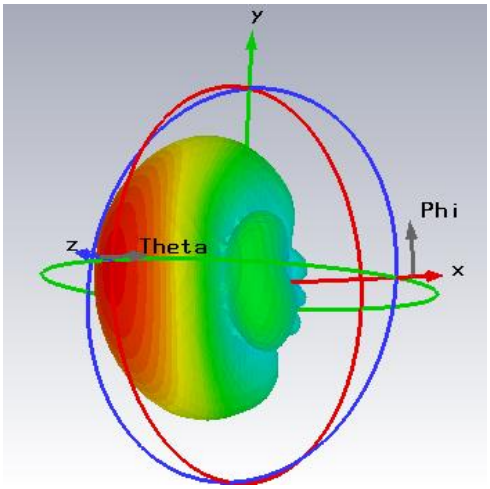

Figure (4.37): 3D radiation pattern for corner fed four element linear array antenna

4.5.7 Dual-Polarized antenna array

In the microstrip antenna field, there has been increasing interest in the dual-polarization operation, which provides more information for aperture radars, doubles the capacity of communication systems, fights against the multipath fading in land mobile communications by means of the polarization-diversity, and increases the transmit–receive isolation of transceivers or

transponders, etc. (Zhong, Yang, & Cui, Corner-Fed Microstrip Antenna Element and Arrays for Dual-Polarization Operation, 2002). Some of the dual-polarization designs utilize multilayered structures, which make the configuration more complicated and increase the manufacturing cost (Zhong, Ahmed, & Qasim, Low Cost Corner-Fed Microstrip Antenna Array With Dual Polarization, 1999) .

The gap-coupled microstrip antenna suffers from poor isolation between ports when fed from two edges as shown in Figure (4.38). The simulated S_{21} between the two ports is presented Figure (4.39). This clearly shows that this design is not appropriate for dual polarized antennas.

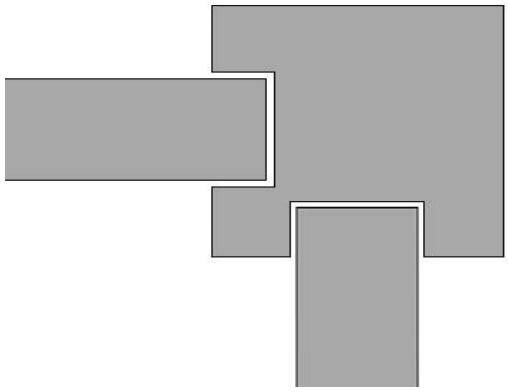

Figure (4.38): dual-polarized gap-coupled fed patch antenna

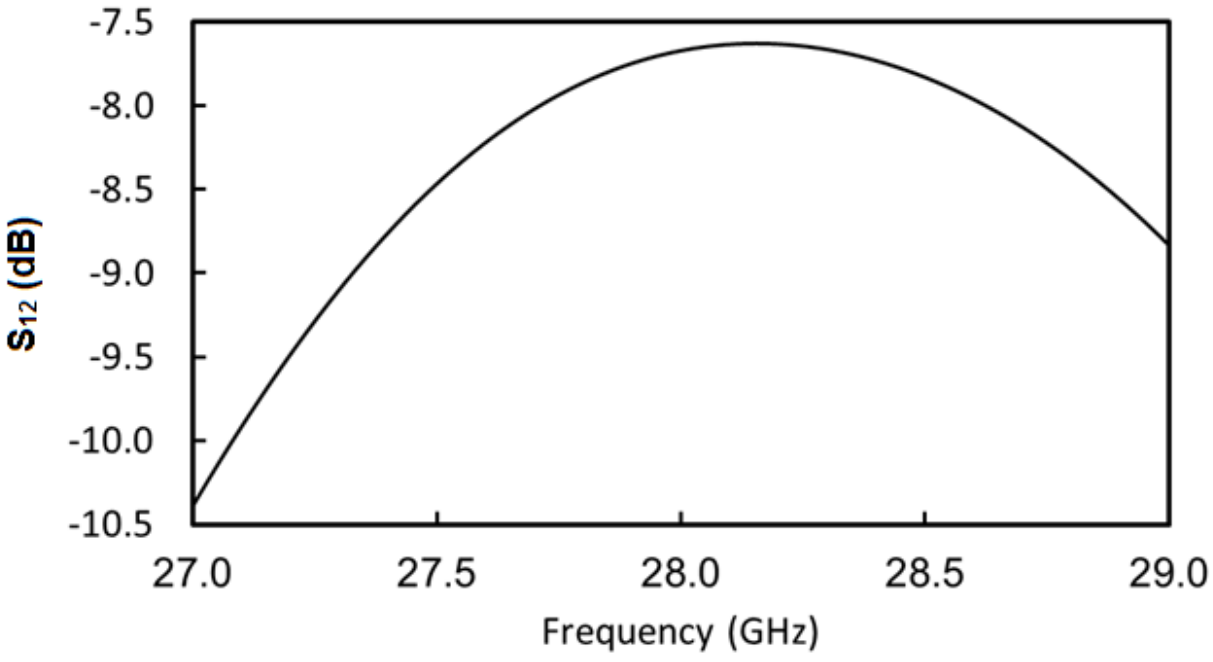

Figure (4.39): Simulated S_{21} between two feeders vs. frequency

The edge fed design shown in Figure (4.40) shows better isolation between ports as presented in Figure (4.41).

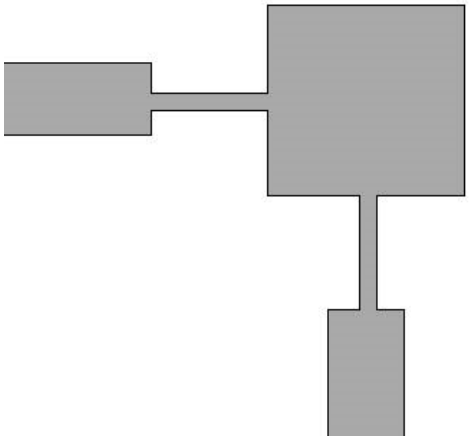

Figure (4.40): dual-polarized edge fed patch antenna

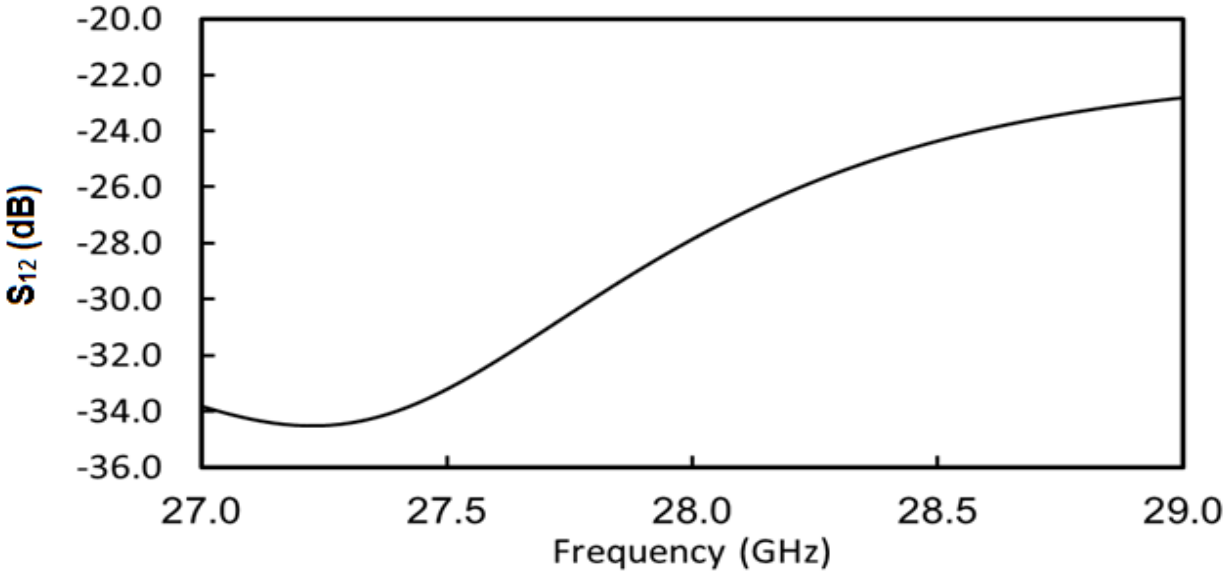

Figure (4.41): Simulated S_{21} between two feeders vs. frequency

A dual polarized linear array of an edge-fed patch antenna is presented in (Hamberger, Drexler, Trummer, Siart, & Eibert, 2016).

4.5.8 Dual polarized single element Corner-fed antenna

A dual-corner-fed square patch is proposed to realize the dual polarization operation. A good isolation between two ports is achieved. The antenna geometry is presented in Figure (4.42) and the simulated S_{21} between the two feeders is shown in Figure (4.43).

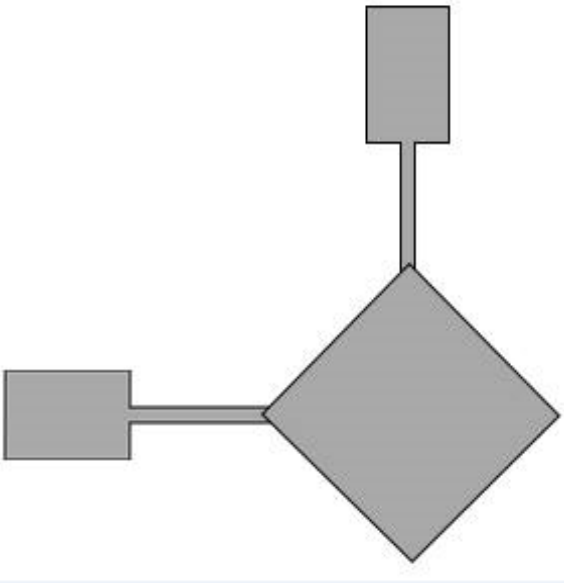

Figure (4.42): dual polarized corner fed single element (Zhong, Yang, & Cui, Corner-Fed Microstrip Antenna Element and Arrays for Dual-Polarization Operation, 2002)

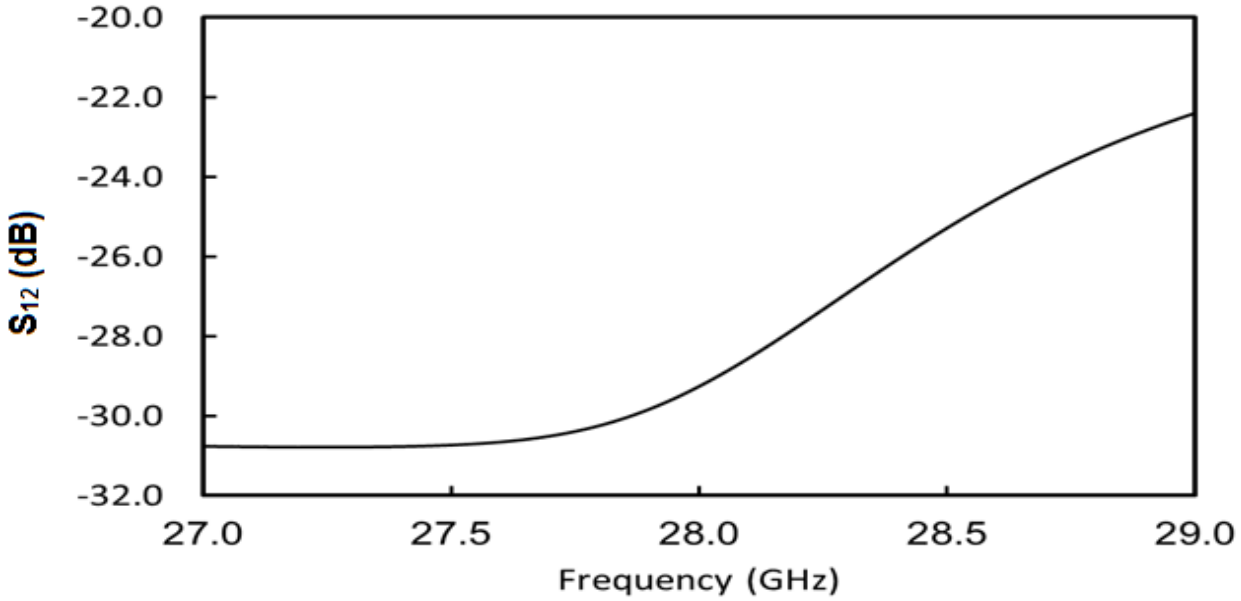

Figure (4.43): Simulated S_{21} between two feeders vs. frequency

4.5.9 Dual polarized 2×2 planar array Corner-fed antenna

A 2x2 6 GHz planar dual polarized antenna array of corner-fed microstrip patch antenna is presented in (Zhong, Yang, & Cui, Corner-Fed Microstrip Antenna Element and Arrays for Dual-Polarization Operation, 2002). A 2by2 dual polarized antenna array at 28 GHz is presented as shown in Figure (4.44). The simulated S_{11} of the array is presented in Figure (4.45). The array has an S_{11} <-10 dB bandwidth of 780 MHz. A good isolation between array feeders as shown in Figure (4.46) where S_{12} has the best value at 28GHz which equals -60dB. Figure (4.47) presents the simulated gain of the array. fed 2by2 antenna array has a max gain of 12.51 dB at 28 GHz. Figure (4.48) presents the radiation pattern of the array. The array has a half power beamwidth (HPBW) of 45.6 degree and 36.7 degree in the E and H planes respectively.

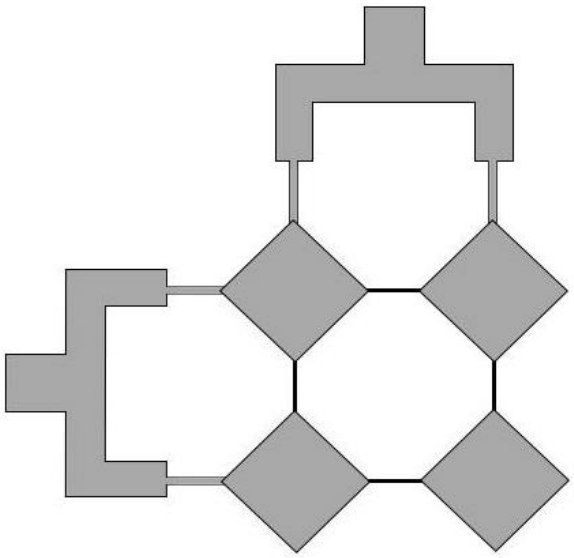

Figure (4.44): dual polarized corner fed 2by2 antenna

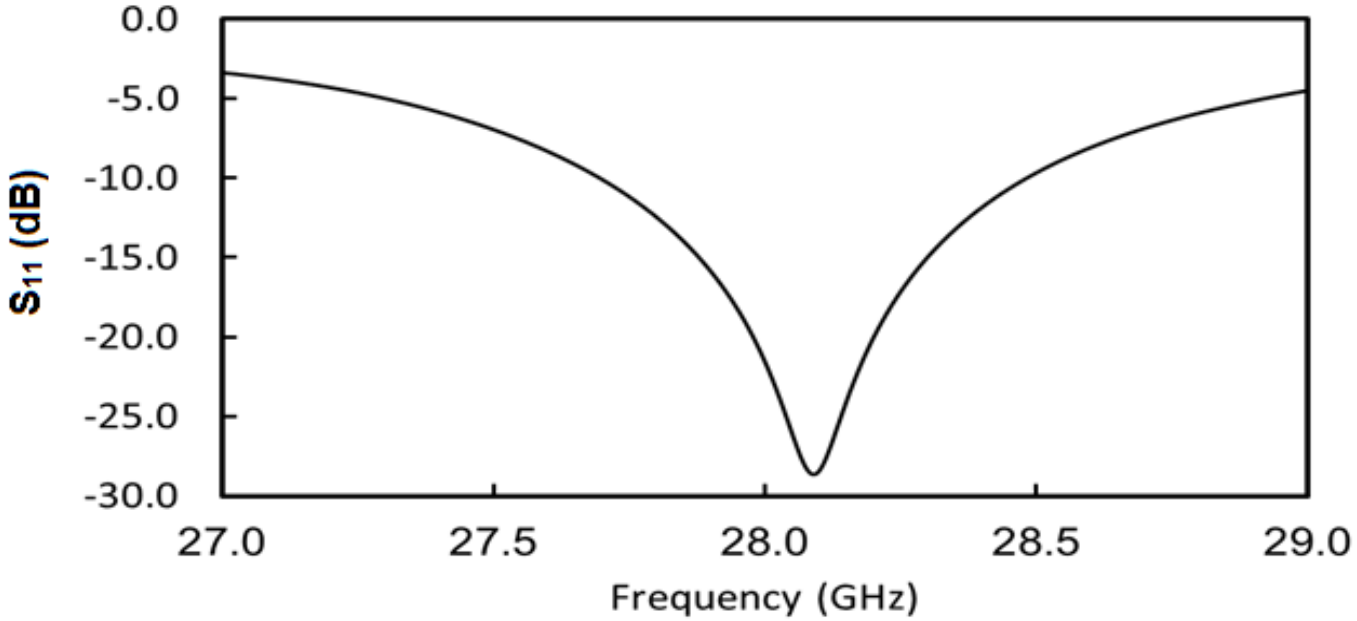

Figure (4.45): Simulated antenna S_{11} vs. frequency for corner fed 2by2 antenna array

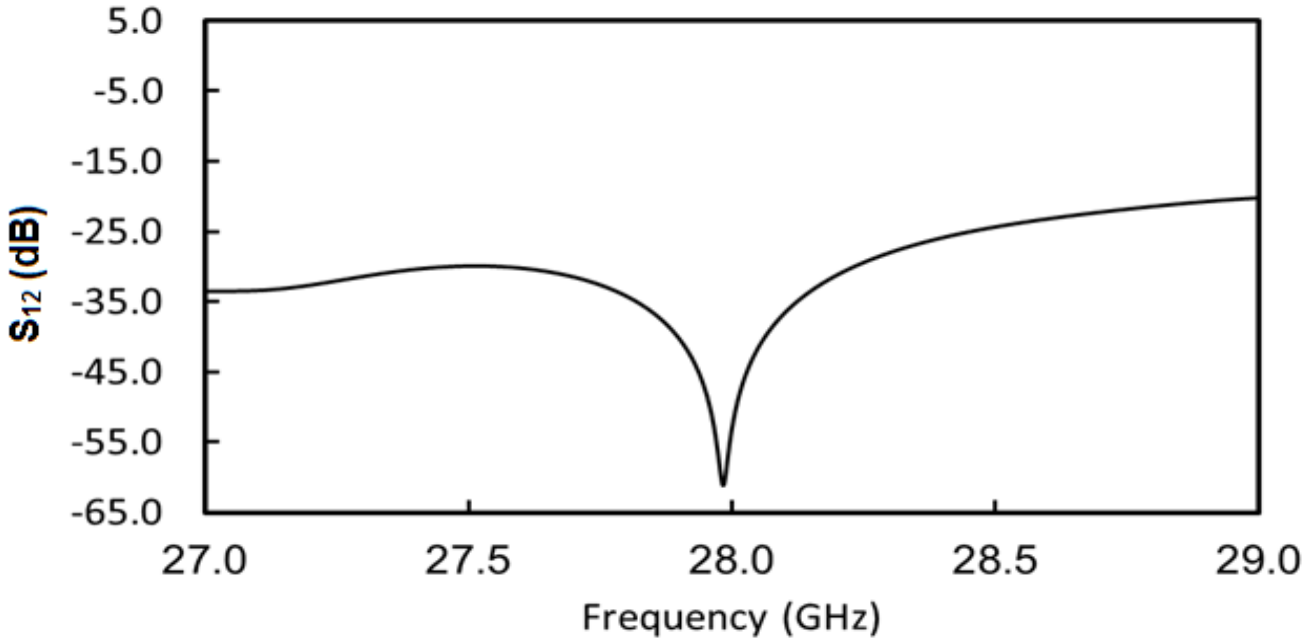

Figure (4.46): Simulated S_{21} between two feeders vs. frequency

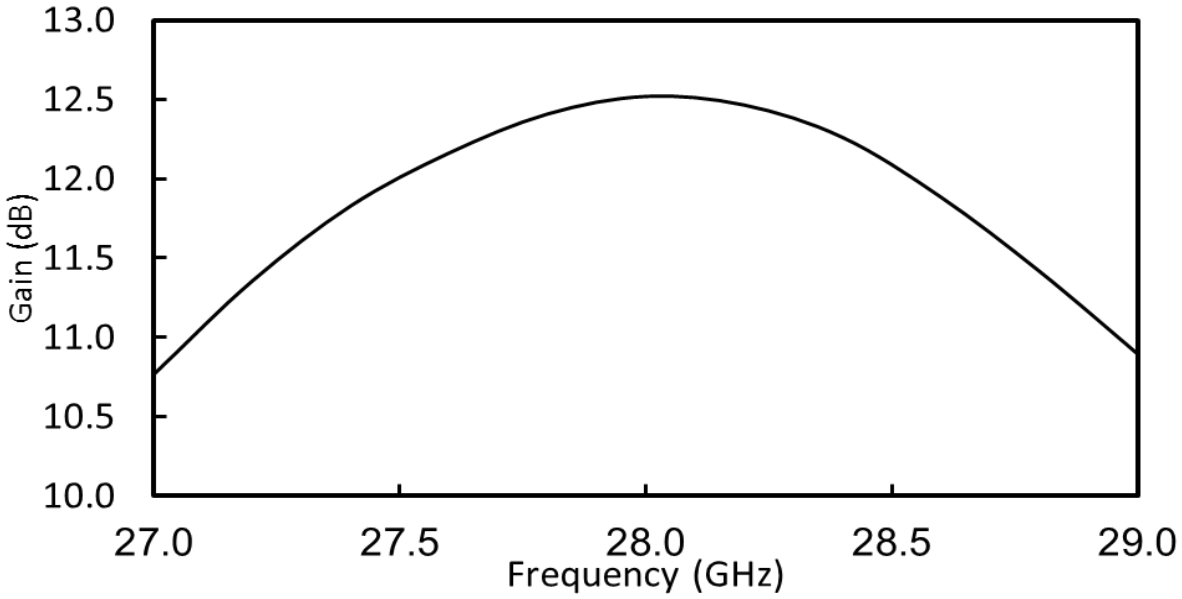

Figure (4.47): Simulated gain vs. frequency for corner fed 2by2 antenna array

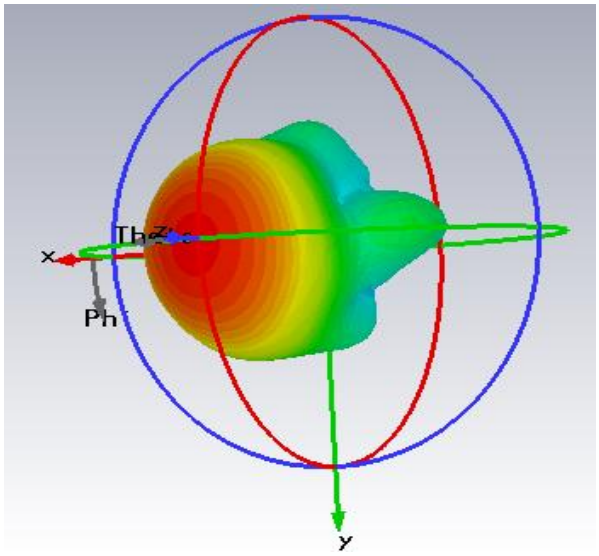

Figure (4.48): 3D radiation pattern pattern (realized gain)

4.5.10 Dual polarized 4×4 planar array Corner-fed antenna

A 4x4 6 GHz planar dual polarized antenna array of corner-fed microstrip patch antenna is presented in (Zhong, Yang, & Cui, Corner-Fed Microstrip Antenna Element and Arrays for Dual-Polarization Operation, 2002). A 4by4dual polarized antenna array at 28 GHz is presented as shown in Figure (4.49). The simulated S_{11} of the array is presented in Figure (4.50). The array has an S_{11} <-10 dB bandwidth of 784 MHz. A good isolation between array feeders as shown in Figure (4.51), where S_{12} has the best value at 28GHz which equals -39.7dB. Figure (4.52) presents the simulated gain of the array. fed 2by2 antenna array has a max gain of 16.53 dB at 28 GHz. Figure (4.53) presents the radiation pattern of the array.

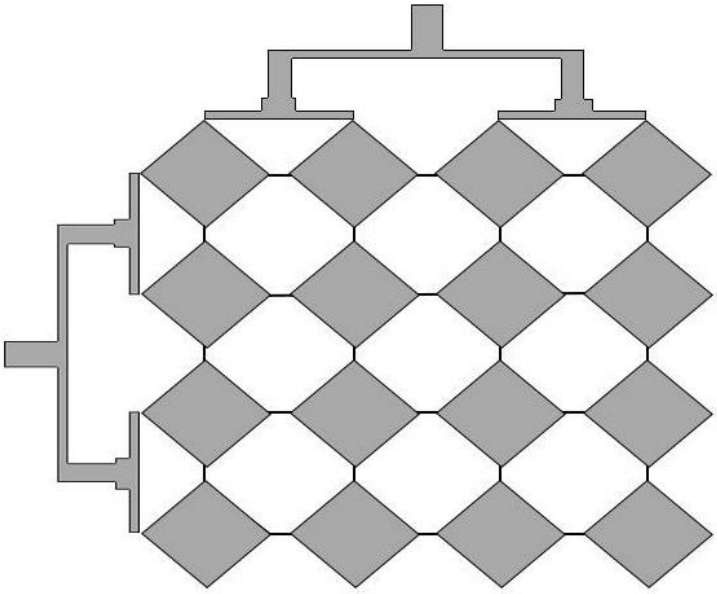

Figure (4.49): dual polarized corner fed 4by4 antenna array

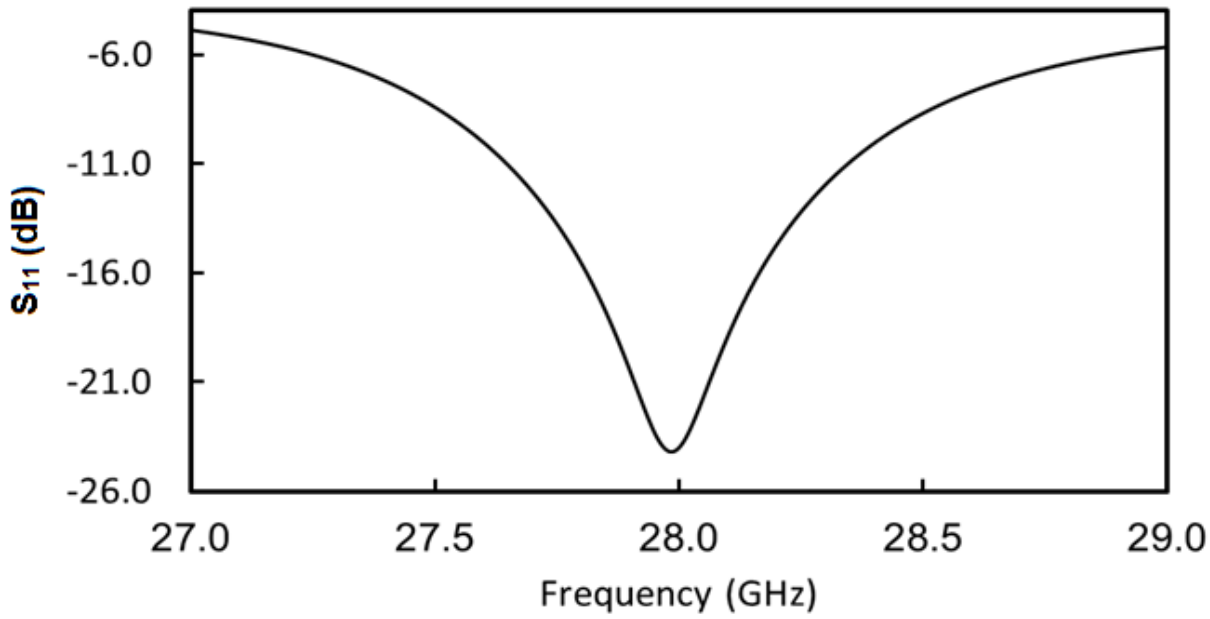

Figure (4.50): Simulated antenna S_{11} vs. frequency for corner fed 4by4 antenna array

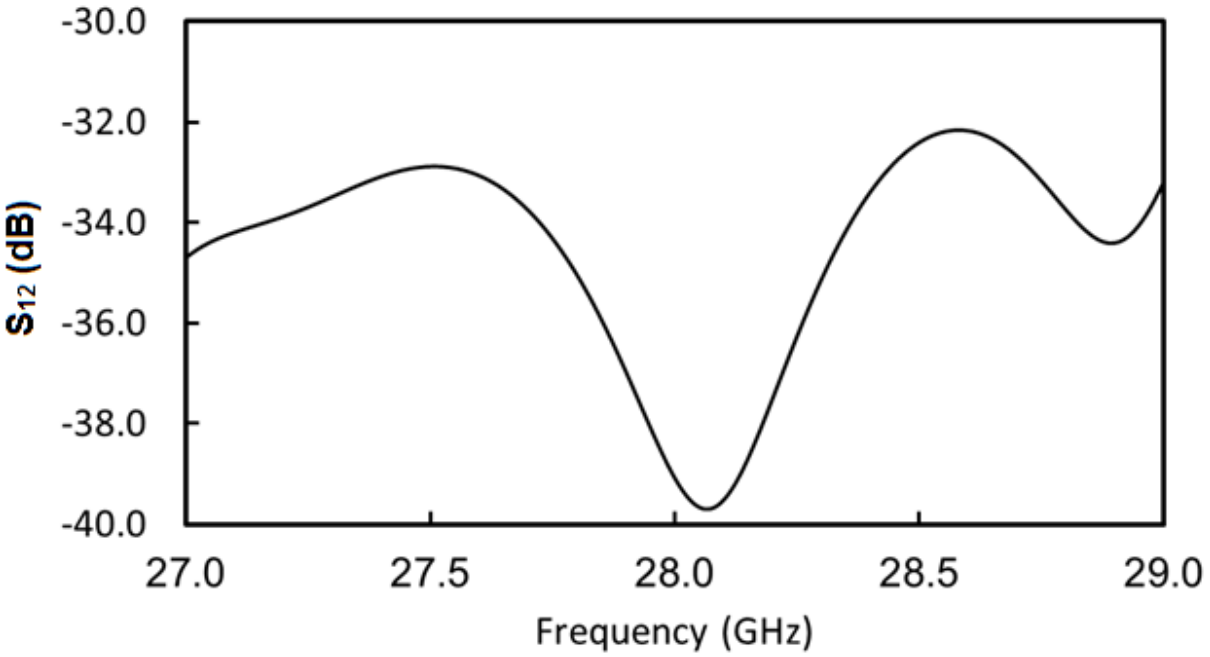

Figure (4.51): Simulated S_{21} between two feeders vs. frequency

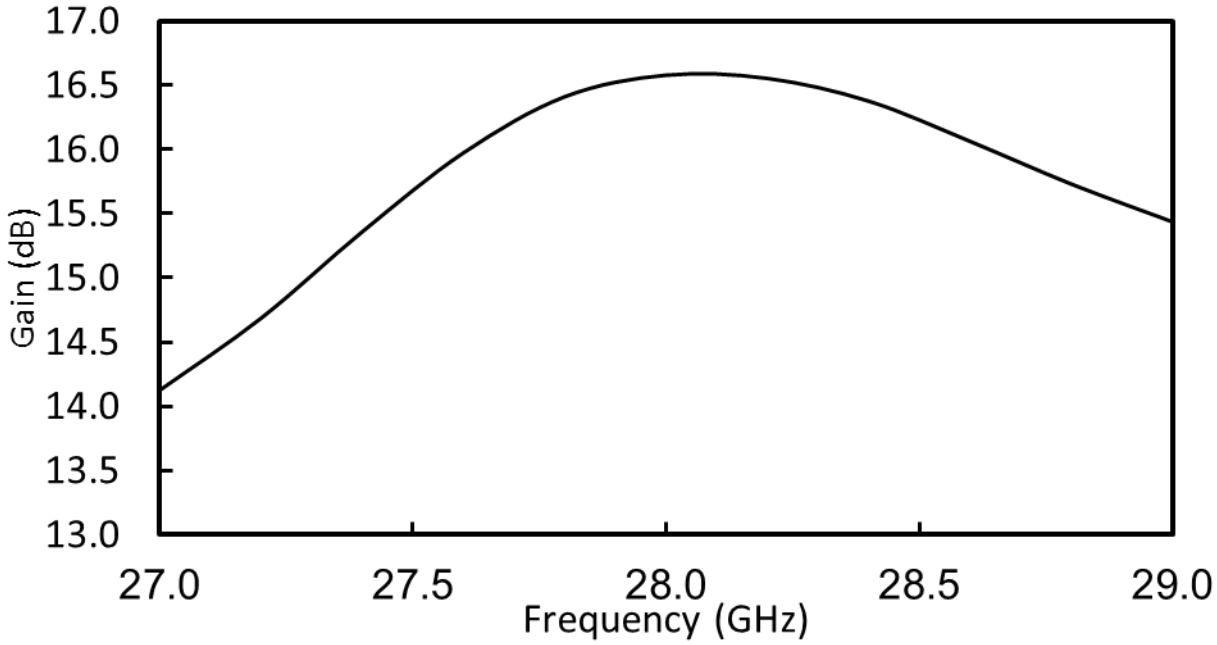

Figure (4.52): Simulated gain vs. frequency for corner fed 4by4 antenna array

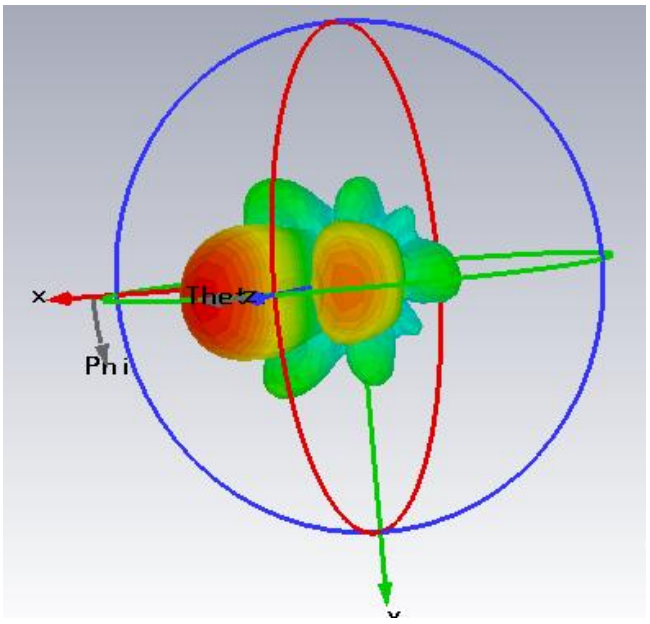

Figure (4.53): 3D radiation pattern

Chapter 5
Conclusion and Future Work

Chapter 5

Conclusions and Future Work

5.1 Conclusion:

In this work, an efficient antenna at 28GHz for 5G communications applications has been successfully designed.

First of all, a parametric study of different parameters that affect antenna performance, (such as antenna type, feeding technique, substrate dielectric constant, substrate thickness, substrate loss tangent, etc.…) was performed using CST simulation software. According to this study, the best substrate material in terms of efficiency and bandwidth is RT-duroid-5880 with dielectric constant ε_r = 2.2 and thickness (h) =0.381 mm.

Several feeding techniques have been studied, and an efficient bandwidth has been obtained with gap-coupled fed single antenna, which has a 1226 MHz bandwidth, FBW (4.38%) and the radiation efficiency equal to 91.8%.

Mutual coupling between two adjacent array elements was studied in order to achieve compact design and wider scanning angle. Defected Ground Structure (DGS) technique was used to reduce the mutual coupling with a rectangular slot in the ground. The slot was optimized to obtain the best isolation (better than -20 dB) and its dimensions were (8.3*0.8) mm^2.

This single element was used in a corporate linear array at different elements number (2×1, 4×1, 8×1 and 16×1). Increasing array elements number results in higher gain value and wider scanning angle, so the gains of that arrays are (9.01 dB, 12.02 dB, 14.6 dB and 17.3 dB respectively).

Dual polarized antenna array is one of the 5G communications requirements, and corner fed microstrip antenna is a good choice to achieve this goal. Corner-fed microstrip antenna element and arrays for dual-polarization operation were designed.

5.2 Future work:

- The linear and planar arrays in this thesis could be fabricated in order to compare the Simulation results and the measurement results.
- Enhance the bandwidth for the corner fed planar dual-polarized antenna array.
- Design dual frequency antenna at mm-wave frequencies to support 5G communications applications.

References

References

Radartutorial.eu. (n.d.). (Radar Basics - Patch Antennas) Retrieved from http://www.radartutorial.eu/06.antennas/Microstrip%20Antenna.en.html

Advanced millimeter-Wave Technologies. (2009). Chichester, U.K.: J. Wiley & Sons.

Agarwal, A. (2017). *The 5th Generation Mobile Wireless Networks- Key Concepts, Network Architecture and Challenges*. (Pubs.sciepub.com) Retrieved from http://pubs.sciepub.com/ajeee/3/2/1/

Ahmadi, S. (2016). Toward 5G Xilinx Solutions and Enablers for Next-Generation Wireless Systems. *White Paper: Xilinx MPSoCs and FPGAs*.

Alhalabi, R. A. (2010). High Efficiency Planar and RFIC-Based Antennas for Millimeter-Wave Communication Systems. *PHD thesis*.

Al-Hasan, M. J., Denidni, T. A., & Sebak, A. R. (2014). Mllimeter-wave Hybrid Isolator for Mutual-Coupling Reduction Applications. *16th International Symposium on Antenna Technology and Applied Electromagnetics (ANTEM)*, 1-2.

Alreshaid, A. T., Hammi, O., & Sharawi, M. S. (2015). A Millimeter Wave Switched Beam Planar Antenna Array. *2015 IEEE International Symposium on Antennas and Propagation & USNC/URSI National Radio Science Meeting*.

Alreshaid, A., Hammi, O., Sharawi, M., & Sarabandi, K. (2015). A compact millimeter-wave slot antenna array for 5G standards. *2015 IEEE 4th Asia-Pacific Conference on Antennas and Propagation (APCAP)*.

Andrews, J. G., Buzzi, S., Choi, W., Hanly, S. V., Lozano, A., Soong, A. C., & Zhang, J. C. (2014). What Will 5G Be? *IEEE Journal on Selected Areas in Communications, 32*(6), 1065-1082.

Antenna-Theory.com - Fractional Bandwidth. (2017). Retrieved Feb 28, 2017, from http://www.antenna-theory.com/definitions/fractionalBW.php

Arya, A. K., Patnaik, A., & Kartikeyan, M. V. (2011). A Compact Array with Low Mutual Coupling using Defected Ground Structures. *IEEE Applied Electromagnatics Conference(AEMC)*, 1-4.

Ashraf, M. A., Haraz, O. M., & Alshebeili, S. (2015). Compact size enhanced gain switched beam conformal antipodal tapered slot antenna system for 5G MIMO wireless communication. *2015 IEEE 11th International Conference on Wireless and Mobile Computing, Networking and Communications (WiMob)*.

Ayoub, F., & Christodoulou, C. T. (2014). The effect of feeding techniques on the bandwidth of millimeter-wave patch antenna arrays. *2014 United States National Committee of URSI National Radio Science Meeting (USNC-URSI NRSM)*.

Balanis, C. (2005). *Antenna theory*. Hoboken, New Jersey: Wiley.

Balanis, C. A. (2008). *MODERN ANTENNA.* Canada: A JOHN WILEY & SONS, INC.

Bancroft, R. (2009). *Microstrip and printed antenna design.* Raleigh, NC: SciTech publishing.

Bevelacqua, P. (2017). *Antenna-theory.com*. (Antenna-Theory.com - Rectangular Microstrip (Patch) Antenna - Feeding Methods) Retrieved from http://www.antenna-theory.com/antennas/patches/patch3.php

Bevelacqua, P. (n.d.). *Antenna-theory.com*. (Antenna Efficiency) Retrieved from http://www.antenna-theory.com/basics/efficiency.php

Carver, K., & Mink, J. (1981). Microstrip antenna technology. *IEEE Transactions on Antennas and Propagation, 29*(1), 2-24.

CHAKRAVARTHY, S. S. (2016). Comparative study on different feeding techniques of rectangular patch antenna. *2016 Thirteenth International Conference on Wireless and Optical Communications Networks (WOCN).*

Chen, Z., & Zhang, Y. (2013). FR4 PCB Grid Array Antenna for Millimeter-Wave 5G Mobile Communications. *IEEE MTT-S International Microwave Workshop Series onRF and Wireless Technologies for Biomedical and Healthcare Applications* .

Civerolo, M. P. (2010). Aperture Coupled Microstrip Antenna Design and Analysis. *Faculty of California Polytechnic State University(master thesis).*

Forum for Electronics. (2017). (Total radiation efficiency = antenna efficiency) Retrieved from http://www.edaboard.com/thread187838.html

Gampala, G., & Reddy, C. J. (2016). Design of millimeter wave antenna arrays for 5G cellular applications using FEKO. *2016 IEEE/ACES International Conference on Wireless Information Technology and Systems (ICWITS) and Applied Computational Electromagnetics (ACES).*

Gampala, G., & Reddy, C. J. (2016). Design of Millimeter Wave Antenna Arrays for 5G Cellular Applications using FEKO.

Gang, R., Bhartia, P., Bahl, I., & Ittipiboon, A. (2001). *Microstrip Antenna Design Handbook.* Boston: Artech House.

Garg, R. (2001). *Microstrip antenna design handbook.* Boston, MA: Artech House.

Garg, R., Bhartia, P., Bahl, I., & Ittipiboon, A. (2001). *Microstrip antenna design handbook.* Boston: Artech House.

Garg, R., Bhartia, P., Bahl, I., & Ittipiboon, A. (2001). *Microstrip Antenna Design Handbook.* Boston: Artech House.

Ghosh1, J., Ghosal, S., Mitra, D., & Chaudhuri, S. R. (2016). Mutual Coupling Reduction between Closely Placed Microstrip Patch Antenna Using Meander Line Resonator. *Progress In Electromagnetics Research Letters, 59,* 115–122.

Grilo, M., & Correra, F. S. (2015). Rectangular Patch Antenna on Textile Substrate Fed by Proximity Coupling. *Journal of Microwaves, Optoelectronics and Electromagnetic Applications, 14*.

Hamberger, G. F., Drexler, A., Trummer, S., Siart, U., & Eibert, T. F. (2016). A planar dual-polarized microstrip 1D-beamforming antenna array for the 24GHz ISM-band. *2016 10th European Conference on Antennas and Propagation (EuCAP)*.

HARAZ, O. M., ELBOUSHI, A., ALSHEBEILI, S. A., & SEBAK, A.-R. (2014). Dense Dielectric Patch Array Antenna With Improved Radiation Characteristics Using EBG Ground Structure and Dielectric Superstrate for Future 5G Cellular Networks. *IEEE Access*.

Hartley, P. (2017). *Gimme 5: What to Expect from 5G Wireless Networks | FreshMR*. (Marketstrategies.com) Retrieved from http://www.marketstrategies.com/blog/2015/03/gimme-5-what-to-expect-from-5g-wireless-networks/

HONG, J.-S., & LANCASTER, M. J. (2001). *Microstrip Filters for RF/Microwave Applications.* NEW YORK / CHICHESTER / WEINHEIM / BRISBANE / SINGAPORE / TORONTO: JOHN WILEY & SONS, INC.

Hong, W., Ko, S., Lee, Y., & Baek, K. (2015). Multi-polarized antenna array configuration for mmWave 5G mobile terminals. *2015 International Workshop on Antenna Technology (iWAT)*.

Hong, W., Ko, S.-T., Lee, Y., & Baek, K.-H. (2015). Multi-polarized Antenna Array Configuration for mmWave 5G Mobile Terminals. *The 2015 International Workshop on Antenna Technology*, 60-61.

Hong, W., KwanghunBaek, Lee, Y., & Kim, Y. G. (2014). Design and Analysis of a Low-Profile 28 GHz Beam Steering Antenna Solution for Future 5G Cellular Applications. *2014 IEEE MTT-S International Microwave Symposium (IMS2014)*.

Hu, C.-N., Yu, C.-H., Hsaio, T.-W., & Lin, D.-P. (2015). Design of a mm-wave microstrip antenna array. *2015 International Workshop on Electromagnetics: Applications and Student Innovation Competition (iWEM)*.

Huang, Y., & Boyle, K. (2008). *Antennas from Theory to Practice.* Chichester: A John Wiley and Sons, Ltd, Publication.

Huang, Y., & Boyle, K. (2008). *ANTENNAS FROM THEORY TO PRACTICE.* Chichester, UK: John Wiley & Sons Ltd.

Hui, H. T. (n.d.). Mutual Coupling in Antenna Arrays. *University of Waterloo (Waterloo)*.

Jamaluddin, M. h., Kamarudin, M., & Khalily, M. (2016). Rectangular Dielectric Resonator Antenna Array for 28 GHz Applications. *Progress In Electromagnetics Research C, 63*, 53–61.

Jamaluddin, M. h., Kamarudin, M., & Khalily, M. (2016). Rectangular Dielectric Resonator Antenna Array for 28 GHz Applications. *Progress In Electromagnetics Research, 63*, 53–61.

Jang, K., Khattak, M. K., Jeon, J., Kim, H., & Kahng, S. (2015). Handheld beamforming antennas adoptable to 5G wireless connectivity. *2015 International Workshop on Antenna Technology (iWAT)*.

Jr., G. R., Junhong Zhang, S. N., & Rappaport, T. S. (2013). Path Loss Models for 5G Millimeter Wave Propagation Channels in Urban Microcells. *IEEE Global Communications Conference, Exhibition & Industry Forum*, 9-13.

K., G. C., & Parui, S. K. (2013). Reduction of mutual coupling between E-shaped microstrip antennas by using a simple microstrip I-section. *Microwave and Optical Technology Letters*, *55*, 2544–2549.

Kim, T., Bang, I., & Sung, D. K. (2014). Design Criteria on a mmWave-based Small Cell with Directional Antennas. *IEEE 25th International Symposium on Personal*, 103-107.

Kraus, J. D. (1988). *Antennas.* New York - McGrow-Hill.

Kraus, J. D., & Marhefka, R. J. (2002). *Antennas for all Applications.* New York - McGrowHill.

Lee, J., Song, Y., Choi, E., & Park, J. (2015). mmWave Cellular Mobile Communication for Giga Korea 5G Project. *Proceedings of APCC2015 copyright*.

Lee, J., Song, Y., Choi, E., & Park, J. (2015). mmWave Cellular Mobile Communication for Giga Korea 5G Project. *Proceedings of APCC2015 copyright*.

Liu, D. D., Gaucher, M. B., Pfeiffer, D. U., & Grzyb, D. J. (2009). *ADVANCED MILLIMETER-WAVE TECHNOLOGIES.* West Sussex: John Wiley & Sons Ltd.

Nair, A., Bharati A., S., & S.S., T. (2015). Design of Rectangular Microstrip 4x2 Patch Array Antenna at 2.4 GHz for WLAN Application. *2015 Second International Conference on Advances in Computing and Communication Engineering*.

Ojaroudiparchin, N., Shen, M., & Frolund, G. (2015). Multi-Layer 5G Mobile Phone Antenna for Multi-User MIMO Communications. *23rd Telecommunications forum TELFOR 2015*.

Ononchimeg, S., Bang, J.-H., & Ahn, B.-C. (2010). A NEW DUAL-POLARIZED GAP-FED PATCH Antenna. *Progress In Electromagnetics Research C, 14*, 79–87.

Orfanidis, S. J. (2004). *Electromagnetic Waves & Antennas.* Rutgers University.

Pan, B. C., Tang, W. X., & Qi, M. Q. (2017). *Reduction of the spatially mutual coupling between dual-polarized patch antennas using coupled metamaterial slabs*. Retrieved from http://www.nature.com/articles/srep30288

Pozar, D. (1992). Microstrip antennas. *Proceedings of the IEEE*, *80*(1), 79-91.

POZAR, D. M. (1992). Microstrip Antennas. *PROCEEDINGS OF THE IEEE, 80*.

Pozar, D. M. (1996). A Review of Aperture Coupled Microstrip Antennas.

Pozar, D. M. (2012). *Microwave Engineering.* John Wiley & Sons, Inc.

Pozar, D. (n.d.). Surface wave effects for millimeter wave printed antennas. *1983 Antennas and Propagation Society International Symposium*.

Puttaswamy, P., & Murthy, P. S. (2014). Analysis of loss tangent effect on Microstrip antenna gain. *Int. Journal of Applied Sciences and Engineering Research*, 6.

Revolvy, L. (2017). *"5G" on Revolvy.com*. (Revolvy.com) Retrieved from https://www.revolvy.com/main/index.php?s=5G

RT/duroid® 5880 Laminates. (2017). Retrieved from https://www.rogerscorp.com/acs/products/32/RT-duroid-5880-Laminates.aspx

S.Sarkar. (2013). Design of a Compact Microstrip Antenna using Capacitive Feed and Parasitic Patch for Ultra-Wideband Application. *International Journal of Scientific and Research Publications, 3*(6).

Sadiku, M. N. (2007). *Elements of electromagnetics.* New York: Oxford University Press.

Sahoo, S., Hota, M., & Barik, K. (2017). *5G Network a New Look into the Future: Beyond all Generation Networks*. (Pubs.sciepub.com) Retrieved from http://pubs.sciepub.com/ajss/2/4/5

Salehi, M., Motevasselian, A., Tavakoli, A., & Heidari, a. T. (2006). MUTUAL COUPLING REDUCTION OF MICROSTRIP ANTENNAS USING DEFECTED GROUND STRUCTURE. *Iran Telecommunication Research Center (ITRC) for financial support.*

Senic, D., zivkovic, Z., simic, M., & Sarolic, A. (2014). Rectangular patch antenna: Design, wideband properties and loss tangent influence. *2014 22nd International Conference on Software, Telecommunications and Computer Networks (SoftCOM)*.

Senic, D., Zivkovic, Z., Simic, M., & Sarolic, A. (2014). Rectangular patch antenna: Design, wideband properties and loss tangent influence. *2014 22nd International Conference on Software, Telecommunications and Computer Networks (SoftCOM)*.

SILVER, S. (1949). *MICROWAVE ANTENNA THEORY AND DESIGN.* NEW YORK, TORONTO LONDON: McGRAW-HILL BOOK CO,MPANY, INC.

Stutzman, W., & Thiele, G. (2013). *Antenna theory and design.* John Wiley & Sons, Inc.

Tang, X., Qing, X., Liu, W., Nasimuddin, Zhai, G., & Chen, Z. N. (2016). Effect of Mutual Coupling on Ka-band Circularly Polarized Beam Scanning Antenna Array. *2016 IEEE International Symposium on Antennas and Propagation (APSURSI)*, 2193 - 2194.

Uncategorized | mansipruthi. (2017). (Mansipruthi.wordpress.com) Retrieved from https://mansipruthi.wordpress.com/category/uncategorized/

Volakis, J. L. (2007). *Antenna engineering handbook.* New York: Toronto.

Yang, X. M., Liu, X. G., Zhu, X. Y., & Cui, T. J. (2012). Reduction of mutual coupling between closely packed patch antenna using waveguide metamaterials. *IEEE Antennas and Wireless Propagation, 11*, 389–391.

Yu, A., & Zhang, X. (2003). A novel method to improve the performance of microstrip antenna arrays using a dumbbell EBG structure. *IEEE Antennas Wireless Propagation Letters, 2*, 170–172.

Yu, Y., Yi, L., Liu, X., & Gu, Z. (2016). Mutual Coupling Reduction of Dual-Frequency Patch Antenna Arrays. *ACES JOURNAL, 31*.

Zhao, H., Mayzus, R., Sun, S., Samimi, M., S., J. K., A., . . . T. (2013). 28 GHz Millimeter Wave Cellular Communication Measurements for Reflection and Penetration Loss in and around Buildings in New York City. *IEEE International Conference on Communications (ICC)*, 9-13.

Zhong, S.-S., Ahmed, M., & Qasim, G. (1999). Low Cost Corner-Fed Microstrip Antenna Array With Dual Polarization. *1999 Asia Pacific Microwave Conference. APMC'99. Microwaves Enter the 21st Century. Conference Proceedings (Cat. No.99TH8473)*.

Zhong, S.-S., Yang, X.-X., & Cui, J.-H. (2002). Corner-Fed Microstrip Antenna Element and Arrays for Dual-Polarization Operation. *IEEE TRANSACTIONS ON ANTENNAS AND PROPAGATION, 50*, 1473-1479.